2018

High-throughput microfluidic assay devices for culturing of soybean and microalgae and microfluidic electrophoretic ion nutrient sensor

Zhen Xu
Iowa State University

High-throughput microfluidic assay devices for culturing of soybean and microalgae and microfluidic electrophoretic ion nutrient sensor

by

Zhen Xu

A dissertation submitted to the graduate faculty

in partial fulfillment of the requirements for the degree of

DOCTOR OF PHILOSOPHY

Major: Electrical Engineering

Program of Study Committee:
Liang Dong, Co-major Professor
Ratnesh Kumar, Co-major Professor
Robert J Weber
Michael Castellano
Fernando Miguez

The student author, whose presentation of the scholarship herein was approved by the program of study committee, is solely responsible for the content of this dissertation. The Graduate College will ensure this dissertation is globally accessible and will not permit alterations after a degree is conferred.

Iowa State University

Ames, Iowa

2018

NOMENCLATURE v
ACKNOWLEDGMENTS vii
ABSTRACT viii
CHAPTER 1. INTRODUCTION 1
1.1 Introduction to bioenergy 1
1.1.1 Biofuel and biofuel generation 2
1.2 Introduction to soybean, Phytophthora sojae, and humidity 2
1.2.1 Phytophthora sojae 3
1.2.2 Humidity 4
1.2.3 State-of-art controlled humidity technology 5
1.2.3.1 Greenhouse controlled humidity technology 6
1.2.3.2 In-laboratory large-scale controlled humidity technology 7
1.2.3.3 On-chip controlled humidity technology 8
1.3 Microalgae and algal cell culture 11
1.3.1 Biomass 11
1.3.2 Microalgae 12
1.3.3 State-of-art microalgae cultivation technology 13
1.3.3.1 Open pond microalgae cultivation technology 14
1.3.3.2 Photobioreactor 15
1.3.3.3 In-laboratory microalgae cultivation technology 16
1.3.3.4 On-chip microalgae cultivation technology 18
1.4 Soil nutrient sensor 21
1.4.1 Soil health 21
1.4.2 State-of-art soil nutrient sensor 22
1.4.2.1 Coaxial impedance dielectric reflectometry method 23
1.4.2.2 Atomic absorption spectroscopy 23
1.4.2.3 Ion sensitive field effect transistor method 24
1.4.3 Capillary electrophoresis 24
1.4.4 Capillary electrophoresis based on on-chip technology 25

1.5 Problems, Objective, Goal and Approach 26
1.5.1 Limitation of current humidity control technology 26
1.5.2 Challenge of current microalgae culture technology 26
1.5.3 Limitation of current soil sensors 27
1.5.4 Objectives and basic approaches of this thesis 27
References 29
CHAPTER 2. HUMIDITY ASSAY FOR PLANT-PATHOGEN INTERACTIONS IN MINIATURE CONTROLLED DISCRETE HUMIDITY ENVIRONMENTS WITH GOOD THROUGHPUT 37
Abstract 37
2.1 Introduction 38
2.2 Device Design 40
2.3 Device characterization 44
2.3 Humidity in the soybean-Phytophthora sojae interaction 46
2.4 Temperature, size scaling & other configurations 50
2.5 Conclusions 54
References 55
CHAPTER 3. MICROFLUIDIC CHIP FOR AUTOMATED SCREENING OF CARBON DIOXIDE CONDITIONS FOR MICROALGAL CELL GROWTH 58
Abstract 58
3.1 Introduction 59
3.2 Device Design 61
3.3 Experimental 66
3.4 Results and Discussion 67
3.5 Conclusions 71
References 71
CHAPTER 4. MULTIWELL-PLATE-BASED MICROALGAL BIOREACTOR ARRAY FOR HIGH-THROUGHPUT SCREENING OF CO2 CONCENTRATION CONDITIONS ON MICROALGAE GROWTH 76
Abstract 76
4.1 Introduction 76
4.2 Material and Method 78
4.2.1 Concept of multi-well-plate-based microalgal bioreactor 78
4.2.2 Fabrication and assembly 79
4.2.3 Transmitted light intensity and colorimetric detection 80
4.2.4 Cell incubation and on-chip culture 80

4.3 Results 81
4.4 Discussion 84
4.5 Conclusions 85
References 86
CHAPTER 5. NUTRIENT SENSING USING CHIP SCALE ELECTROPHORESIS AND IN SITU SOIL SOLUTION EXTRACTION 88
Abstract 88
5.1 Introduction 88
5.2 Principle and Design 92
5.2.1 Principle 92
5.2.2 Electrophoretic Microchip 93
5.2.3 Fabrication Process 94
5.2.4 Programmable High-Voltage Power Supply Unit 95
5.2.5 Conductivity detection unit 96
5.2.6 Soil solution extraction 98
5.3 Electrophoretic Chip Testing 100
5.4 Results and Discussion 101
5.4.1 Separation of ions 101
5.4.2 Sensitivity and detection-limit from single ion detection 102
5.4.3 Soil solution testing 104
5.5 Integration System (not part of the IEEE Sensors paper) 108
5.6 Conclusion 108
References 109
CHAPTER 6. CONCLUSIONS 113

NOMENCLATURE

P.sojae	Phytophthora sojae
CO_2	Carbon Dioxide
FEA	Finite Element Analysis
PDMS	Polydimethylsiloxane
DI	Deionized
IBA	Isobornyl Acrylate
PMMA	Poly(methyl methacrylate)
TWh	Terawatt-hours
GW	gigawatt
AH	Absolute humidity
RH	Relative humidity
MEMS	Microelectromechanical systems
PBR	Photobioreactor
LED	Light-emitting diode
ISE	Ion-selective electrode
IC	Ion chromatography
NO_3^-	Nitrate ion
NH_4^+	Ammonium ion
PO_4^{3-}	Phosphate
MCC	Microfluidic cell culture
RuBisCo	Ribulose-1,5-bisphosphate carboxylase-oxygenase
TLI	Transmitted light intensity

GSV	Grayscale value
C.	Chlamydomonas
TAP	Tris-acetate-phosphate
SPME	Solid-phase microextraction
EOF	Electro-osmotic flow
C4D	Capacitively coupled conductivity detection
MES	2-[N-Morpholino] ethanesulfonic acid
HIS	Histidine
DI	Deionized
LOD	Limit of detection
DNA	Deoxyribonucleic acid

ACKNOWLEDGMENTS

This dissertation summarizes the research work during my Ph.D. program in Iowa State University. I appreciate all the help from all the people who guided and supported me during this period.

First, I would like to thank my committee chair and major professor, Dr. Liang Dong. Thanks for his support and patient guidance. Here, I want to thank Dr. Ratnesh Kumar for his support and instruction. I also want to thank my committee members, Dr. Robert J Weber, Dr. Michael Castellano, and Dr. Fernando Miguez, for their guidance and instruction throughout the whole process of this research. Here, I specially want to express my sincere appreciation to Dr. Ashfaq A. Khokhar for his great help and support during the last year of my PhD study.

Second, I want to express my gratitude for Dr. Yinjun Wang, Dr. Dan Stessman, Dr. Martin H Spalding, Dr. Binod B Sahu, Dr. Prashant Singh, and Dr. Madan K. Bhattacharyya for the collaboration on the humidity array and microalgae projects and providing helpful discussions. I want to offer my appreciation and thanks to my colleagues in Laboratory for MEMS & Lab-Chips: Depeng Mao, Huawei Jiang, Jikang Qu, Peng Liu, Qiugu Wang, Seval Yavas, Shawana Tabassum, Xuan Qiao, Xinran Wang, Yifei Wang, Yuncong Chen, and Yueyi Jiao.

The research presented in the thesis was supported in part by the U.S. National Science Foundation under Grant Nos. CCF-1331390, IIP-1602089, DBI-1352819, IOS-1650182, United States Department of Agriculture's National Institute of Food and Agriculture program under Grant No. 2013-68004-20374, and Iowa State University’s the Crop Bioengineering Consortium.

In addition, I want to express my gratitude for my parents who always are my strong backing no matter what kind of difficulties I come across.

ABSTRACT

In the past decade, there are significant challenges in agriculture because of the rapidly growing global population. Meanwhile, microfluidic devices or lab-on-a-chip devices, which are a set of micro-structure etch or molded into glass, silicon wafer, PDMS, or other materials, have been rapidly developed to achieve features, such as mix, separate, sort, sense, and control biochemical environment. The advantages of microfluidic technologies include high-throughput, low cost, precision control, and high sensitive. In particular, they have offered promising potential for applications in medical diagnosis, drug discovery, and gene sequencing. However, the potential of microfluidic technologies for application in agriculture is far from being developed. This thesis focuses on application of microfluidic technologies in agriculture. In this thesis, three different types of microfluidic systems were developed to present three approaches in agriculture investigation.

Firstly, this report a high throughput approach to build a steady-state discrete relative humidity gradient using a modified multi-well plate. The customized device was applied to generate a set of humidity conditions to study the plant-pathogen interaction for two types of soybean beans, Williams and Williams 82.

Next, a microfluidic microalgal bioreactor is presented to culture and screen microalgae strains growth under a set of CO_2 concentration conditions. C. reinhardtii strains CC620 were cultured and screened in the customized bioreactor to validate the workability of the system. Growth rates of the cultured strain cells were analyzed under different CO_2 concentrations. In addition, a multi-well-plate-based microalgal bioreactor array was also developed to do long-term culturing and screening. This work showed a promising microfluidic bioreactor for in-line screening based on microalgal culture under different CO_2 concentrations.

Finally, this report presents a microchip sensor system for ions separation and detection basing electrophoresis. It is a system owning high potential in various ions concentration analysis with high specificity and sensitivity. In addition, a solution sampling system was developed to extract solution from soil.

All those presented technologies not only have advantages including high-throughput, low cost, and high sensitive, but also have good extensibility and robustness. With simple modification, those technologies can be expanded to different application areas due to experimental purposes. Thus, those presented microfluidic technologies provide new approaches and powerful tools in agriculture investigation. Furthermore, they have great potential to accelerate the development of agriculture.

CHAPTER 1. INTRODUCTION

1.1 Introduction to bioenergy

Energy, which is defined as the property that must be transferred to an object to perform work, or to heat in physical, is indispensable in daily life [1]. The final global energy consumption is 109613 TWh in 2014 [2]. Due to the contradiction between development requirement and limited energy resource, people gradually turn their attention to renewable resource, such as solar, wind, tides, hydroelectric power, and geothermal heat [3]. Renewable energy, which is collected from renewable resource, contributed 19.3% to human's global energy consumption in 2015 as shown in Fig. 1.1. Bioenergy, one of most important renewable energy made from biomass through thermochemical or biology process, becomes more and more favored worldwide.

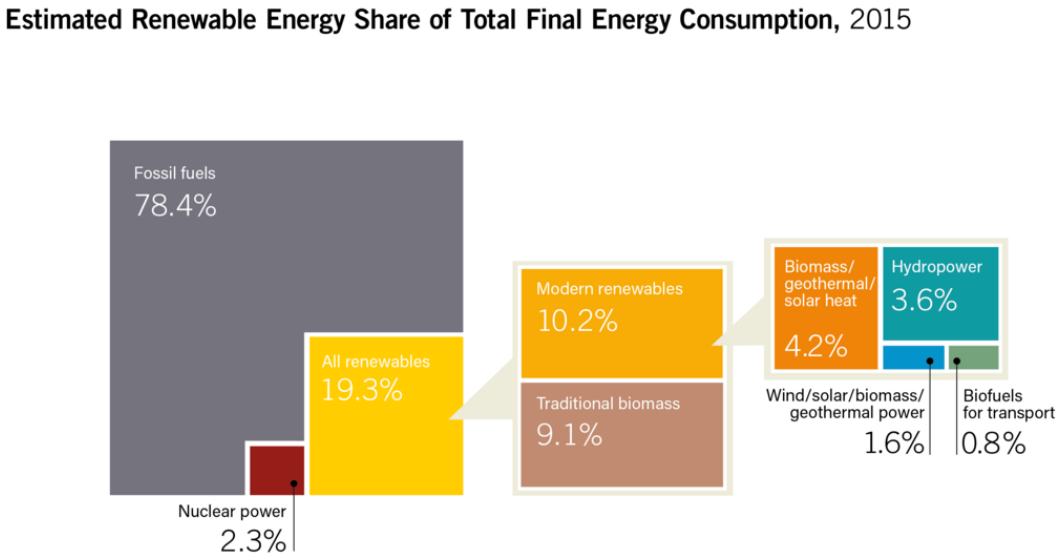

Figure 1.1 *Consumption of Renewable Energy Percentage of Total Final Energy in 2015 [4].*

1.1.1 Biofuel and biofuel generation

Different from traditional fossil fuels that produced by geological processes from prehistoric biological matter, biofuel is a fuel that made through conversion of biomass or contemporary carbon fixation, such as photosynthesis. Biofuel can be in solid, liquid, or gas form. Bioethanol and biodiesel are two most common biofuel products. Bioethanol is widely used as a gasoline additive and biodiesel is used as diesel additive [7]. With development of biofuel, it is divided into three generations as shown in Fig. 1.2. First-generation biofuels are those biofuels made from food crops grown on arable land. Productions from food crops [8], such as sugar [9], cellulose, and vegetable oil, can be converted into bioethanol or biodiesel via transesterification, or yeast fermentation. Second-generation biofuels are extracted from materials that derived from feedstock of lignocellulosic, non-food materials and special grown energy crops [10, 11]. Lots of research work was taken to maximize production from renewable carbon and hydrogen sources. Third-generation biofuels are extended to algal biomass production to remove non-fuel component and reduce production costs [12, 13]. Recently, a new generation biofuel, the four generation biofuels, was proposed. The four-generation biofuels are focus on photobiological solar fuels and electro-fuels. It is a technology that can convert solar energy or electric energy into fuel by new synthetic biology method [14].

1.2 Introduction to soybean, Phytophthora sojae, and humidity

As an important source for biomass, agricultural crops and its residues catch enough attention. In United States, several crops are specifically being grown and harvested for biofuel production. Soybean, which is only listed after corn, is the second most important row crop in United States.

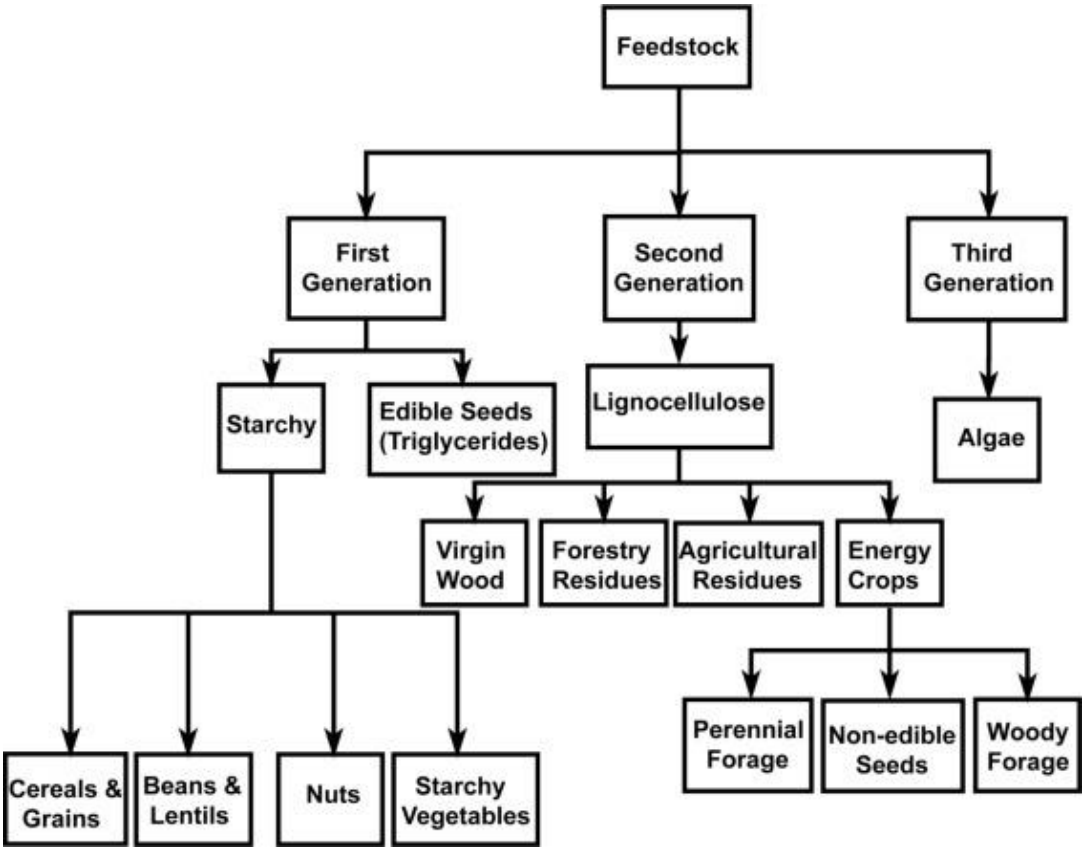

Figure 1.2 *Three generations feedstock classification. [15] Reprinted with permission from Elsevier.*

1.2.1 Phytophthora sojae

Due to Wrather's report on 2006, various diseases lead to over 2.6 billion dollars' losses in field every year. Specially, Phytophthora sojae (P. sojae), which a wide spread pathogen present in all soybean production areas, causes around 0.3 billion dollars' losses [16]. P. sojae is an oomycete and a soil-borne pathogen. Specially, it has a parasitic relationship with soybean. P. sojae usually infects seeds, root, and stem causing rot under favorable environment condition. Once infecting P. sojae, the root and stem will turn brown and some other symptoms will also be displayed, including chlorosis of leaves. (Fig. 1.3). In the past over decades, soybean-P. sojae interaction, a classical model plant-pathogen interaction, has been widely studied because of the economic loss causing by the disease. Currently, the primary method of control for P.sojae is host resistance, including R-gene

mediated resistance, root resistance, and partial resistance [17]. Different single-resistance genes (Rps genes) have been identified and utilized to study R-gene mediated resistance approach [18]. Of these, the Rps1-k locus was cloned and introduced to overcome the oomycete pathogen. Furthermore, only not gene, but also environmental conditions, such as temperature, light density, supplication of nitrogen, moisture, greatly influenced the expression of plant disease. High-throughput phenotyping tools that studying interaction between plants and biological species under different environment conditions are rarely achieved.

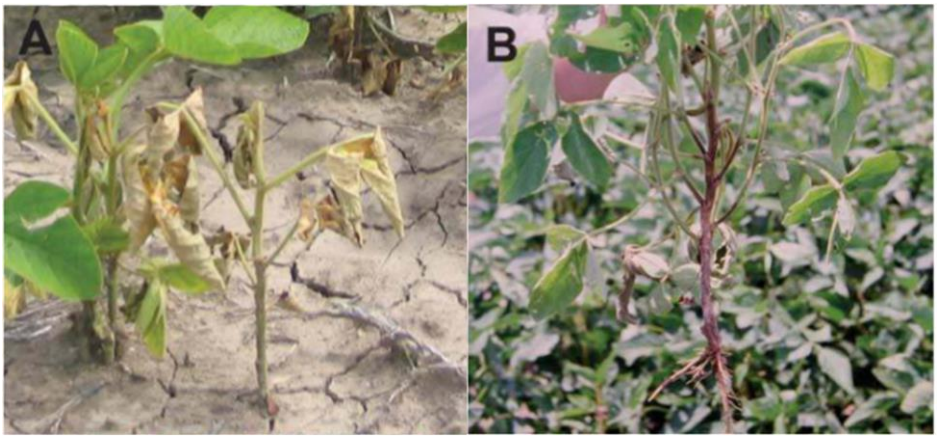

Figure 1.3 *Disease symptoms of Phytophthora sojae on soybean. (A) Seedlings' damping off. (B) Stem rot. Pictures courtesy of Anne Dorrance, Ohio State University. [19]. Reprinted with permission from John Wiley and Sons*

1.2.2 Humidity

Humidity presents the mass of water vapour in the air. Absolute humidity is the ratio of total mass of water vapour to a certain volume of air, which can be expressed as:

$$\mathrm{AH} = \frac{m_{\mathrm{H_2O}}}{V_{net}} \tag{1-1}$$

Where AH, $m_{\mathrm{H_2O}}$, and V_{net} are absolute humidity, mass of water vapor, and volume of the air including water vapor [27]. The absolute humidity varies with by temperature and pressure. Relative humidity, which means the partial pressure of water vapor in the equilibrium vapor

pressure of water at a given temperature, is a more common concept used to represent moisture level in air in weather forecasts and reports. It is represented as:

$$\mathrm{RH} = \frac{p_{\mathrm{H_2O}}}{p^*_{\mathrm{H_2O}}} \tag{1-2}$$

Where RH, $p_{\mathrm{H_2O}}$, and $p^*_{\mathrm{H_2O}}$ are relative humidity, partial pressure of water vapor, and equilibrium vapor pressure of water [28]. Relative humidity is valued as a percentage generally. A high relative humidity means a moisture environment at a given temperature.

Plant phenotypes are the result of interaction between plant genotype and environment. Various environmental condition, such as light, temperature, nutrient, oxygen, and so on, influence plant diseases. Among these environmental factors, RH plays an important role in disease infection. To our interest, the mechanism between RH and expression of the soybean-P. sojae interaction is unclear.

1.2.3 State-of-art controlled humidity technology

Due to the importance of humidity in plant growth, controlled humidity environment approaches have good potential in agriculture research [29-31]. Traditional controlled humidity systems are usually built in greenhouse and large-scale growth chamber. A well-established humidity system requires sensors, controlled water circulatory system, and air circulatory system, to achieve and to maintain a specified humidity level [32, 33]. A simple commercial air humidity-regulating controllable plant growth chamber is obtained by the combination of humidifiers and dehumidifiers with temperature-humidity sensors [34]. However, those technology-based greenhouse and growth chambers are limited in providing one specified humidity. Disadvantages as insufficient flexibility and low accuracy are displayed when using those greenhouse or growth chambers to create a large number of variable humidity levels, which increasing cost and affecting throughput of various humidity

research.

Recently, many applications focusing high-throughput arrays have been implemented. For instance, researchers have used developed microelectromechanical systems (MEMS) technology to generate stable and precise soluble gradients of biochemicals in a high-throughput way [35, 36]. Once molecular concentration gradients are built in the system, the system could be used to study cell migration [37], cancer chemotaxis [38], bacteria growth [39], and optimization of reaction conditions [40] in cell biology research.

1.2.3.1 Greenhouse controlled humidity technology

Greenhouses are the most common technology using for controlling the growing environment of plants. Current greenhouse technology already achieved accurate control of humidity, temperature, light, CO_2, and other environment factors in a closed system. In a greenhouse system, researcher can optimize growth environment for plant growth while preventing waste of energy, water, and nutrients.

Figure 1.4 shows an automatic greenhouse system developed to grow plant. The greenhouse consists of a controller, a RH and temperature sensor, an injection system, an air conditioner a water filter system and a dehumidifier system. The system is built based on control-feedback mechanism. The controller allows user to set required parameters. For example, RH and temperature can be set as 60% at 25 Celsius degree. Once the parameters are confirmed, the greenhouse system starts to run through feedback loops: the temperature and humidity sensor obtains temperature and humidity, sets datas to processer; processer compares the temperature and humidity with the upper and lower limits that have been set and command controller to take correspond action.

Figure 1.4 *Custom design of a humidifier system for a greenhouse [41].*

1.2.3.2 In-laboratory large-scale controlled humidity technology

Greenhouse controlled humidity technology is regards as the most reliable approach to obtain certain humidity for plant growth. But, in-laboratory facilities are still required for studying the performance of plant in an accurately controlled humidity environment. Plant growth chambers, cultivation rooms have emerged as the most widely used tool for comparing hundreds of plants in a given condition.

Plant growth chambers provide precise controls of environment parameters, such as temperature, humidity, and light cycle, to simulate natural plant growth status in experimental plant science research [42]. Since plant growth chamber provide complete control of the environment inside the chamber, researcher can study the effect of different environment factors on plant growth in isolate system. Weiss Technik has developed unsurpassed accurate and reliable plant growth chambers which controls temperature, humidity and lighting (Figure 1.5).

The traditional in-laboratory plant growth chambers, however, suffer from high cost of instruments because of large amounts of experiment requirement base on relatively complicate environment factors for plant growth. And also, the chamber size limits the mobility of the system.

Figure 1.5 *Fitotron® SGC 120 Plant growth chamber [43].*

1.2.3.3 On-chip controlled humidity technology

Recently, microfluidics, as a rapid developed technology in last decade, has been widely used in many field. Microfluidics have several advantages, including micron scale channel matching size of cell, relative independent culture environment in multi channels, fast mass transfer and heat transfer, and parallel experiments [44]. Therefore, it has a great potential to generate controllable molecular concentration gradients in a rapid way. Many microfluidic devices or systems have been developed to achieve real-time screening of the behaviour or responses of various cells or seeds under multiple environment factors [45, 46].

Microfluidic gradient generation methods can be classified into four types: convection mixing-based method [35], laminar flow diffusion-based method [47], static diffusion-based method [48], and geometric metring mixing-based method [44], as shown in Fig 1.6. The gradient generators have been proved as a good platform for biology research.

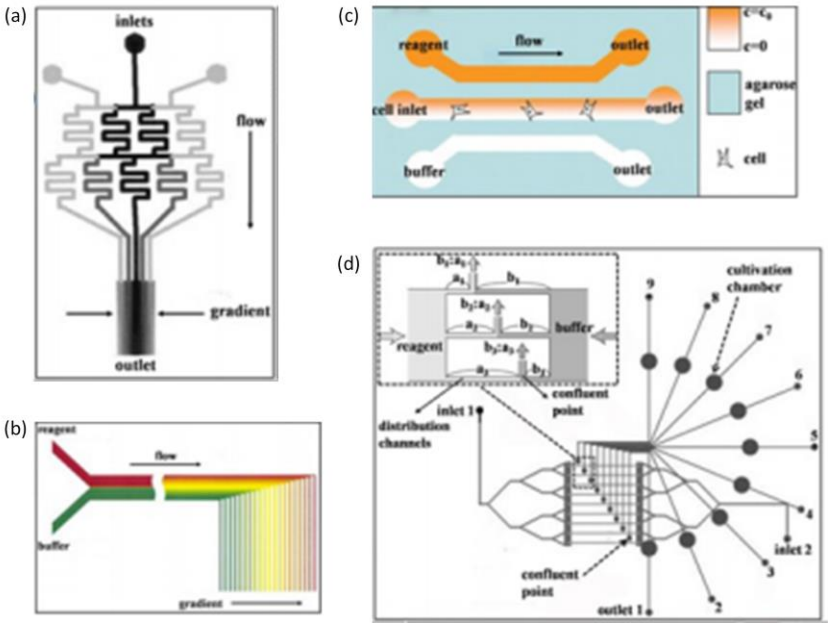

Figure 1.6 *Gradient generator based on different method (a) Convection mixing-based method. (b) Laminar flow diffusion-based method. (c) Static diffusion-based method. (d) Geometric metering mixing-based method [44]. Reprinted with permission from Elsevier*

Due to its simple channel structure, laminar flow diffusion-based system is the most widely used gradient generation platform. Recently, a set of microfluidic devices have been developed to generate concentration gradients using laminar flow diffusion-based methods [36, 49-52]. This method can manipulate chemical concentrations at a small scale, thus accelerating biology investigation [35, 53-58]. However, it is always required an external pumping system to build varying concentrations using the laminar flow diffusion-based method. Another approach is using free-diffusion process to build concentration gradients between two sources due to concentration difference. But a drawback of the method is hard to maintain a long-time concentration gradient [59, 60]. In Figure 1.7, Kang et al. presented

an approach using a convective-diffusive balance to generate concentration gradients along the direction of flow [61]. Taking advantage of fast mass diffusion in small scale device, the controllable concentration gradients can be established in less than one minute. In Figure 1.8, Du et al. used the combination of convection and diffusion to establish controllable concentration gradients of molecules in a microfluidic device in a rapid way [62]. Here, a passive pump is required to induce forward flow. And this simple and rapid approach generate a high-throughput platform to test response of cells in a gradient of a cardiac toxin concentration.

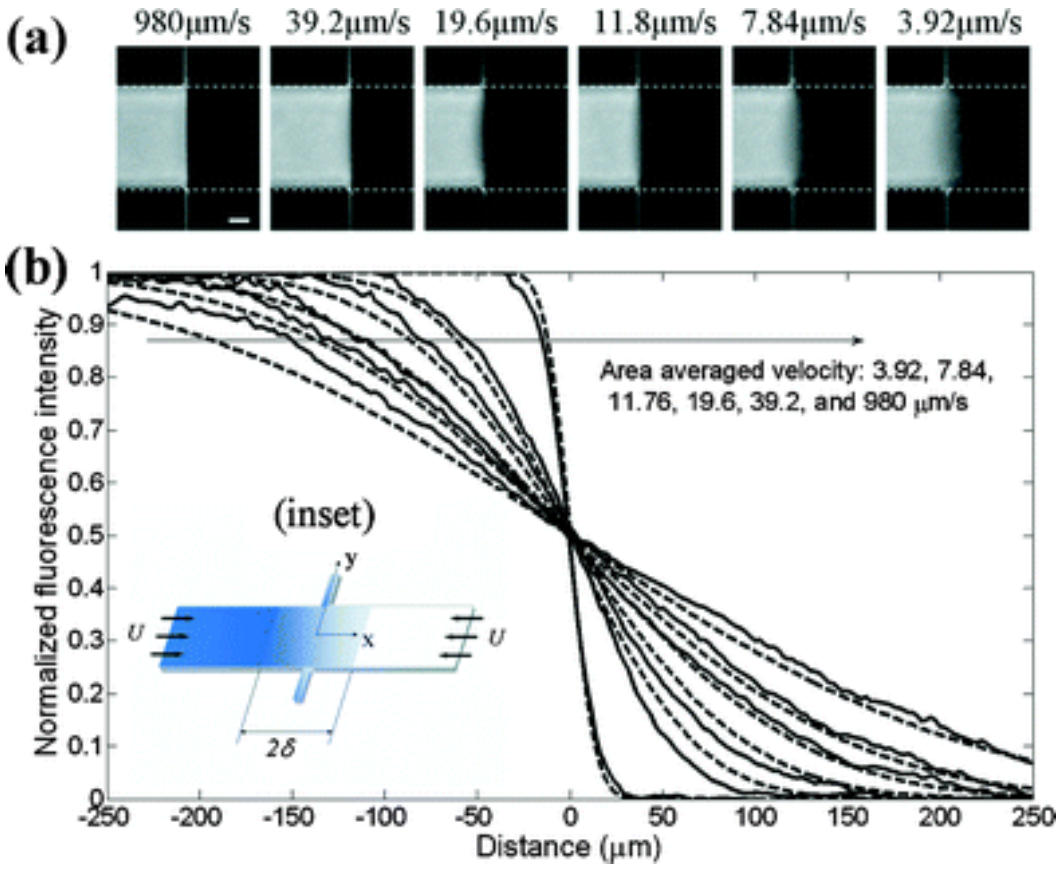

Figure 1.7 *(a) Rhodamine 6G fluorescence images of six different convective velocities. The scale bar is 200 μm. (b) Comparison of concentration gradient between the experimental data (solid lines) and the theoretical data (dashed lines).[61]. Reprinted with permission from RSC.*

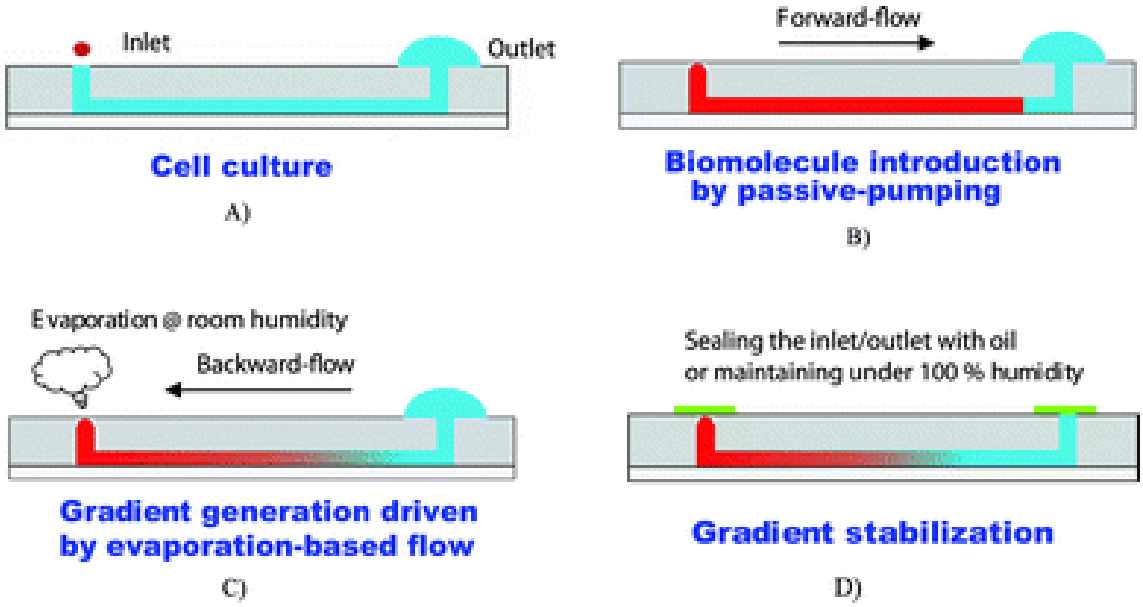

Figure 1.8 *Schematic of the gradient generation and stabilization process: A) filling the Microfluidic channel with culture medium initially, with a large droplet on the outlet and a small drop on the inlet; B) pumping a forward flow using a passive pump; C) generating a concentration gradient of molecules via the evaporation-based backward flow; D) stabilizing the gradient by stopping the evaporation. [62] Reprinted with permission from RSC.*

1.3 Microalgae and algal cell culture

1.3.1 Biomass

Biomass is an organic renewable energy source derived from living organisms [5]. Different from other natural resources such as petroleum, coal, and nuclear fuel, biomass is based on the carbon cycle. The sources for biomass can be classified as six types: forestry crops, agricultural crops, sewage, industry residues, animal residues, and municipal solid waste, as shown in Fig. 1.9. Biomass can be used as energy source in both directly and indirectly ways. One way to use is directly combusting to product heat. Another way is applying thermal, chemical, or biochemical method to convert biomass to various forms of biofuel, such as methane gas, ethanol, and biodiesel, for further use.

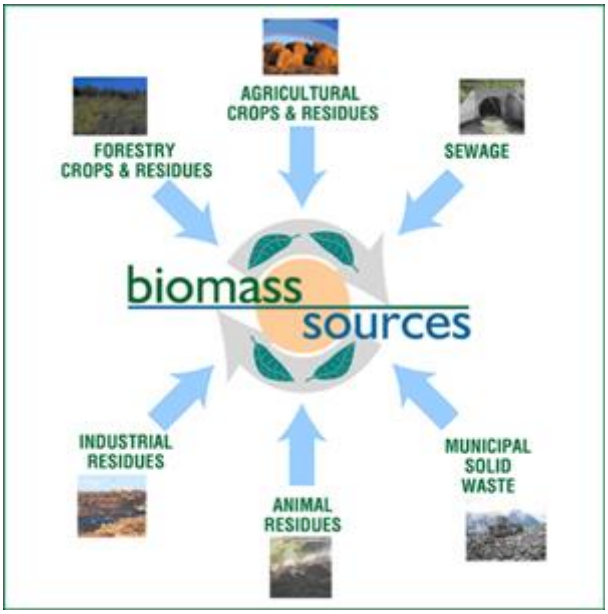

Figure 1.9 *Biomass sources [6].*

1.3.2 Microalgae

Microalgae, one of the oldest living microbes on the earth, have more than 300000 species [20]. Among those species, the size of microalgae is between a few micrometers and hundreds of micrometers. Microalgae plays an important role in the earth ecosystem as the capable of performing photosynthesis. Similar as higher plant, microalgae produce oxygen and use carbon dioxide simultaneously through photosynthesis process. Nearly 50 percent of atmospheric oxygen is produced by microalgae [21]. Comparing energy crops, microalgae have many advantages. First, microalgae are more tolerant to environment factors, including temperature, pH and CO_2 concentration, which make algae cell reserve more lipids [24]. Lipids can be converted to oil production, such as biodiesel. Second, because of the simple structure of cells, microalgae can convert solar energy more efficiently [22, 23]. And microalgae can absorb water, CO_2, and other nutrients in a more efficient way due to the aqueous environment. Third, microalgae have a shorter growth cycle and their biodiesel production can be 15-300 times higher than crops on an area basis [25]. Forth, microalgae

can growth on nonagricultural soil using wastewater, which can save huge volume of drink water. Therefore, microalgae have the potential to be a powerful source of renewable bioenergy. A brief algal biofuel pipeline shows the processes from microalgae to biodiesel in Figure 1.10.

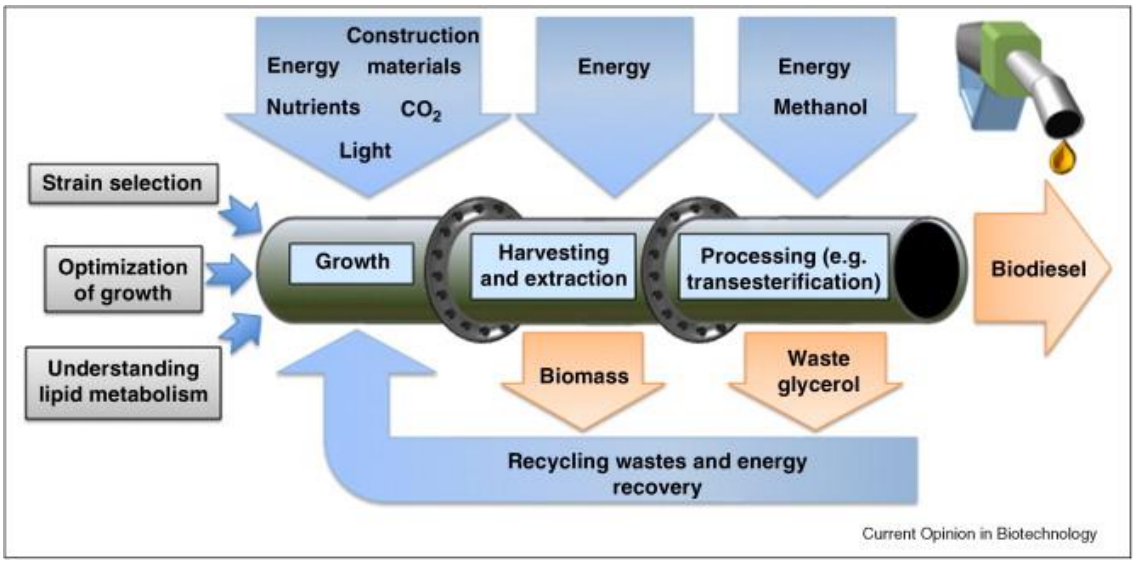

Figure 1.10 *Algal biofuel pipeline, showing the processes from microalgae to biodiesel [26]. Reprinted with permission from Elsevier.*

1.3.3 State-of-art microalgae cultivation technology

Microalgae cultivation system is a system designed around the algae strain to be grown. Because of the great potential as a source of biorenewable energy fuel, researchers are working on develop better microalgae strains and better culturing approaches through genetic and bioprocess engineering to increase production of microalgal oil. A number of algae cultivation technologies have been developed or under development to maximize algae growth for fuel production [63-66]. Traditionally, microalgal cells are cultured in large-scale systems. The system can be either open pond [64] or closed [66]. Both two types of system have its own advantages and disadvantages. And Those cultivation systems are widely used in research and commercial production. Recently, with rapid development of MEMS system,

several microfluidic devices were developed to grow microalgal cells [67], examine their lipid production [68], and test toxin response to different environment conditions [69]. These studies have shown great promise of applying microfluidic technology to culture and analyse microalgal cells in microalgae research.

1.3.3.1 Open pond microalgae cultivation technology

Open ponds system and closed photobioreactors (PBRs) are two most common large-scale microalgae cultivation systems. Open pond systems are the first and most studied approach for microalgae cultivation. There are several existed open pond systems and raceway ponds is the most widely used open pond microalgae cultivation system [70]. Open pond microalgae cultivation systems are good for mass cultivation of algae with relatively low cost and easily cleaning [73]. Among those systems, the paddle-wheel raceway pond is the most popular one because of its highest productive. Raceway pond cultivation system consists of paddle wheel, water and nutrient inlet, CO_2 bubblers, baffle, light source, and vortex generator (in Figure 1.11 and Figure 1.12(a)). The raceway pond system has an extremely low cost with a simple structure to construct, which make it the most economical microalgae cultivation system [24].

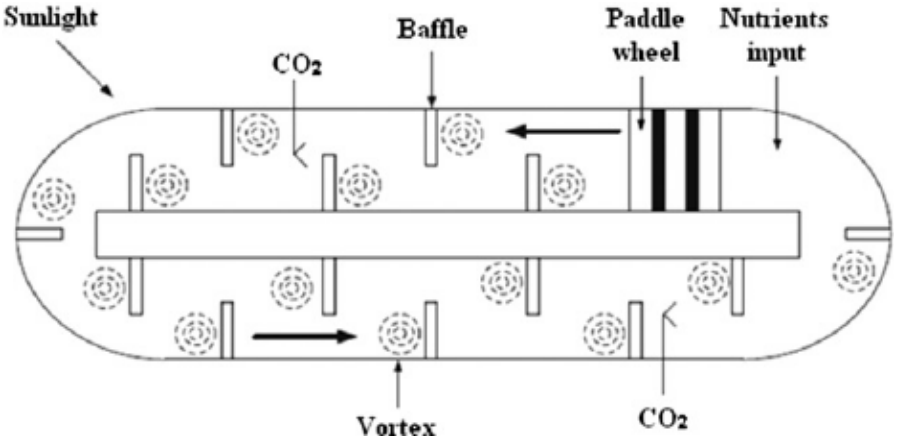

Figure 1.11 *Conceptual open raceway pond to culture microalgae [71]. Reprinted with permission from Elsevier*

Figure 1.12 *Large-scale PBRs (a) raceway pond, (b) flat-plate PBRs, (c) tubular type PBRs, (d) horizontal type PBRs and (e) Vectical column type PBRs [72]. Reprinted with permission from Elsevier.*

1.3.3.2 Photobioreactor

Due to the drawbacks of open pond microalgae cultivation systems in research, such as unevenly control of culture conditions, limited in short-term cell culture, low efficiency, requirement of large mass land, easily contaminated [73], most of the microalgae research uses PBRs instead of open ponds systems. A PBR is a close cultivation system that simulates growth environment for microbes. It contains solar light, or artefact light, energy, heat, CO_2 and nutrient. Obviously, as a closed cultivation system, PBRs eliminate the risk of contamination and have a better control of the conditions for microalgae growth. With a more precise control of culture environment, PBRs are efficient in increasing productivity.

Among various of closed microalgae cultivation systems, flat-plate, tubular, vertical-column and internally-illuminated PBRs are four most common one. As shown in Figure 1.12(b), flat-plate PBRs take advantage of large illumination surface area to maximize the utilization of solar light energy [73]. High photosynthetic efficiencies can be achieved in flat-plate PBRs. There are also some limitation of flat-plate PBRs. The most obvious one is

culture temperature are hard to control in flat-plate PBRs. Tubular PBRs is another suitable closed cultivation system for outdoor algae mass cultures [73]. Tubular PBRs are usually made by glass or plastic and external air pump or airlift system is implemented to recirculate cultures (in Figure 1.12(c)). Tubular PBRs also utilize large illumination surface area to achieve good biomass productivity but have poor mass transfer and difficulty in culture temperature control [74-76]. Vertical-column PBRs, containing many vertical tubes that are lined up, are another type of PBRs using airlift system. Comparing other types of PBRs, Vertical-column PBRs are relatively low-cost PBRs for easy operation (in Figure 1.12(e)). They are especially good for culturing immobilization of algae. However, the cost is still high in construction materials [77]. Most of PBRs are take solar light or external artefact light as energy source. Internally-illuminated PBRs are a type of PBRs that have internal light system, which makes the system can utilize both solar and artificial light source [79]. The design can provide continuously light source and maximize biomass productivity.

1.3.3.3 In-laboratory microalgae cultivation technology

Large-scale microalgae cultivation is regard as the most widely used technology to culturing and harvest biomass from microalgae. But, the study of characterization of microalgae is necessary to build small scale culture systems with in-laboratory facility. Current in-laboratory microalgae studies are conducted by culturing microalgal cells in flasks, dishes, multi-well plates [80], and small-scale photobioreactors [81, 82]. Laboratory-scale PBR, which is the most widely used approach in man biotechnological research and production facilities, is designed based on the traditional glass fermenters. Similarly, a laboratory-scale PBR consists of a standard glass vessel, an external light source, head nozzles integrated with sensor for gas exchange (in Figure 1.13). The designed PBR simulates natural growth environment for microalgal cells by providing suitable conditions

for photosynthesis. Photon Systems Inc. developed a computer-controlled monitoring cultivation instrument for growth of algae. The instrument consists of cultivation vessel, light source, optical sensor, bubble humidifier, air pump, and bubble interruption valve. The system achieves precise control of light, temperature, gas and medium regime through connected computer (in Figure 1.14).

Those developed in-laboratory cultivation technologies have made great contribution to understanding the effects of various culture factors, such as light, temperature, CO_2, pH, nutrient, on microalgae growth. However, considering the numerous microalgal strains and combinatorial nature of many culture factors, high throughput approaches that screening and tracking algae growth responding is still required.

Figure 1.13 *Microalgae photobioreactor to cultivate microalgae at laboratory scales [83].*

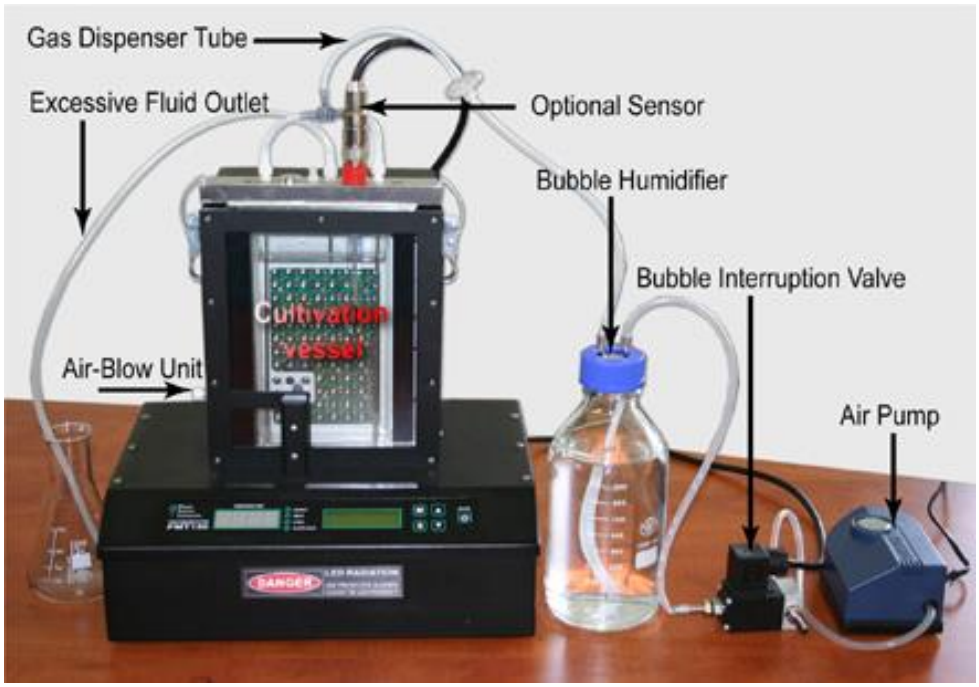

Figure 1.14 *Photobioreactor FMT 150, Photon Systems Inc. [84].*

1.3.3.4 On-chip microalgae cultivation technology

Recently, microfluidic has been widely researched and applied to enable to study biochemical process in miniaturized and integrated devices automatically and concurrently [85, 86]. Using various microfluidic device for cell culture is becoming increasingly common in cell biology study. Recently, many microfluidics-based platforms have been developed for cell culturing, manipulation, and detection in high-throughput bioassays [87-89]. Specially, several microfluidic devices were developed to culture microaglal cells, examine lipid production and response to different environment conditions [63, 67, 68, 90-93]. Kim et al. (shown in Figure 1.15) devised microfluidic PBRs to screen microalgal oil production under different light conditions [94]. They achieved 64 different light conditions in a microfluidic PBR array and applied the PBR array to study algal growth and oil production under different light conditions. Compared to traditional convectional flask-scale PBRs, Kim's device has 250 times higher throughput. Zheng et al. (shown in Figure 1.16) developed a

microfluidic device using microalgal cells to test toxicity of many chemicals [69]. In Zheng's design, the cultivation system consists of a concentration gradient generator (CCG), a diffusible culturing module, and a valve system. Marine microalgal cells were cultured for toxicity testing and screening on the developed platform. Dewan et al. (shown in Figure 1.17) generated immobilized arrays of microfluidic drops to investigate growth kinetics of microalgae [95]. In Dewan's system, single microalgal cell was trapped, cultured, observed, measured in a nanolitre-scale droplet and compared with other cells in the array. Furthermore, the culture system can be maintained for long-term experiments by controlling the permeation of water in and out of the device. Those studies have shown great promise of microfluidic technology in microalgae research.

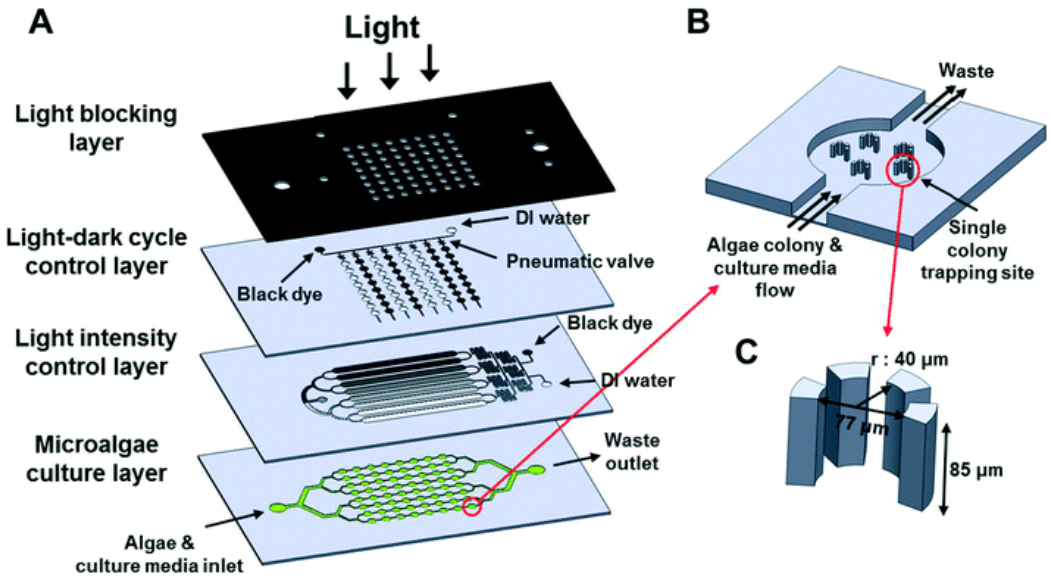

Figure 1.15 *Schematic of the microfluidic microalgal photobioreactor array for high-throughput culture. (A) Schematic of the four-layer platform– a light blocking layer, a microfluidic light–dark cycle control layer, a microfluidic light intensity control layer, and a microalgae culture layer. (B) Schematic of a single culture unit with five single-colony trapping sites. (C) Schematic of a single-colony trapping site having four micropillars. [94] Reprinted with permission from RSC.*

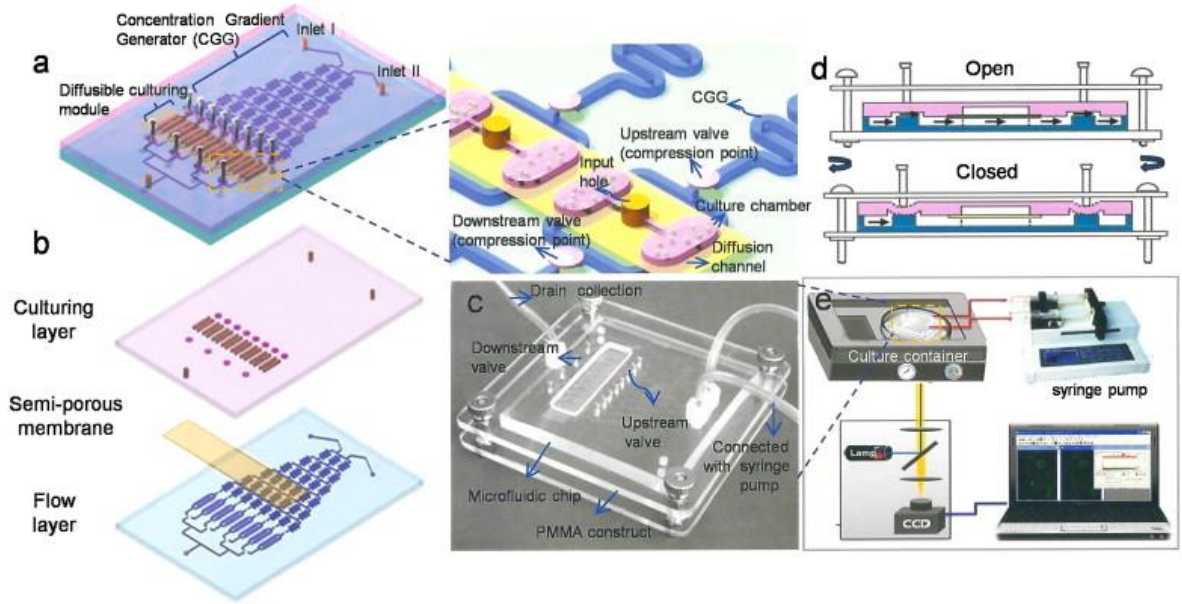

Figure 1.16 *Schematic and photograph of the microfluidic device (a) Schematic of the multiple layers structure. (b) Three layers of the microfluidic microchip device-culturing layer, semi-porous membrane and the flow layer. (c) Photograph of the fabricated microfluidic device. (d) Crossing view of valve operation. (e) Schematic of the microfluidic device based system for toxicity assessment [69]. Reprinted with permission from Elsevier.*

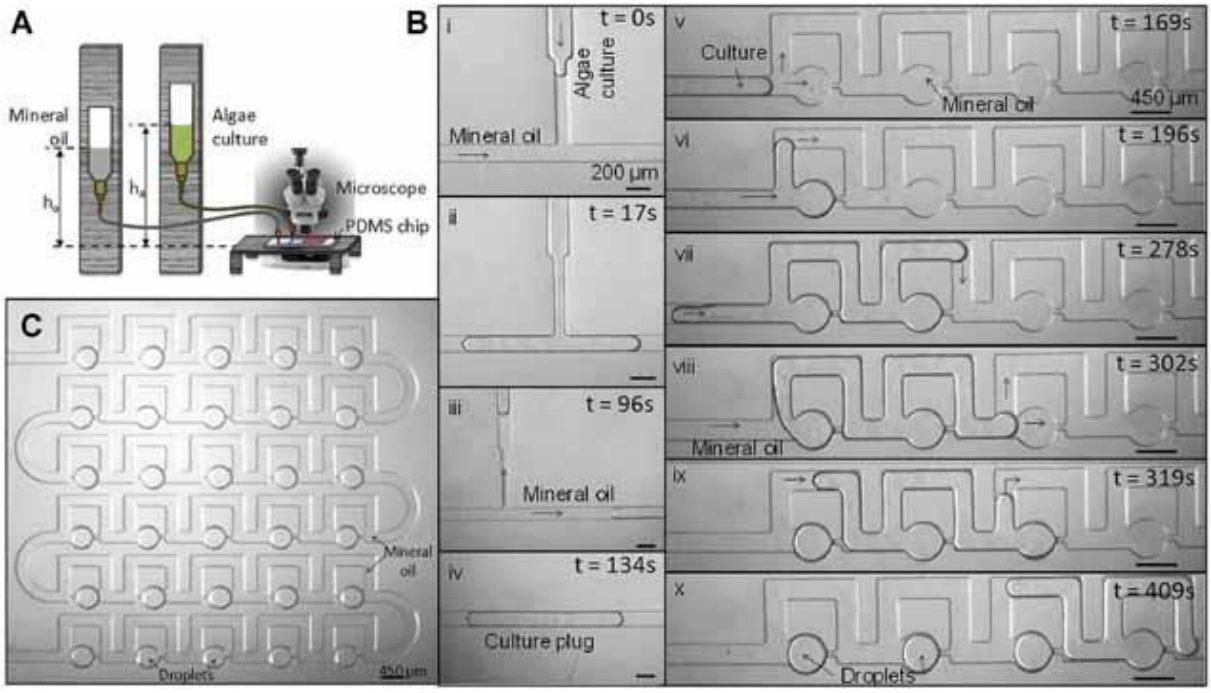

Figure 1.17 *Droplet trapping system : (A) schematic of the experimental setup, (B) time-stamped images showing the formation of single algae culture plug (i–iv) and droplet arrays (v–x), and (C) the microchip with a matrix of 30 trapped droplets. [95]. Reprinted with permission from Elsevier.*

1.4 Soil nutrient sensor

As a major component of the Earth's ecosystem, soil acts as a medium for plant growth. It also plays a key role in the nutrients recycling system. Since sustainable agriculture is garnering increasing support and acceptance, environment health, especially soil health, becomes important for optimizing agriculture production and minimizing environmental cost. Soil nutrient sensors, which are developed to achieve soil health monitoring, plays an expedient role in modern agriculture.

1.4.1 Soil health

Soil health is used to value the capacity of soil to maintain the quality of a living ecosystem [96]. Assessing soil health is a complicate process since the need to consider not only integrating physical, chemical, and biological properties, but also its utility to humans and efficiency of resource use. There are lots of parameters that indicate health status of soil, including moisture, salinity, pH, forms of N, and available nutrients [96]. Among those parameters, soil nutrient, which indicates capacity to support crop growth and environment hazard [96], is of great societal interest.

Nitrogen (N) is one of the vital elements for plant. Nitrogen is not only an essential element of plant proteins, but also a component of DNA. It is indispensable for plant structures and metabolic process. Besides, nitrogen also plays a key role in photosynthesis of plant. With sufficient Nitrogen, plants stay in high rates of photosynthesis and exhibit vigorous growth. When the supply of Nitrogen is insufficient, plant, including flowering and fruiting, will be severely disordered. However, plants cannot take nitrogen directly from atmosphere and soil. Instead, plants absorb nitrogen forms, including ammonium and nitrate, from soil. Thus, concentrations of nitrate and ammonium are an important standard for accessing soil health.

1.4.2 State-of-art soil nutrient sensor

To maintain good soil status, to optimize the amount of fertilizer, to increase crop production, it is important to monitor the concentration of soil nutrients [97]. Therefore, soil nutrient sensors, which realize in-situ measurement of nutrient in soil, play a key role in soil nutrient management [98, 99]. Over the past two decades, different types of soil sensors have been developed for measuring soil properties, including soil moisture [100], pH [101], temperature [102], heavy metal [103], and nutrients [104]. A variety of devices based on different principles, including electrical [105], electromagnetic [106], optical [107], radiometric [108], mechanical [109], acoustic [110], and electrochemical [111], were applied in soil nutrient sensing. Among those developed technologies, ion chromatography (IC) [112], spectrophotometry [113], electrochemical [114], and ion-selective electrodes (ISEs), are mostly widely used technologies to detect soil's nutrient ions in practices. Compared to other two approaches, IC and spectrophotometry-based systems have higher precision in measurement. However, they are limited to laboratory application without the ability to realize in-situ measurement. ISE-based sensors, which convert the conductance change of a membrane based on the activity of a selected ion in a solution into an electrical signal, are developed for field deployable soil nutrient sensor. Marx's group developed an approach using ISE based measurement to do quantitative analysis and simultaneously mapping on soil pH, and available sodium contents (in Figure 1.18). But, ISE method relies on specific ion-selective membranes that may not available for many ions, may degrade over time.

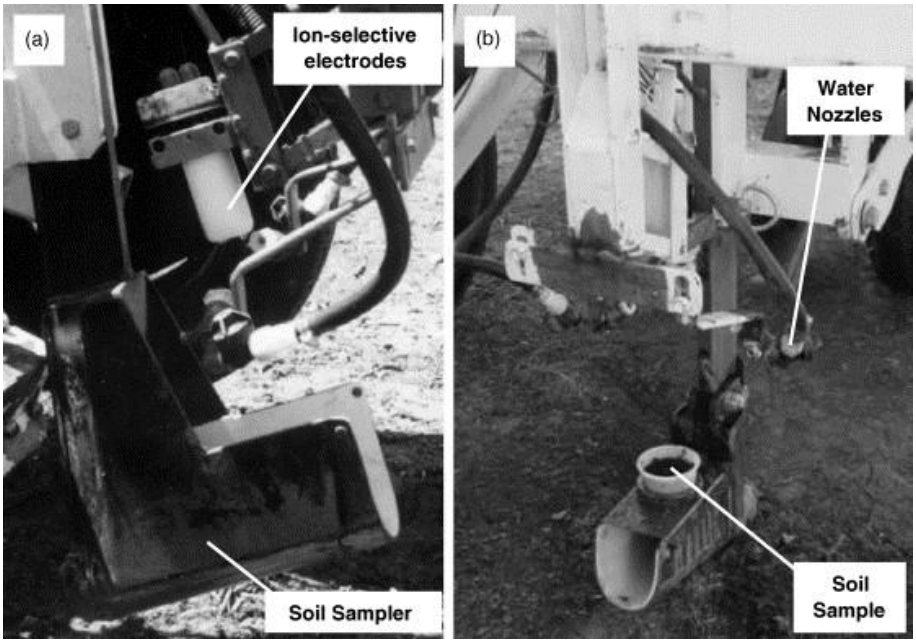

Figure 1.18 *Soil sampler based ISEs (a) mapping soil pH, (b) laboratory experiment. [115]. Reprinted with permission from Elsevier.*

1.4.2.1 Coaxial impedance dielectric reflectometry method

The coaxial impedance dielectric reflectometry method, which was developed by the physics department at Dartmouth College, is based on Maxwell's equations [126]. The system firstly generates an electromagnetic signal using an oscillator and sends the signal into the soil. Then the sensor detects the amplitude of the reflected signal and delivers the signal to an onboard microcontroller to calculate the impedance based on Maxwell's equations. Later, calculated impendence is converted to soil moisture value. It is a method with high measure accuracy. Furthermore, it can be used for most types of soil without calibration. A company, the HydraProbe, has already developed a commercial sensor based on coaxial impedance dielectric reflectometry method.

1.4.2.2 Atomic absorption spectroscopy

Atomic absorption spectroscopy, which using the absorption of optical radiation by atoms to assess the concentration of analytes, is one of the most widely used an analytical

technique to determine chemical elements in soil [127]. Here, a sample has to be atomized first and then be irradiated by optical radiation. The absorbance of the sample will be detected, analysed, and converted to concentration. It is a high accuracy technique and can be used for analyse over 70 different elements. However, due to the large size of the system, it is limited to laboratory application.

1.4.2.3 Ion sensitive field effect transistor method

Introducing microelectronics technology intro ion selective electrode technology, a new method was developed to analyse soil nutrient based on ion selective field effect transistors [128]. Different from traditional ion selective field effect transistor, the surface of the transistor was modified with an ion selective membrane. When selected ions go through the membrane, it will cause a gate voltage shift and lead to a drain current shift consequently. The sensor has advantages, including miniaturized size, low cost, high sensitivity, and in-soil measurement.

1.4.3 Capillary electrophoresis

Capillary electrophoresis, separating ions based on the difference of electrophoretic motility of ions under an applied electrical field, has been widely used for DNA separation [116], chemical reactions screening [117], biomolecules analysis [118], and clinical diagnostics [119]. A capillary electrophoresis system usually consists of a high-voltage power supply, a sample inject and separate system, a capillary tube, a detector, and a data logger (in Figure 1.19). Optical absorption or fluorescence detectors, allowing for a single-molecular level sensitivity, are the most common signal detectors applying in electrophoresis instruments.

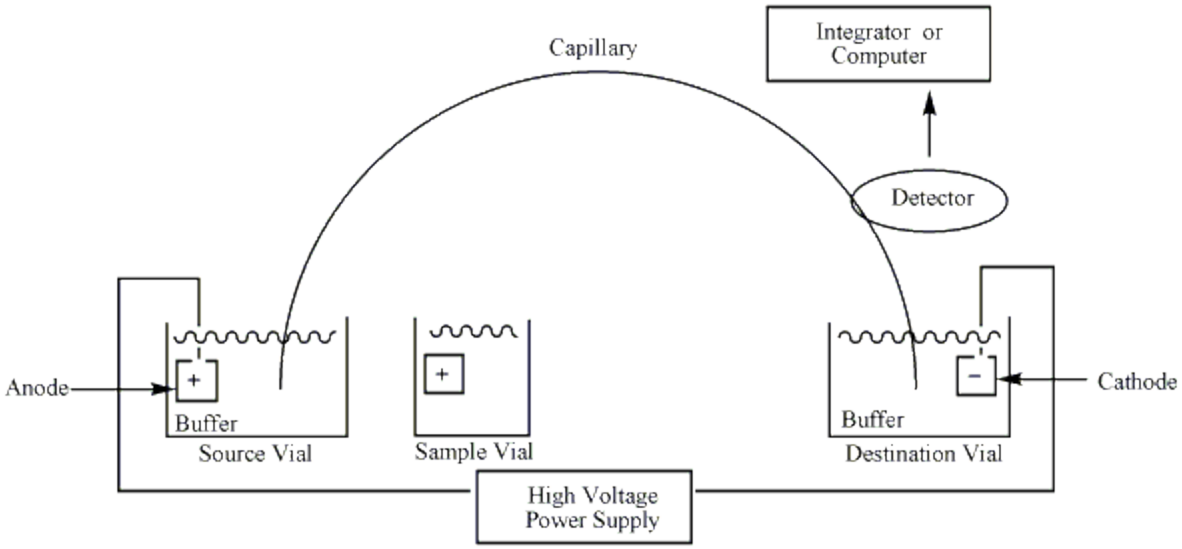

Figure 1.19 *Diagram of capillary electrophoresis system [120].*

1.4.4 Capillary electrophoresis based on on-chip technology

Compared to traditional or commercial capillary electrophoresis-based devices, microfluidic devices, which have advantages in miniaturization and portability, is receiving considerable attention in chemical analysis and biological assays [121]. Furthermore, microchip-scale electrophoresis system for capillary electrophoretic separation and detection has higher separation efficiency, shorter analysis time, higher sensitivity, and lower sample consumption [122-124]. Smolka et al. developed a electrophoresis-based sensor to achieve on-site analysis of collected soil sample. The presented sensor consists of a microfluidic chip and a conductivity detector. The introduced sample ions were separated in an applied electrical field and ion concentrations were detected by a conductivity measurement. Through this device, multiple ions (NO_3^-, NH_4^+, PO_4^{3-}) in extracted sample solution were separated and detected.

1.5 Problems, Objective, Goal and Approach

1.5.1 Limitation of current humidity control technology

Humidity, one of major environmental factors in affecting plant disease infection, is gotten enough attention in research of plant science and cell biology. Greenhouses and growth chambers are the most common systems using to control humidity environments currently. However, the existed technologies are unable to create multi-levels of humidity in an efficient way. While a lot of investment have been made to build various controlled environment consequently, flexible approaches for discrete humidity environments generation is far from enough.

1.5.2 Challenge of current microalgae culture technology

Considering the numerous microalgal strains and combinatorial nature of many culture factors, current practice microalgal conventional culture systems, such as open pond systems and PBRs, appear less suitable for rapid, high throughput screening and tracking algae growth responding to different growth conditions. Also due to large volumes of the conventional culture systems, it is relatively difficult to achieve spatially uniform environmental conditions within a single reactor with agitation by shaking, rotating, or bubbling. Furthermore, in-line monitoring and quantification of algal growth in these culture systems is rarely achieved. While several microfluidic devices were developed to grow micralgal cells and examine their lipid production, those systems were not integrated an in-line analysis feature, or only built one single culture environment as low efficiency. Also, the responding of micralgal cells to different CO_2 concentrations, a key factor in photosynthesis of microalgae, is rarely studied in microfluidic based microalgae culture device. There is an

urgent need to develop a strategy to achieve in-line monitoring and analyzing of microalgae growth under different CO_2 environments in a high throughput way in the small device.

1.5.3 Limitation of current soil sensors

While most of practice soil sensors were designed based on ISE or optical absorption mechanism, they always rely on specific ISE membranes or light source at specific wavelength range. Capillary electrophoresis, as efficient tool for ion separation, is widely used for multiple ions separation, detection, and precise analysis in biology and plant science. However, commercial electrophoresis instruments are bulky and not suitable for in-situ applications. Comparing with current commercial electrophoresis instruments, the microchip-based electrophoresis devices overcome the drawback as bulky without scarifying sensitivity. Furthermore, microfluidic devices have advantages as low sample consumption, high sensitivity, and high throughput. Even though a number of microfluidic electrophoresis systems have been developed, the application to soil nutrient detection has not been addressed.

1.5.4 Objectives and basic approaches of this thesis

The first objective of the thesis is to a new simple method to obtain a controlled discrete humidity gradient in miniature multi-plate like devices rapidly. The designed goals for this objective are listed below:

- To design a miniature multi-plate like devices for obtaining a controlled discrete humidity. Through the combinatory effects of evaporation, convection and diffusion, the device not only generates stable discrete humidity gradient within a few minutes, but also maintains the generated stable humidity gradient for long-term experiment purpose.

- To demonstrate the workability of the device on Soybean-P. sojae interaction investigation. By analyzing the responses of soybeans to P. sojae after a 48-hour culturing, the most suitable humidity environment for generating compatible soybean-P. sojae interaction was studied.
- To proof the flexibility of the approach. Different spatial distribution of humidity can be manipulated flexibly via setting up the multiple water and desiccant drying agent sources at different wells.

The second objective is to develop a microfluidic microalgal bioreactor to study the growth of microalgae under different CO_2 concentrations. The specific goals for this objective are listed below:

- To develop a microfluidic microalgal bioreactor to simulated natural growth environment for microalgae. The present approach not only achieves multiple CO_2 concentrations environments for paralleled experiments on one single chip, but also allows in-line observation and analysis.
- To study growth characterization of C. reinhardtii strain CC620 under different CO_2 concentration conditions. C. reinhardtii strain CC620 was cultured in accurate CO_2 conditions using the developed platform. Two different analysis methods are introduced to realize real-time screening.

The third objective is to conduct a microchip-based electrophoresis nutrient sensing system to separate, detect, and quantify nutrient ions in soil sample solutions. The goals for this objective are listed below:

- To design and build a microchip-based nutrient sensing system to separate and detect nutrient ions. The system not only does solution analysis via ion separation and

detection, but also does solution extraction for soil and solution transportation before electrophoresis process. To validate the system, a mixture of nutrient ions in soil solution were separate and detected with distinguishing peaks.

- To quantify nutrient ions in soil sample solutions.

References

1. R.L. Lehrman, "Energy is not the ability to do work." *The Physics Teacher* 11.1 (1973): 15-18.

2. http://www.iea.org/publications/freepublications/publication/KeyWorld2016.pdf

3. O. Ellabban, H. Abu-Rub, F. Blaabjerg. "Renewable energy resources: Current status, future prospects and their enabling technology." *Renewable and Sustainable Energy Reviews* 39 (2014): 748-764.

4. http://www.ren21.net/gsr-2017/assets/img/Figure_01_GSR_2017-large.png

5. https://www.energy.gov/science-innovation/energy-sources/renewable-energy/bioenergy

6. http://bearadtech.com/wp-content/uploads/2014/09/Biomass.jpg

7. https://en.wikipedia.org/wiki/Biofuel#First-generation_biofuels

8. Y.D. Hang, and E. E. Woodams. "Enzymatic production of reducing sugars from corn cobs." *LWT-Food Science and Technology* 34.3 (2001): 140-142.

9. S. Limtong, S. Chutima, and W. Yongmanitchai. "Production of fuel ethanol at high temperature from sugar cane juice by a newly isolated Kluyveromyces marxianus." *Bioresource technology* 98.17 (2007): 3367-3374.

10. M. Simpson-Holley, A. Higson, and G. Evans. "Bring on the biorefinery." *Chemical engineer* 795 (2007): 46-48.

11. S.N. Naik, V.V. Goud, P.K. Rout, and A.K. Dalai, "Production of first and second generation biofuels: a comprehensive review." *Renewable and sustainable energy reviews* 14.2 (2010): 578-597.

12. G. Dragone, B.D. Fernandes, A.A. Vicente, and J.A. Teixeira, "Third generation biofuels from microalgae." *Current research, technology and education topics in applied microbiology and microbial biotechnology* 2 (2010): 1355-1366.

13. F. Alam, S. Mobin, and H. Chowdhury. "Third generation biofuel from Algae." *Procedia Engineering* 105 (2015): 763-768.

14. E.M. Aro, "From first generation biofuels to advanced solar biofuels." *Ambio* 45.1 (2016): 24-31.

15. S. K. Bardhan, G. Shelaka, M. E. Gorman, and M. Ali Haider. "Biorenewable chemicals: Feedstocks, technologies and the conflict with food production." *Renewable and Sustainable Energy Reviews* 51 (2015): 506-520.

16. J. A. Wrather and S. R. Koenning, "Estimates of disease effects on soybean yields in the United States 2003 to 2005." *Journal of nematology* 38.2 (2006): 173.

17. A.E. Dorrance, H. Jia, and T. S. Abney. "Evaluation of soybean differentials for their interaction with Phytophthora sojae." *Plant Health Prog* (2004).

18. D. Qutob, P.T. Hraber, B.W. Sobral, and M. Gijzen, "Comparative analysis of expressed sequences in Phytophthora sojae." *Plant Physiology* 123.1 (2000): 243-254.

19. B.M. Tyler, "Phytophthora sojae: root rot pathogen of soybean and model oomycete." *Molecular plant pathology* 8.1 (2007): 1-8.

20. S. A. Scott, M. P. Davey, J. S. Dennis, I. Horst, C. J. Howe, D. J. Lea-Smith and A. G. Smith, *Current opinion in biotechnology*, 2010, 21, 277-286.

21. B. Metz, O.R. Davidson, P.R. Bosch, R. Dave, L.A. Meyer, "Contribution of working group II to the fourth assessment report of the intergovernmental panel on climate change, 2007." *Climate change* (2007).

22. A. Melis, "Solar energy conversion efficiencies in photosynthesis: minimizing the chlorophyll antennae to maximize efficiency." *Plant science* 177.4 (2009): 272-280.

23. M. Packer, "Algal capture of carbon dioxide; biomass generation as a tool for greenhouse gas mitigation with reference to New Zealand energy strategy and policy." *Energy Policy* 37.9 (2009): 3428-3437.

24. Y. Chisti, "Biodiesel from microalgae." *Biotechnology advances* 25.3 (2007): 294-306.

25. M.G. Babu, and K. A. Subramanian. Alternative transportation fuels: utilisation in combustion engines. *CRC Press*, 2013.

26. S.A. Scott, M.P. Davey, J.S. Dennis, I. Horst, C.J. Howe, D.J. Lea-Smith, and A.G. Smith, "Biodiesel from algae: challenges and prospects." *Current opinion in biotechnology* 21.3 (2010): 277-286.

27. SS.A. Wyer, *Treatise on producer-gas and gas-producers by Samuel S Wyer*. 1906.

28. D. Lide. *CRC Handbook of Chemistry and Physics* (85 ed.). CRC Press (2005). pp. 15–25. ISBN 0-8493-0485-7.

29. J.L. Shipp, Y. Zhang, D.W.A. Hunt, and G. Ferguson, "Influence of humidity and greenhouse microclimate on the efficacy of Beauveria bassiana (Balsamo) for control of greenhouse arthropod pests." *Environmental Entomology* 32.5 (2003): 1154-1163.

30. P.B. Reich, and G.A. Robert, "Ambient levels of ozone reduce net photosynthesis in tree and crop species." *Science* 230.4725 (1985): 566-570.

31. K.A. Mott, and D.F. Parkhurst. "Stomatal responses to humidity in air and helox." *Plant, Cell & Environment* 14.5 (1991): 509-515.

32. O. Körner, and H. Challa. "Process-based humidity control regime for greenhouse crops." *Computers and Electronics in Agriculture* 39.3 (2003): 173-192.

33. O. Körner, and H. Challa. "Temperature integration and process-based humidity control in chrysanthemum." *Computers and electronics in agriculture* 43.1 (2004): 1-21.

34. J.S. Perret, A.M. Al-Ismaili, and S.S. Sablani. "Development of a humidification–dehumidification system in a quonset greenhouse for sustainable crop production in arid regions." *Biosystems engineering* 91.3 (2005): 349-359.

35. N.L. Jeon, S.K. Dertinger, D.T. Chiu, I.S. Choi, A.D. Stroock, & G.M. Whitesides, "Generation of solution and surface gradients using microfluidic systems." *Langmuir* 16.22 (2000): 8311-8316.

36. S.K. Dertinger, D.T. Chiu, N.L. Jeon, & G.M. Whitesides, "Generation of gradients having complex shapes using microfluidic networks." *Analytical Chemistry* 73.6 (2001): 1240-1246.

37. I. Barkefors, S. Le Jan, L. Jakobsson, E. Hejll, G. Carlson, H. Johansson, J. Jarvius, J.W. Park, N.L. Jeon, and J. Kreuger, "Endothelial cell migration in stable gradients of vascular endothelial growth factor a and fibroblast growth factor 2 effects on chemotaxis and chemokinesis." *Journal of Biological Chemistry* 283.20 (2008): 13905-13912.

38. W. Saadi, S.J. Wang, F. Lin, & N.L. Jeon, "A parallel-gradient microfluidic chamber for quantitative analysis of breast cancer cell chemotaxis." *Biomedical microdevices* 8.2 (2006): 109-118.

39. J. Diao, L. Young, S. Kim, E.A. Fogarty, S.M. Heilman, P. Zhou, M.L. Shuler, M. Wu, and M.P. DeLisa, "A three-channel microfluidic device for generating static linear gradients and its application to the quantitative analysis of bacterial chemotaxis." *Lab on a Chip* 6.3 (2006): 381-388.

40. N. Damean, L.F. Olguin, F. Hollfelder, C. Abell, and W.T. Huck, "Simultaneous measurement of reactions in microdroplets filled by concentration gradients." *Lab on a Chip* 9.12 (2009): 1707-1713.

41. http://www.klbict.co.uk/gcse/theory/5_3/5_3_3_feedback.htm

42. F. Katagiri, D. Canelon-Suarez, K. Griffin, J. Petersen, R.K. Meyer, M. Siegle, and K. Mase, "Design and Construction of an Inexpensive Homemade Plant Growth Chamber." *PloS one* 10.5 (2015): e0126826.

43. http://weiss-na.com/product/sgc-plant-growth-chamber/?category

44. C. Hu, J. Liu, H. Chen, and F. Nie, "Microfluidic Platforms for Gradient Generation and its Applications." *Biochem Anal Biochem* 6.320 (2017): 2161-1009.

45. S. E. Hulme, S. S. Shevkoplyas, A. P. McGuigan, J. Apfeld, W. Fontana and G. M. Whitesides. "Lifespan-on-a-chip: microfluidic chambers for performing lifelong observation of C. elegans." *Lab on a Chip* 10.5 (2010): 589-597.

46. S. Okushima, T. Nisisako, T. Torii, and T. Higuchi. "Controlled production of monodisperse double emulsions by two-step droplet breakup in microfluidic devices." *Langmuir* 20.23 (2004): 9905-9908.

47. G.A. Cooksey, C.G. Sip, and A. Folch. "A multi-purpose microfluidic perfusion system with combinatorial choice of inputs, mixtures, gradient patterns, and flow rates." *Lab on a Chip* 9.3 (2009): 417-426.

48. E. Berthier, J. Surfus, J. Verbsky, A. Huttenlocher, and D. Beebe, "An arrayed high-content chemotaxis assay for patient diagnosis." *Integrative Biology* 2.11-12 (2010): 630-638.

49. T. M. Keenan and A. Folch, "Biomolecular gradients in cell culture systems." *Lab on a Chip* 8.1 (2008): 34-57.

50. M. A. Holden, S. Kumar, E. T. Castellana, A. Beskok and P. S. Cremer, "Generating fixed concentration arrays in a microfluidic device." *Sensors and Actuators B: Chemical* 92.1 (2003): 199-207.

51. R. F. Ismagilov, A. D. Stroock, P. J. Kenis, G. Whitesides and H. A. Stone, "Experimental and theoretical scaling laws for transverse diffusive broadening in two-phase laminar flows in microchannels." *Applied Physics Letters* 76.17 (2000): 2376-2378.

52. B. R. Gorman and J. P. Wikswo, "Characterization of transport in microfluidic gradient generators." *Microfluidics and Nanofluidics* 4.4 (2008): 273.

53. A. Khademhosseini, R. Langer, J. Borenstein and J. P. Vacanti, Proc. Natl. "Microscale technologies for tissue engineering and biology." *Proceedings of the National Academy of Sciences of the United States of America* 103.8 (2006): 2480-2487.

54. A. Shamloo, N. Ma, M.-m. Poo, L. L. Sohn and S. C. Heilshorn, "Endothelial cell polarization and chemotaxis in a microfluidic device." *Lab on a chip* 8.8 (2008): 1292-1299.

55. B. G. Chung, L. A. Flanagan, S. W. Rhee, P. H. Schwartz, A. P. Lee, E. S. Monuki and N. L. Jeon, "Human neural stem cell growth and differentiation in a gradient-generating microfluidic device." *Lab on a Chip* 5.4 (2005): 401-406.

56. J. Pihl, J. Sinclair, E. Sahlin, M. Karlsson, F. Petterson, J. Olofsson and O. Orwar, "Microfluidic gradient-generating device for pharmacological profiling." *Analytical Chemistry* 77.13 (2005): 3897-3903.

57. B. G. Chung, F. Lin and N. L. Jeon, "A microfluidic multi-injector for gradient generation." *Lab on a Chip* 6.6 (2006): 764-768.

58. M. Yang, J. Yang, C.-W. Li and J. Zhao, "Generation of concentration gradient by controlled flow distribution and diffusive mixing in a microfluidic chip." *Lab on a Chip* 2.3 (2002): 158-163.

59. B. Mosadegh, C. Huang, J. W. Park, H. S. Shin, B. G. Chung, S.-K. Hwang, K.-H. Lee, H. J. Kim, J. Brody and N. L. Jeon, "Generation of stable complex gradients across two-dimensional surfaces and three-dimensional gels." *Langmuir* 23.22 (2007): 10910-10912.

60. V. V. Abhyankar, M. A. Lokuta, A. Huttenlocher and D. J. Beebe, "Characterization of a membrane-based gradient generator for use in cell-signaling studies." *Lab on a Chip* 6.3 (2006): 389-393.

61. T. Kang, J. Han and K. S. Lee, "Concentration gradient generator using a convective–diffusive balance." *Lab on a Chip* 8.7 (2008): 1220-1222.

62. Y. Du, J. Shim, M. Vidula, M. J. Hancock, E. Lo, B. G. Chung, J. T. Borenstein, M. Khabiry, D. M. Cropek and A. Khademhosseini, "Rapid generation of spatially and temporally controllable long-range concentration gradients in a microfluidic device." *Lab on a Chip* 9.6 (2009): 761-767.

63. A. Han, H. Hou, L. Li, H. S. Kim and P. de Figueiredo, "Microfabricated devices in microbial bioenergy sciences." *Trends in biotechnology* 31.4 (2013): 225-232.

64. S. Boussiba, E. Sandbank, G. Shelef, Z. Cohen, A. Vonshak, A. Ben-Amotz, S. Arad and A. Richmond, "Outdoor cultivation of the marine microalga Isochrysis galbana in open reactors." *Aquaculture* 72.3-4 (1988): 247-253.

65. R. Hase, H. Oikawa, C. Sasao, M. Morita and Y. Watanabe, "Photosynthetic production of microalgal biomass in a raceway system under greenhouse conditions in Sendai city." *Journal of bioscience and bioengineering* 89.2 (2000): 157-163.

66. C.Y. Chen, K.L. Yeh, R. Aisyah, D.J. Lee and J.-S. Chang, "Cultivation, photobioreactor design and harvesting of microalgae for biodiesel production: a critical review." *Bioresource technology* 102.1 (2011): 71-81.

67. R.A. Erickson and R. Jimenez, "Microfluidic cytometer for high-throughput measurement of photosynthetic characteristics and lipid accumulation in individual algal cells." *Lab on a Chip* 13.15 (2013): 2893-2901.

68. R.E. Holcomb, L.J. Mason, K.F. Reardon, D.M. Cropek and C.S. Henry, "Culturing and investigation of stress-induced lipid accumulation in microalgae using a microfluidic device." *Analytical and bioanalytical chemistry* 400.1 (2011): 245-253.

69. G. Zheng, Y. Wang, Z. Wang, W. Zhong, H. Wang and Y. Li, "An integrated microfluidic device in marine microalgae culture for toxicity screening application." *Marine pollution bulletin* 72.1 (2013): 231-243.

70. M.A. Borowitzka, "Commercial production of microalgae: ponds, tanks, tubes and fermenters." *Journal of biotechnology* 70.1 (1999): 313-321.

71. N. Moazami, A. Ashori, R. Ranjbar, M. Tangestani, R. Eghtesadi, and A.S. Nejad, "Large-scale biodiesel production using microalgae biomass of Nannochloropsis." *Biomass and bioenergy* 39 (2012): 449-453.

72. J.P. Bitog, I.B. Lee, C.G. Lee, K.S. Kim, H.S. Hwang, S.W. Hong, I.H. Seo, K.S. Kwon, K.S. and E. Mostafa, "Application of computational fluid dynamics for modeling and designing photobioreactors for microalgae production: a review." *Computers and Electronics in Agriculture* 76.2 (2011): 131-147.

73. C.U. Ugwu, H. Aoyagi, and H. Uchiyama. "Photobioreactors for mass cultivation of algae." *Bioresource technology* 99.10 (2008): 4021-4028.

74. G. Torzillo, B. Pushparaj, F. Bocci, W. Balloni, R. Materassi, and G. Florenzano, "Production of Spirulina biomass in closed photobioreactors." *Biomass* 11.1 (1986): 61-74.

75. A. Richmond, S. Boussiba, A. Vonshak, and R. Kopel, "A new tubular reactor for mass production of microalgae outdoors." *Journal of Applied Phycology* 5.3 (1993): 327-332.

76. E. Molina, J. Fernández, F.G. Acién, and Y. Chisti."Tubular photobioreactor design for algal cultures." *Journal of biotechnology* 92.2 (2001): 113-131.

77. A.S. Mirón, M.C.C. Garcıa, F.G. Camacho, E.M. Grima, and Y. Chisti, 2002. "Growth and biochemical characterization of microalgal biomass produced in bubble column and airlift photobioreactors: studies in fed-batch culture." *Enzyme and Microbial Technology* 31.7 (2002): 1015-1023.

78. https://subitec.com/de/bildergalerien-mikroalge-und-photobioreaktor/18-produktions-und-forschungsanlagen#

79. J.C. Ogbonna, S. Toshihiko, and H. Tanaka, "An integrated solar and artificial light system for internal illumination of photobioreactors." *Journal of Biotechnology* 70.1 (1999): 289-297.

80. A. Saeed and M. Iqbal, "Immobilization of blue green microalgae on loofa sponge to biosorb cadmium in repeated shake flask batch and continuous flow fixed bed column reactor system." *World Journal of Microbiology and Biotechnology* 22.8 (2006): 775-782.

81. L. Giannelli, A. Scoma, and G. Torzillo. "Interplay between light intensity, chlorophyll concentration and culture mixing on the hydrogen production in sulfur - deprived Chlamydomonas reinhardtii cultures grown in laboratory photobioreactors." *Biotechnology and bioengineering* 104.1 (2009): 76-90.

82. E. Jacob-Lopes, C.H.G. Scoparo, M.I. Queiroz, and T.T. Franco, "Biotransformations of carbon dioxide in photobioreactors." *Energy Conversion and Management* 51.5 (2010): 894-900.

83. https://upload.wikimedia.org/wikipedia/commons/b/b1/Bioreaktor_quer2.jpg

84. http://www.psi.cz/img/products/photobioreactors/bubble_line.jpg

85. H. Jiang, Z. Xu, M.R. Aluru, and L. Dong, "Plant chip for high-throughput phenotyping of Arabidopsis." *Lab on a Chip* 14.7 (2014): 1281-1293.

86. S. H. Au, S.C. Shih, and A.R. Wheeler. "Integrated microbioreactor for culture and analysis of bacteria, algae and yeast." *Biomedical microdevices* 13.1 (2011): 41-50.

87. D. Mark, S. Haeberle, G. Roth, F. von Stetten and R. Zengerle, "Microfluidic lab-on-a-chip platforms: requirements, characteristics and applications." *Microfluidics Based Microsystems*. Springer, Dordrecht, 2010. 305-376.

88. G. B. Salieb-Beugelaar, G. Simone, A. Arora, A. Philippi and A. Manz, "Latest developments in microfluidic cell biology and analysis systems." *Analytical chemistry* 82.12 (2010): 4848-4864.

89. G. M. Whitesides, "What comes next?." *Lab on a Chip* 11.2 (2011): 191-193.

90. D.-H. Lee, C. Y. Bae, J.-I. Han and J.-K. Park, "In situ analysis of heterogeneity in the lipid content of single green microalgae in alginate hydrogel microcapsules." *Analytical chemistry* 85.18 (2013): 8749-8756.

91. J. Pan, A. L. Stephenson, E. Kazamia, W. T. Huck, J. S. Dennis, A. G. Smith and C. Abell, "Quantitative tracking of the growth of individual algal cells in microdroplet compartments." *Integrative Biology* 3.10 (2011): 1043-1051.

92. A. Schaap, Y. Bellouard and T. Rohrlack, "Optofluidic lab-on-a-chip for rapid algae population screening." *Biomedical optics express* 2.3 (2011): 658-664.

93. A. Schaap, T. Rohrlack and Y. Bellouard, "Optical classification of algae species with a glass lab-on-a-chip." *Lab on a Chip* 12.8 (2012): 1527-1532.

94. H. S. Kim, T. L. Weiss, H. R. Thapa, T. P. Devarenne and A. Han, "A microfluidic photobioreactor array demonstrating high-throughput screening for microalgal oil production." *Lab on a Chip* 14.8 (2014): 1415-1425.

95. A. Dewan, J. Kim, R. H. McLean, S. A. Vanapalli and M. N. Karim, "Growth kinetics of microalgae in microfluidic static droplet arrays." *Biotechnology and bioengineering* 109.12 (2012): 2987-2996.

96. D.L. Karlen, M.J. Mausbach, J.W. Doran, R.G. Cline, R.F. Harris, and G.E. Schuman, "Soil quality: a concept, definition, and framework for evaluation (a guest editorial)." *Soil Science Society of America Journal* 61.1 (1997): 4-10.

97. M. Yokota, T. Okada, and I. Yamaguchi. "An optical sensor for analysis of soil nutrients by using LED light sources." *Measurement Science and Technology* 18.7 (2007): 2197.

98. P.C. Robert, "Precision agriculture: a challenge for crop nutrition management." *Plant and soil* 247.1 (2002): 143-149.

99. N. Zhang, M. Wang, and N. Wang. "Precision agriculture—a worldwide overview." *Computers and electronics in agriculture* 36.2 (2002): 113-132.

100. F. Kizito, C. Campbell, G. Campbell, D. Cobos, B. Teare, B. Carter and J. Hopmans, "Frequency, electrical conductivity and temperature analysis of a low-cost capacitance soil moisture sensor." *Journal of Hydrology* 352.3-4 (2008): 367-378.

101. S. Staggenborg, M. Carignano and L. Haag, "Predicting soil pH and buffer pH in situ with a real-time sensor." *Agronomy journal* 99.3 (2007): 854-861.

102. T. Jackson, K. Mansfield, M. Saafi, T. Colman and P. Romine, "Measuring soil temperature and moisture using wireless MEMS sensors." *Measurement* 41.4 (2008): 381-390.

103. Z. Zou, A. Jang, E. MacKnight, P.-M. Wu, J. Do, P. L. Bishop and C. H. Ahn, "Environmentally friendly disposable sensors with microfabricated on-chip planar bismuth electrode for in situ heavy metal ions measurement." *Sensors and Actuators B: Chemical* 134.1 (2008): 18-24.

104. J. V. Sinfield, D. Fagerman and O. Colic, "Evaluation of sensing technologies for on-the-go detection of macro-nutrients in cultivated soils." *Computers and Electronics in Agriculture* 70.1 (2010): 1-18.

105. D. Corwin and S. Lesch, "Characterizing soil spatial variability with apparent soil electrical conductivity: I. Survey protocols." *Computers and electronics in agriculture* 46.1 (2005): 103-133.

106. K. Sudduth, S. Drummond and N. Kitchen, "Accuracy issues in electromagnetic induction sensing of soil electrical conductivity for precision agriculture." *Computers and electronics in agriculture* 31.3 (2001): 239-264.

107. E. Ben-Dor and A. Banin, "Near-infrared analysis as a rapid method to simultaneously evaluate several soil properties." *Soil Science Society of America Journal* 59.2 (1995): 364-372.

108. J. Reeves, G. McCarty and T. Mimmo, "The potential of diffuse reflectance spectroscopy for the determination of carbon inventories in soils." *Environmental pollution* 116 (2002): S277-S284.

109. R. Verschoore, J. Pieters, T. Seps, Y. Spriet and J. Vangeyte, "Development of a sensor for continuous soil resistance measurement." *Precision Agriculture*. Wageningen Academic Publishers, Wageningen, The Netherlands (2003): 689-695.

110. R.L. Raper, T.E. Grift, and M.Z. Tekeste. "A portable tillage profiler for measuring subsoiling disruption." *Transactions of the ASAE* 47.1 (2004): 23.

111. S. Birrell and J. Hummel, "Multi-sensor ISFET system for soil analysis." *Precision agriculture* 97 (1997): 459-468.

112. Tu, Qiang, Willie Johnson Jr, and Brian Buckley. "Mercury speciation analysis in soil samples by ion chromatography, post-column cold vapor generation and inductively coupled plasma mass spectrometry." *Journal of analytical atomic spectrometry* 18.7 (2003): 696-701.

113. C.W. Chang, D. A. Laird, M. J. Mausbach and C. R. Hurburgh, "Near-infrared reflectance spectroscopy–principal components regression analyses of soil properties." *Soil Science Society of America Journal* 65.2 (2001): 480-490.

114. R. R. Price, J. W. Hummel, S. J. Birrell and I. S. Ahmad, "Rapid nitrate analysis of soil cores using ISFETs." *Transactions of the ASAE* 46.3 (2003): 601.

115. V.I. Adamchuk, E.D. Lund, B. Sethuramasamyraja, M.T. Morgan, A. Dobermann, and D.B. Marx, "Direct measurement of soil chemical properties on-the-go using ion-selective electrodes." *Computers and Electronics in Agriculture* 48.3 (2005): 272-294.

116. A. T. Woolley, D. Hadley, P. Landre, A. J. deMello, R. A. Mathies and M. A. Northrup, "Functional integration of PCR amplification and capillary electrophoresis in a microfabricated DNA analysis device." *Analytical Chemistry* 68.23 (1996): 4081-4086.

117. M. W. Lada, T. W. Vickroy and R. T. Kennedy, "High temporal resolution monitoring of glutamate and aspartate in vivo using microdialysis on-line with capillary electrophoresis with laser-induced fluorescence detection." *Analytical chemistry* 69.22 (1997): 4560-4565.

118. C. S. Effenhauser, G. J. Bruin, A. Paulus and M. Ehrat, "Integrated capillary electrophoresis on flexible silicone microdevices: analysis of DNA restriction fragments and detection of single DNA molecules on microchips." *Analytical Chemistry* 69.17 (1997): 3451-3457.

119. C. L. Colyer, T. Tang, N. Chiem and D. J. Harrison, "Clinical potential of microchip capillary electrophoresis systems." *Electrophoresis* 18.10 (1997): 1733-1741.

120. https://upload.wikimedia.org/wikipedia/commons/3/37/Capillaryelectrophoresis.png

121. H. Craighead, "Future lab-on-a-chip technologies for interrogating individual molecules." *Nature* 442.7101 (2006): 387-393.

122. D. R. Reyes, D. Iossifidis, P.-A. Auroux and A. Manz, "Micro total analysis systems. 1. Introduction, theory, and technology." *Analytical chemistry* 74.12 (2002): 2623-2636.

123. P.A. Auroux, D. Iossifidis, D. R. Reyes and A. Manz, "Micro total analysis systems. 2. Analytical standard operations and applications." *Analytical chemistry* 74.12 (2002): 2637-2652.

124. A. T. Woolley and R. A. Mathies, "Ultra-high-speed DNA fragment separations using microfabricated capillary array electrophoresis chips." *Proceedings of the National Academy of Sciences* 91.24 (1994): 11348-11352.

125. M. Smolka, D. Puchberger-Enengl, M. Bipoun, A. Klasa, M. Kiczkajlo, W. Śmiechowski, P. Sowiński, C. Krutzler, F. Keplinger, and M.J. Vellekoop, "A mobile lab-on-a-chip device for on-site soil nutrient analysis." *Precision Agriculture* 18.2 (2017): 152-168.

126. F.M. Francisca, and M. A. Montoro. "Measuring the dielectric properties of soil–organic mixtures using coaxial impedance dielectric reflectometry." *Journal of Applied Geophysics* 80 (2012): 101-109.

127. https://en.wikipedia.org/wiki/Atomic_absorption_spectroscopy

128. J. Artigas, A. Beltran, C. Jimenez, A. Baldi, R. Mas, C. Domınguez, and J. Alonso. "Application of ion sensitive field effect transistor based sensors to soil analysis." *Computers and electronics in agriculture* 31.3 (2001): 281-293.

CHAPTER 2. HUMIDITY ASSAY FOR PLANT-PATHOGEN INTERACTIONS IN MINIATURE CONTROLLED DISCRETE HUMIDITY ENVIRONMENTS WITH GOOD THROUGHPUT

A paper published in *Biomicrofluidics*

Zhen Xu, Huawei Jiang, Binod Bihari Sahu, Sekhar Kambakam, Prashant Singh,

Xinran Wang, Qiugu Wang, Madan K. Bhattacharyya, and Liang Dong

Abstract

This paper reports a highly economical and accessible approach to generate different discrete relative humidity conditions in spatially separated wells of a modified multi-well plate for humidity assay of plant-pathogen interactions with good throughput. We demonstrated that a discrete humidity gradient could be formed within a few minutes and maintained over a period of a few days inside the device. The device consisted of a freeway channel in the top layer, multiple compartmented wells in the bottom layer, a water source, and a drying agent source. The combinational effects of evaporation, diffusion, and convection were synergized to establish the stable discrete humidity gradient. The device was employed to study visible and molecular disease phenotypes of soybean in responses to infection by Phytophthora sojae, an oomycete pathogen, under a set of humidity conditions, with two near-isogenic soybean lines, Williams and Williams 82, that differ for a Phytophthora resistance gene (Rps1-k). Our result showed that at 63 % relative humidity, the transcript level of the defense gene GmPR1 was at minimum in the susceptible soybean line Williams and at maximal level in the resistant line Williams 82 following P. sojae CC5C infection. In addition, we investigated the effects of environmental temperature, dimensional and geometrical parameters, and other configurational factors on the ability of the device to generate miniature humidity environments. This work represents an exploratory effort to

economically and efficiently manipulate humidity environments in a space-limited device and shows a great potential to facilitate humidity assay of plant seed germination and development, pathogen growth, and plant-pathogen interactions. Since the proposed device can be easily made, modified, and operated, it is believed that this present humidity manipulation technology will benefit many laboratories in the area of seed science, plant pathology, and plant-microbe biology, where humidity is an important factor that influences plant disease infection, establishment, and development.

2.1 Introduction

The Controlled humidity environments are highly desired in plant science and agriculture research [1-3]. The ability to generate stable and controllable humidity conditions is of significant benefit for assaying the role of air water content in seed germination and plant development and growth, and studying interactions between plants and biological species (e.g., microbes, pathogens, and pests) [4]. Current greenhouse and growth chamber technologies require sensors and computer-assisted water spray and air ventilation to obtain specified humidity levels [5,6]. Air humidity-regulating control of commercial plant growth environments is often obtained by combining humidifier and dehumidifier [7]. These methods have relatively insufficient flexibility and low accuracy in creating a large number of variable humidity levels, thus affecting throughput of various humidity assays in plant sciences. New research and development efforts of considerable magnitude are therefore needed to realize flexible, precise, and economic regulation of humidity environments with high efficiency.

Concentration gradients of diffusible molecules have been flexibly generated in microfluidic lab-chip devices using flow-based or diffusion-based methods [8-12]. These approaches allow for flexible manipulation of chemical concentrations at a small scale, thus

facilitating studying many scientifically important biological phenomena, such as chemotaxis and morphogenesis of single cells and multicellular microorganisms [13-19]. The flow-based method uses an external pumping system to produce stable gradients perpendicular to parallel laminar flows of varying concentrations. The diffusion-based approach produces a chemical concentration gradient along a channel by free-diffusion between two sources, but the resulting gradient is often hard to maintain over long time periods [20, 21]. Kang et al. developed a device that generated concentration gradients parallel to the direction of flow by using a convective-diffusive balance in a counter-flow configuration [22]. Du et al. established spatially and temporally controllable concentration gradients of molecules in a microfluidic device [23]. Nezhad et al. developed diffusion based and flow based gradient microfluidic devices to stimulate pollen tubes [24].

While continuing efforts have been made to realize various miniature controlled environments for different biological applications, it should be pointed out that flexible manipulation of discrete humidity environments is relatively under-researched in miniaturization research and development area for plant science, plant pathology, and plant-microbe biology, where humidity is regarded as one of major environmental factors in affecting plant disease infection, establishment, and development.

Soybean [Glycine max (L.) Merr.] is one of the most important crops with high economic value worldwide. In the United States, soybean is the second most important row crop after corn. It is estimated that soybean suffers yield reduction valued over 2.6 billion dollars annually from various diseases [25]. Among the diseases, Phytophthora root and stem rot caused by Phytophthora sojae alone results in annual soybean yield losses valued around 0.3 billion dollars [26]. P. sojae is an oomycete pathogen and can cause pre-emergence

damping off leading to total crop failure. Owing to its economic importance of the disease, soybean-P. sojae has been widely accepted as a model plant-pathogen interaction for over four decades.

A series of Rps genes has been identified and utilized in breeding Phytophthora resistant soybean cultivars [27]. Of these, the Rps1-k locus was cloned. It contains two genes encoding coiled coil-nucleotide binding-leucine repeat containing proteins [28,29]. Because the oomycete pathogen P. sojae evolves rapidly and overcome the newly introduced Rps genes [30], a better understanding of this model system is becoming essential for designing or creating durable Phytophthora resistant soybean line. Furthermore, plant diseases are greatly influenced by various environmental conditions (e.g., light, temperature, soil water stress, nitrogen, etc.). Among these environmental factors, relative humidity or air water content plays a major role in disease development. Unfortunately, how the environmental humidity factor influences the outcome of the soybean-P. sojae interaction is unknown.

In this paper, we report on the development of a highly economical and accessible miniature device able to create a stable discrete stable humidity gradient in a space suitable for studying humidity requirements of the soybean-pathogen interaction. The proposed multi-well plate-like humidity devices can be easily made, used, and modified by unskilled persons in most biology and agriculture laboratories. We demonstrated the workability of the humidity device in assaying humidity conditions for studying both visible and molecular phenotypes in the Soybean-P. sojae interaction.

2.2 Device Design

The proposed device consists of two layers in a vertical direction (Fig. 2.1a, 1d). The top layer is spatially continuous and capped by a transparent lid. The bottom layer is partitioned into multiple identical wells. These wells are open at the top into the freeway

space of the top layer. Two device configurations, namely I-shaped and U-shaped devices, are studied for the purpose of illustrating and verifying the underlying principle. The I-shaped device has a straight top channel and a linear array of rectangular wells (Fig. 2.1a-c). In the U-shaped device, an array of cylindrical wells locates in the bottom layer and a U-shaped freeway channel is formed in the top layer by using a one-end-opened partition wall (Fig. 2.1d-f). To obtain a discrete humidity gradient, water and desiccant drying agent are respectively preloaded into two wells at the two extreme ends of the bottom layer (Fig. 2.1a, 2.1d). Water vapors evaporate from the water surface of the "source" reservoir and diffuses horizontally towards the desiccant reservoir or "drain" along the continuous top layer of the device (Fig. 2.1b, 2.1e). While passing each well, water vapors diffuse and convect downwards into the wells of the bottom layer. Herein, evaporation, diffusion, and convection are the driving forces for mass transfer of water vapors. The equilibrium concentration gradient of water vapors in the top layer arises from a balance of water evaporation at the source and water absorption by the drying agent at the drain. Therefore, a steady-state discrete humidity gradient is formed within the separated wells of the bottom layer, while a continuous humidity gradient still appears in the top layer of the device (Fig. 2.1c, 2.1f). As long as the water and desiccant drying agent sources are sufficient, the discrete humidity gradient in the wells will remain in its steady state. For example, when humidity of one or multiple wells is changed due to possible absorption of water vapors by plant seeds or pathogens, the water vapors in the top freeway channel will automatically transport into the corresponding wells to compensate for the vapor loss until reaching a new equilibrium vapor gradient through local diffusion and convection.

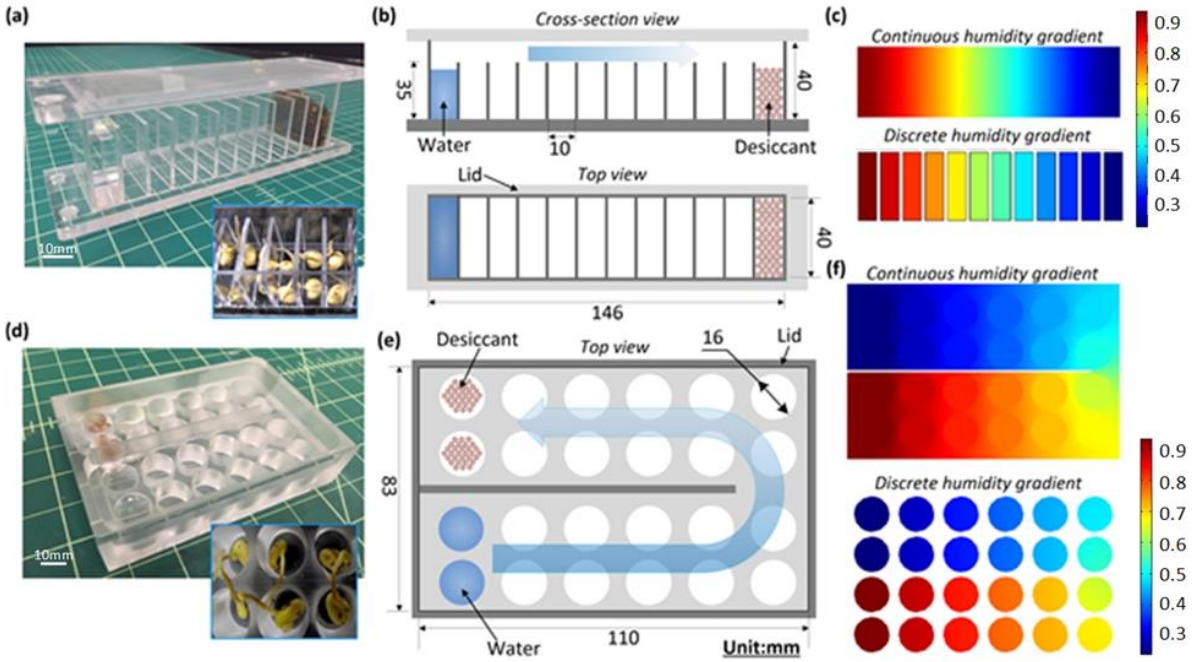

Figure 2.1 *Generation of a discrete humidity gradient in the I-shaped (a-c) and U-shaped (d-f) devices. Device photos are shown in (a) and (d). Schematics with key dimensions are given in (b) and (e). (c) and (f) give humidity gradients (top view) in the top and bottom layers of the I-shaped (c) and U-shaped (f) devices, respectively. Insets in (a) and (d) show soybean in the devices for studying soybean-pathogen interactions.*

To accommodate the size of soybean, the outer dimensions of the device were designed to be 146 mm (length) × 40 mm (width) × 40 mm (height). In the bottom layer, 12 wells were formed and each well was 10 mm long, 35 mm wide, and 35 mm tall. The top layer of the device was comprised of 5 mm deep space between the bottom layer and the transparent slab lid on the top (Fig. 2.1a, 2.1b). The I-shaped device was assembled by gluing multiple pieces of pre-machined transparent poly (methyl methacrylate) or PMMA (1/8-inch thick; Plexiglas; Alsip, USA) using acrylic adhesives (3M8155; 3M; St. Paul, USA). The U-shaped device was designed to be like a commercial 24-well tissue culture plate. The device had the dimensions of 110 mm (L) × 83 mm (W) × 25 mm (H) and the size of each well was 16 mm diameter and 15 mm deep. The top freeway channel was 8 mm in depth (Fig. 2.1d, 2.1e). The digital pattern of the U-shaped device was designed in AutoCAD (Autodesk; San

Rafael, CA) and fabricated with a PMMA block (3/4-inch thick; Plexiglas; Alsip, USA) by using a high-precision milling machine (CNC Masters; Irwindale, USA).

To study dynamic process of generating a discrete humidity gradient in the I-shaped and U-shaped devices, we built a computational model for the devices, based on a finite element analysis (FEA) method based software COMSOL Multiphysics (Burlington, USA). Generally, relative humidity has a linear function with water vapor concentration in the air [31]. The FEA simulations were conducted by establishing an equilibrium relation between the vapour source, the drain with the drying agent, and the moist air concentrations at different locations of the top and bottom layers. A convection-diffusion model was thus used to simulate the humidity gradient generation process in the device based on the convection-diffusion transport equation below:

$$\frac{\partial c}{\partial t} + \nabla \cdot (-D\nabla c) + u \cdot \nabla c = 0 \tag{2-1}$$

where c, D, and u are the concentration, the diffusivity, and the flow rate of water molecules in gaseous state, respectively. The diffusion coefficient D was set as 2.82×10^{-5} m^2/s at room temperature [32]. The flow rate of water molecules u was set at zero due to no external driving force. For normalization purpose, a constant vapor concentration of 1 mol/m^3 was used at the water reservoir and zero concentration was used at the desiccant reservoir. Time increment was set to be 5 seconds to illustrate the time-varying process of forming a discrete humidity gradient. A steady-state analysis was conducted to check uniformity and stability of the generated gradient.

Fig. 2.2a shows time-lapse images of the simulated humidity profiles at different time points in the I-shaped device. Fig. 2.2b shows time-varying humidity in each well of this

device. The simulation result indicates the closer the well was away from the water source, the shorter the time required to establish a stable humidity in the well. Specifically, the shortest establishment time was ~130 sec for the first well (see label #1 in Fig. 2.2a), while the longest time was ~550 sec for the last well (see label #10 in Fig. 2.2a). Fig. 2.2c shows the steady-state humidity gradient in the I-shaped device. Five humidity-tracing lines were set at different depths of the device. The result shows that due to combining the upper freeway channel and the lower compartmented wells, a discrete humidity gradient was well established along the wells in the bottom layer, while a continuous humidity gradient appeared in the top layer and decreased along the diffusing direction (line A in Fig. 2.2c). It should be noted that the humidity of each well was spatially uniform (lines C-E in Fig. 2.2c), except for a small humidity drop at the opening of the well (line B in Fig. 2c). Similarly, we also conducted simulations for the U-shaped device and obtained similar results as shown in Fig. 2.2d-f. In particular, the simulated time of reaching a stable humidity in a well varied from ~140 sec at well #1 to ~820 sec at well #10. It should be noted that the humidity values of wells #5 and #6 at the spatial turning point of the U-shaped device were deviated from a linear fit for all humidity data (Fig. 2.2f). This is because the geometrical constrains of these two wells were not similar to other wells in the same device (Fig. 2.2b).

2.3 Device characterization

To monitor humidity development process in the wells of the lower layer of the device, we inserted four mini relative humidity sensors (SHT11; Sensirion, Staefa, Switzerland) into the wells #1, #5, #6, and #10 (at the half depth of the wells) via the tiny holes punched through the transparent lid. These holes were sealed witch epoxy before measurement. The relative humidity sensors were controlled by a microcontroller board

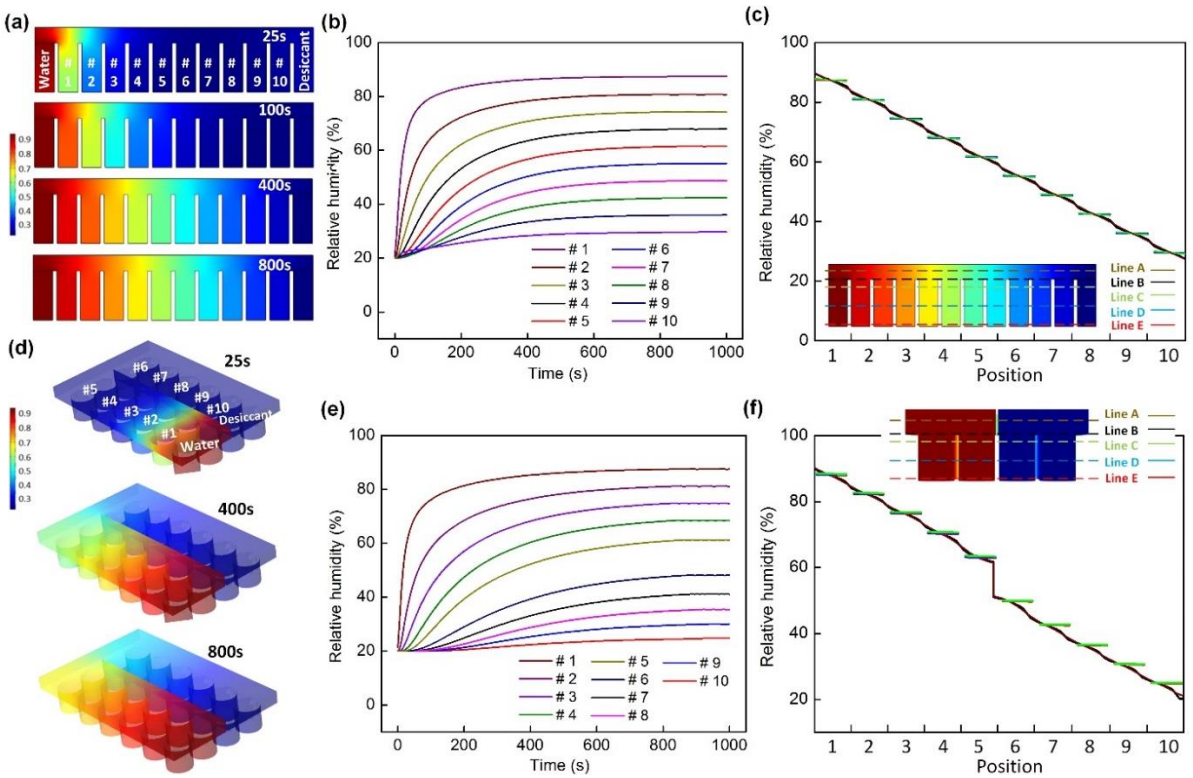

Figure 2.2 *Simulated dynamic process to generate discrete humidity gradients in the I-shaped and U-shaped devices. (a) and (d) give time-lapse images of water vapor movement inside the devices at different time points. (b) and (e) plot simulated relative humidity as a function of time in each well of the I-shaped (b) and U-shaped (e) devices. The wells of the I-shaped and U-shaped devices are numbered from #1 to #10 as shown in (a) and (c), respectively. The water and drying agent reservoirs are not numbered. (c) and (f) give simulated steady-state relative humidity gradient in the continuous top layer (line A), at the interface (line B) between the top and bottom layer, and at the three different depths (lines C-E) in the welled bottom layer, of the I-shaped (c) and U-shaped (f) devices, respectively.*

(Arduino Duemilanove; Arduino LLC, Somerville, USA) to multiplex readouts. Real-time relative humidity data were collected by a built-in program of the Arduino board via USB cable.

Fig. 2.3a shows the measured process of generating a stable discrete relative humidity gradient in the I-shaped device. The result demonstrates that depending on the location of a well, it took about 100 to 600 seconds to reach a steady-state humidity, and that the stabilized humidity remained constant over the tested 48 hours. As expected, the wells closer to the water reservoir require shorter time to establish stable humidity environments. Also, there is a close correspondence between the discrete humidity gradients generated via the FEA

simulation and in the conducted experiments (Fig. 2.3b). Fig. 2.3c indicates that the wells had a decreasing relative humidity from ~91%, next to the water reservoir, to ~22%, next to the desiccant reservoir. In the U-shaped device, the measured discrete relative humidity values and distribution (Fig. 2.3d-f) were similar to the simulation results mentioned. Specifically, the steady-state relative humidity levels were 90%, 82%, 76%, 69%, 63%, 48%, 44%, 37%, 29%, and 21% from well #1 to #10. The lowest relative humidity (21%) was stabilized within ~750 sec, while the highest one (90%) was obtained within ~170 sec.

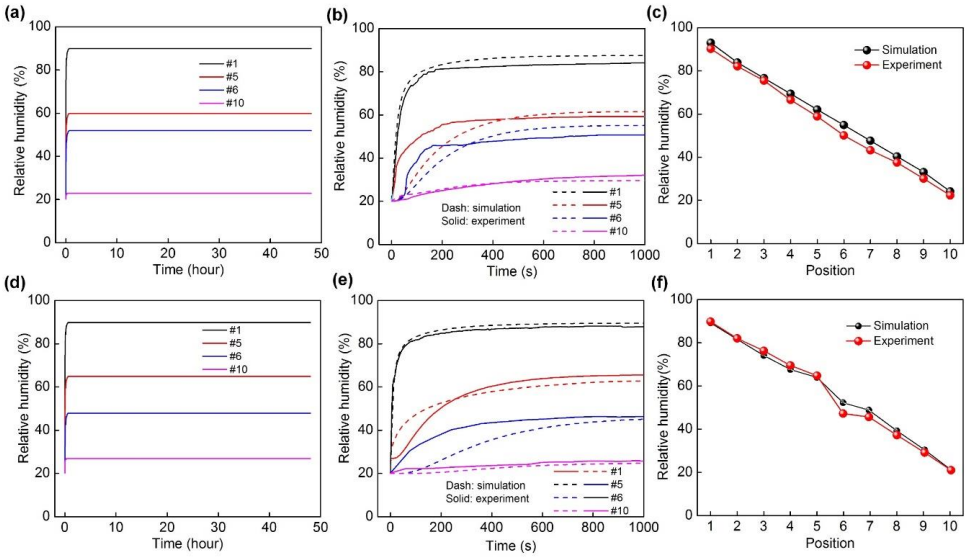

Figure 2.3 *Experimental humidity generation process in four wells (#1, #5, #6, and #10) of the I-shaped and U-shaped devices each, over a 48-hour period (a, d) and a close-up of the first 1000 seconds (b, e). For the purpose of comparison, the simulated results of relative humidity as a function of time are also given in (b, e). Experimental steady-state humidity in each well is given in (c, f). Here (a-c) and (d-f) present the results for the I-shaped and U-shaped devices, respectively.*

2.3 Humidity in the soybean-Phytophthora sojae interaction

Systematic We investigated the influences of the discrete relative humidity gradient generated in the U-shaped device on visible and molecular phenotypes in the soybean-P. sojae interaction. Williams (rps1-k) is susceptible to P. sojae CC5C isolate, while Williams 82 is resistant due to introgression of the Phytophthora resistance Rps1-k gene into the Williams background from the soybean line Kingwa. Two-day old etiolated seedlings of the

soybean cultivars Williams and Williams 82, grown in coarse vermiculites, were either inoculated with P. sojae isolate CC5C zoospores (1×105 spores/ml) or treated with sterile water, and then incubated under a range of relative humidity from 21% to 90% in dark and at 22 ^{o}C for up to 48 h in the U-shaped device (Fig. 2.4). We observed that the development of typical disease phenotypes was depended on humidity conditions. Typical dark brown hypersensitive response was observed for Williams 82, while similar dark brown symptom response was recorded for the susceptible Williams line under lower relative humidity condition (below 45%) due to failure of the pathogen to establish compatible interactions. Seedlings of both lines shriveled when relative humidity was 21%.

To determine the role of humidity on the host responses to pathogen infection, we conducted quantitative RT-PCR (qRT-PCR) for the soybean defense gene GmPR1. Total RNA samples were extracted from the P. sojae-infected or water treated root tissues using the miRNeasy Mini Kit (Qiagen; Venlo, Limburg, The Netherlands). To eliminate any contaminating genomic DNA, we treated the RNA samples with DNase I (Promega; Madison, WI, USA) for 30 min at 37 ^{o}C. RNA samples were evaluated for quality by running on a 0.7% agarose gel and quantified by a NanoDrop ND-1000 spectrophotometer (Thermo Fisher Scientific; Waltham, MA, USA). First-strand cDNAs were synthesized from 2 µg total RNA using M-MLV reverse transcriptase (Promega; Madison, WI, USA) according to the manufacturer's recommendation. Real-time qPCR was performed on an iCycler Real-Time system (Bio-Rad; Hercules, CA, USA). Each reaction was conducted in a final volume of 20 µl containing 10 µl of iTag Universal SYBR Green (Bio-Rad; Hercules, CA, USA), 2.0 µl of cDNA sample, and 200 nM gene-specific primers. The qPCR conditions were as follows: the amplification cycles were composed of 95 ^{o}C for 30 s followed by 40 cycles of 95 ^{o}C for 15s,

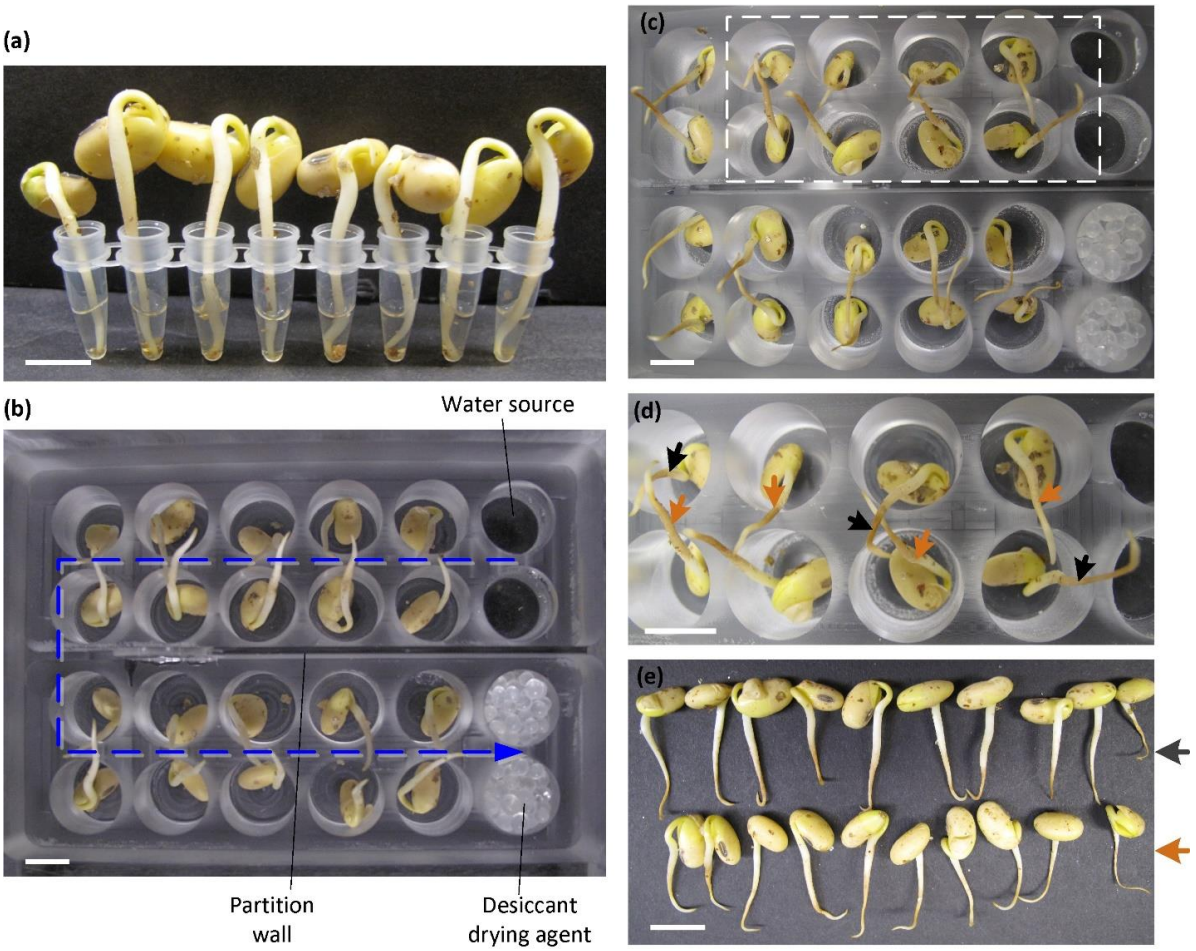

Figure 2.4 *Investigation of the soybean-P. sojae interaction under variable relative humidity conditions. A pair of near isogenic soybean lines that differ for a Phytophthora resistance gene (Rps1-k) was investigated for responses of soybean to the oomycete pathogen under a range of humidity conditions. Two-day old etiolated soybean seedlings of the cultivar Williams (rps1-k) and Williams 82 (Rps1-k) were inoculated with 100 µl P. sojae isolate CC5C zoospores suspension (105 spores/ml) for 30 min as shown in (a). A range of humidity condition was generated by the U-shaped device shown in Fig. 1c. Inoculated seedlings were arranged upside down in the device as shown in (b). Twenty-four hours following inoculation, the seedlings were observed for disease phenotypes (c) and (d). The seedlings shown in (d) are from the zoomed section of (c), shown by a white rectangle. In (d), black arrows show the resistant response of Williams 82 (Rps1-k) to the pathogen, while orange arrows show the susceptible response of Williams (lacking Rps1-k) to the pathogen. In (e), 10 P. sojae infected seedlings under variable humidity condition are shown. The black arrows show resistant response of Williams 82 (upper panel) and the orange arrows show susceptible response of Williams (lower panel) under variable relative humidity condition with the left most seedlings were exposed to 90% relative humidity while the right most ones to 21% relative humidity. Scale bars in (a)-(e) represent 10 mm.*

55 ^{o}C for 30 s and 72 ^{o}C for 30 s and a final extension cycle of 72 ^{o}C for 10 min. At the end of the 40 cycles, a melting curve was generated to analyse the specificity of the reactions. Each cDNA sample was PCR amplified in three replications. The ELF1B transcript level was used as the endogenous control. The relative expression level was calculated as $2^{-\Delta\Delta CT}$ (ΔCT

= CT, gene of interest − CT, ELF1B. ΔΔCT = ΔCT, treatment − ΔCT, 21% relative humidity control). Fig. 2.5 shows relative expression of the soybean defense GmPR1 gene in the roots of etiolated soybean seedlings either treated with water or infected with P. sojae under different humidity conditions. It is expected that in a typical susceptible host response, the GmPR1 levels will be at minimal level. On the other hand, the GmPR1 level will be at maximum level in a typical resistant response governed by recognition of an Rps gene product by its corresponding Avr effector protein encoded by an Avr gene. The result of the humidity assay shown in Fig. 2.5 indicates that at 63% relative humidity, the GmPR1 transcripts are at the minimal level in the infected roots of the susceptible line, Williams, and at the maximal level in the infected roots of the resistant line, Williams. Therefore, this study indicates that for a successful Soybean-P. sojae interaction, the relative humidity should be around 63%.

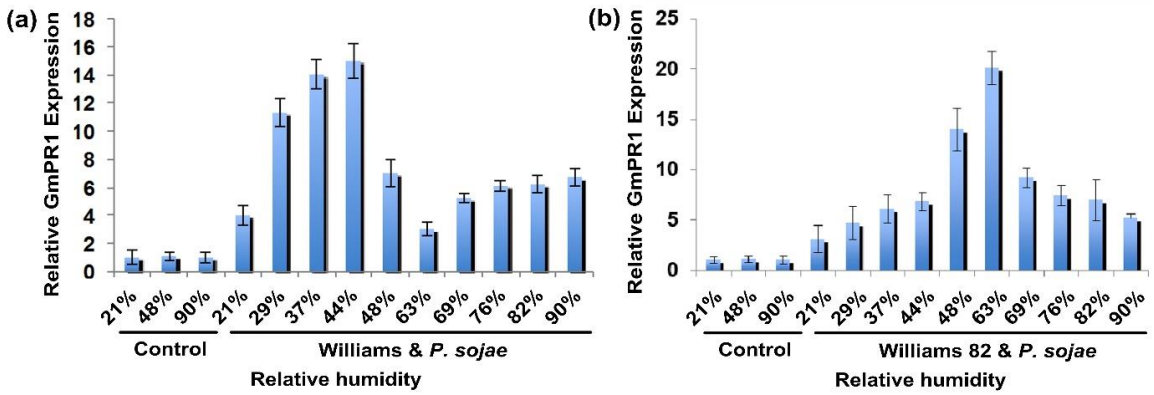

Figure 2.5 *Relative expression of soybean defense GmPR1 gene in infected roots of etiolated soybean seedlings with P. sojae under different humidity conditions as compared to that in the control. (a) Phenotypes of the susceptible and resistant host responses of Williams and Williams 82, respectively, to P. sojae isolate CC5C. (a) Expression of the defense gene GmPR1 in Williams. Control, seedlings treated with water; Williams & P. sojae, compatible interaction or susceptible host response following infection of Williams with P. sojae. (b) Expression of the defense gene GmPR1 in Williams 82. Control, seedlings treated with water; Williams 82 and P. sojae, incompatible interaction or resistant host response following infection of Williams 82 with P. sojae. Histograms show the mean of three biological replications and bars indicate standard errors calculated from standard deviations of three independent biological replications.*

2.4 Temperature, size scaling & other configurations

While the utility of the U-shaped device for determining humidity requirements of the Soybean-P. sojae interaction has been demonstrated, it is also worth studying the effects of environmental temperature and dimensional and geometrical parameters on the device performance in order to further explore other possible applications in the future.

We first studied how environmental temperature influences the formation of discrete humidity gradient within the I-shaped and U-shaped devices. In this experiment, each device was placed on a digital hotplate and a temperature and humidity sensor was inserted into well #6 of the device (Fig. 2.1a, 2.1d). The result shows that as the temperature increases from 22 ^{o}C to 50 ^{o}C, the steady-state humidity of the well decreased from ~52% to ~28% (Fig. 2.6a, 2.6c). Note that relative humidity is defined as the ratio of the partial pressure of water vapour to the equilibrium vapour pressure of water at a temperature. The equilibrium vapour pressure of water vapour increased fast as temperature rose, while the partial pressure of water vapour was little influenced by temperature. As a result, the steady-state humidity decreased with increasing temperature (Fig. 2.6b, 2. 6d).

To accommodate for smaller seeds (e.g., Arabidopsis, rice, etc.) for future research, we also studied the effect of device size on humidity generation of the device. We applied different scaling factors (SF = 1.0, 0.7, 0.5, 0.25, 0.125, 0.1, and 0.05) to the original dimensions of the U-shaped device (Fig. 2.1d, 2.1e). The simulation result shows that the time required to reach a stable humidity level reduced with decreasing device size (Fig. 2.7a). We then manufactured a smaller U-shaped device with the dimensions of 77 mm × 58.1 mm

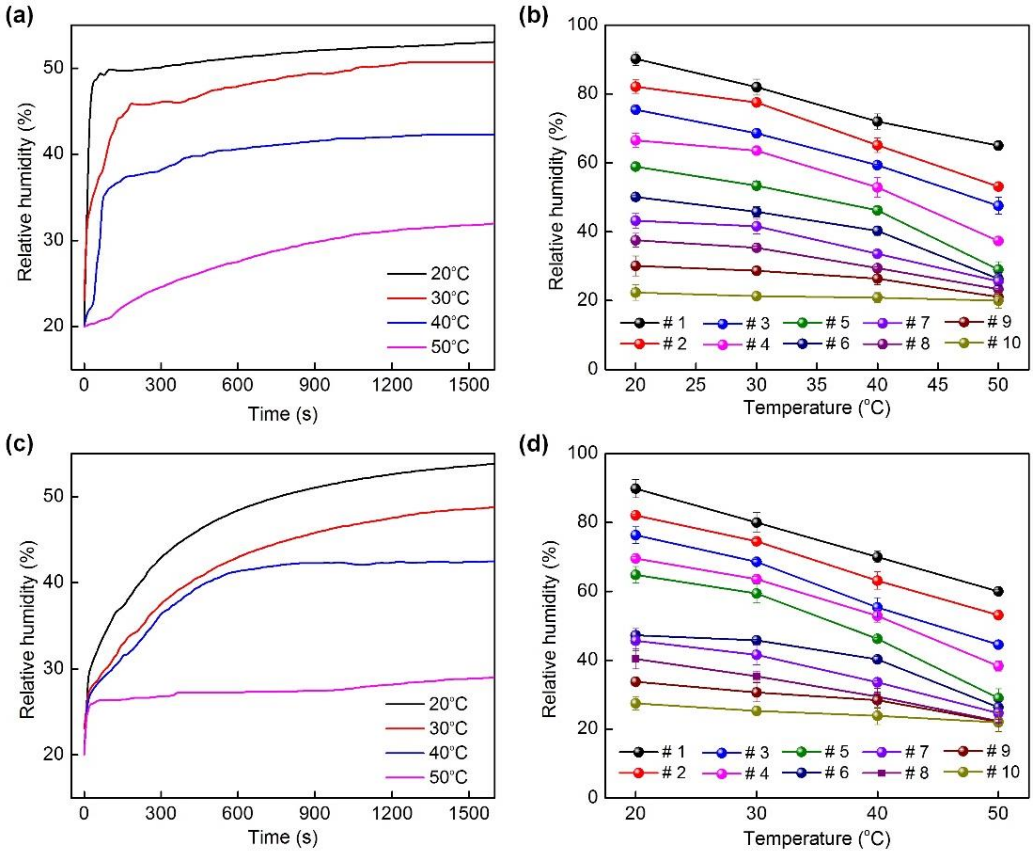

Figure 2.6 *Temperature effect on humidity generation process in a well of the I-shaped (a) and U-shaped (c) device. Steady-state relative humidity as a function of temperature for in all wells of the I-shaped and U-shaped devices are given in (b) and (d), respectively.*

× 17.5 mm (SF = 0.7) to house 24 wells with each being 11.2 mm diameter and 10.5 mm deep. A humidity generation and measurement experiment were also taken on the device, where one end was set as the water source and the other was set as the drying agent source. A thin layer (~1 mm thick) of desiccant powders was laid at the bottom of each well to indicate humidity difference between the wells. At low humidity levels, the colour of the desiccant powders was yellow. As the humidity increased, the desiccant powders became slightly blue. Fig. 2.7b indicates that a stable discrete humidity gradient was established within 6.5 min, almost matching the simulated result (green curve in Fig. 2.7a). We also made a smaller I-shaped device with the dimensions of 44 mm × 32 mm × 6 mm (see the lower panel in Fig.

2.7b). The color change of the desiccant powders indicates that the downscaled I-shaped device had a shorter establishment time of ~1 min (Fig. 2.7b). Therefore, the present method of generating discrete humidity is not limited to the specific dimensions shown above but rather common in different dimensional settings.

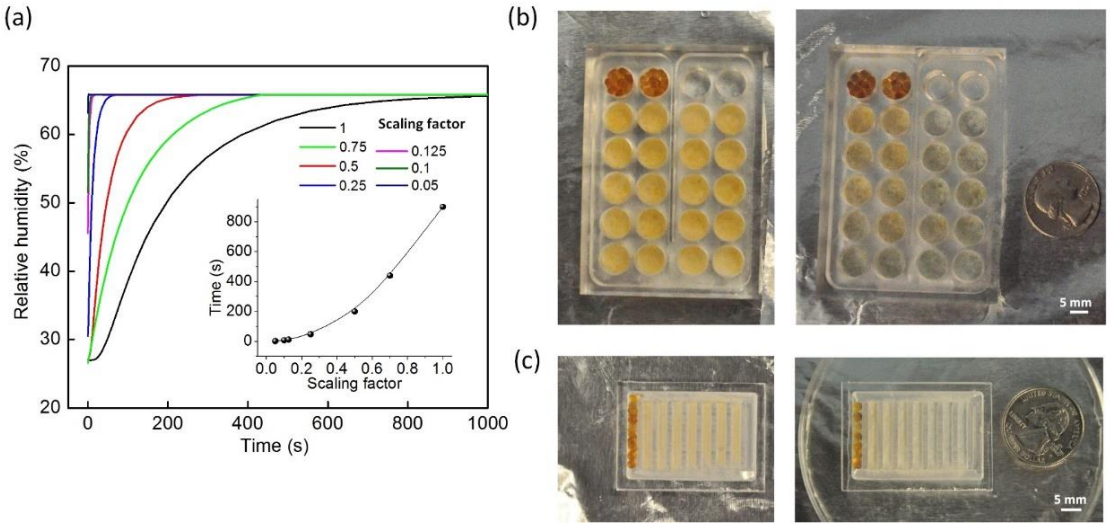

Figure 2.7 *(a) Influence of device size on dynamic humidity generation process of U-shaped device. Inset shows the stabilization time as a function of scaling factor. (b, c) Color change of a thin layer of desiccant powders laid at the bottom of the wells due to different humidity levels of the wells of the downscaled devices.*

Furthermore, by setting up the water and desiccant drying agent sources at different wells of the device, it was possible to flexibly manipulate spatial distributions of discrete humidity within the device. For example, when two desiccant sources located at two extreme ends and one water source located in the middle of the I-shaped device, a terrace-step like distribution of humidity were obtained with the highest level in the middle and the lowest (highest) one at the ends (Fig. 2.8a). In addition, arranging two sets of water and desiccant sources in the I-shaped device as shown in Fig. 2.8c led to a triangular wave-like distribution of humidity superimposed with a step-like modulation. Furthermore, by placing the water and desiccant sources in the center, edge, and/or corner of the device without any partition walls, the humidity distribution within the device could be well defined and predictable. Fig.

2.8d-f shows the discrete humidity gradients generated in three different cases, including (i) that water was loaded in the two wells near the center and the desiccant particles were loaded to the wells in four corners, (ii) that the water and desiccant particles were respectively loaded to the wells near the two short-length edges of the device, and (iii) that the water and desiccant particles located at the wells in the two diagonal corners. In addition, Fig. 8g shows that by setting up three partition walls in the top layer of the U-type device, a serpentine top freeway channel was formed, along which a discrete humidity gradient could be established.

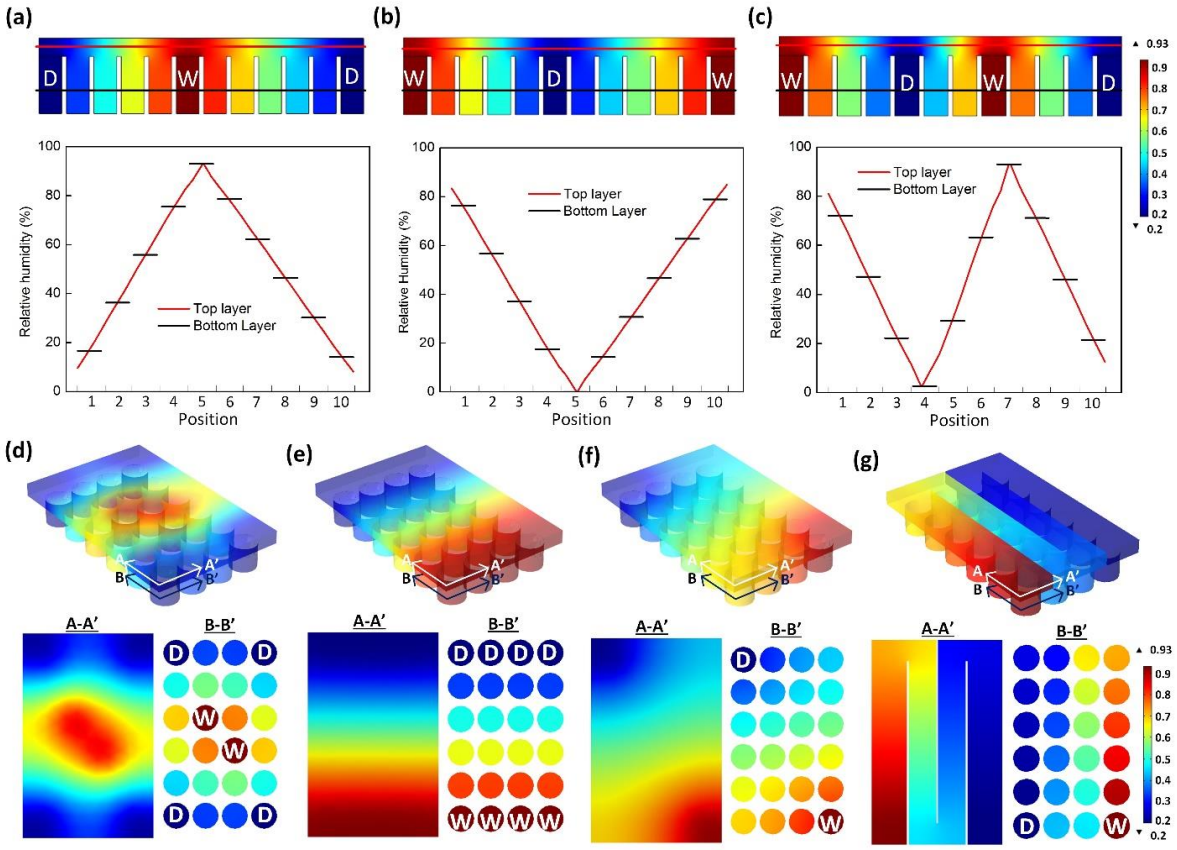

Figure 2.8 *Spatial manipulation of humidity distributions by setting up water and desiccant sources and partition walls at different locations in the I-shaped and U-shaped devices. The letters "D" and "W" represent desiccant and water sources, respectively. In (a)-(c), the plots in the lower row track humidity along the red and black lines in the top and bottom layers, respectively. In (d)-(f), the lower row show distributions of humidity in the two planes (A-A' in the top layer and B-B' in the bottom layer) labelled on each device.*

2.5 Conclusions

We have demonstrated a simple and effective new method to obtain a controlled discrete humidity gradient in miniature multi-plate like devices. The device was composed of a freeway channel in the top layer, multiple compartmented wells in the bottom layer, a water source, and a desiccant source. A stable discrete humidity gradient was generated within up to a few minutes and maintained via the combinatory effects of evaporation, convection and diffusion of water vapors inside the device. We have also demonstrated the workability of the device in studying the soybean-P.sojae interaction at various humidity conditions. Based on the visible and molecular phenotypes of soybean in responses to P. sojae, we came to the conclusion that 63% relative humidity is the most suitable for generating compatible and incompatible interactions in this plant-pathogen interaction.

The present humidity generation method provides sufficient flexibility in manipulating spatial distribution of stable discrete humidity gradient inside a miniature device. This approach can be readily translated into smaller scale devices to accommodate smaller plant species, such as Arabidopsis thaliana [33]. By considering the low cost and ease of fabrication, use, and modification of the device, this method represents a valuable platform for air humidity assay of plant seed germination and development, pathogen growth, and plant-pathogen interaction. In addition, the present device should be useful for many other biological processes where relatively rapid generation and long-term stabilization of discrete air humidity gradient are needed. We believe that the present technology will benefit many research areas including plant science, plant pathology, plant-microbe interaction, and agronomy in general.

Future work includes introduction of additional economic control mechanisms for adjusting other environmental parameters such as light and temperature in the present device

[34,35]. Such a modified humidity device will be a very powerful platform to conduct biological assays for determining role of various environmental factors in plant-pathogen, plant-microbe interactions and also in studying seed germination and plant development.

References

1. J. L. Shipp, Y. Zhang, D. W. A. Hunt and G. Ferguson, "Influence of humidity and greenhouse microclimate on the efficacy of Beauveria bassiana (Balsamo) for control of greenhouse arthropod pests." *Environmental Entomology* 32.5 (2003): 1154-1163.

2. P. B. Reich and R. G. Amundson, "Ambient levels of ozone reduce net photosynthesis in tree and crop species." *Science* 230.4725 (1985): 566-570.

3. K. A. Mott and D. F. Parkhurst, "Stomatal responses to humidity in air and helox." *Plant, Cell & Environment* 14.5 (1991): 509-515.

4. D. J. Hannusch and G. J. Boland, "Interactions of air temperature, relative humidity and biological control agents on grey mold of bean." *European Journal of Plant Pathology* 102.2 (1996): 133-142.

5. K.O. Korner and H. Challa, "Process-based humidity control regime for greenhouse crops." *Computers and Electronics in Agriculture* 39.3 (2003): 173-192.

6. K.O. Korner and H. Challa, "Temperature integration and process-based humidity control in chrysanthemum." *Computers and electronics in agriculture* 43.1 (2004): 1-21.

7. J. S. Perret, A. M. Al-Ismaili and S. S. Sablani, "Development of a humidification–dehumidification system in a quonset greenhouse for sustainable crop production in arid regions." *Biosystems engineering* 91.3 (2005): 349-359.

8. T. M. Keenan and A. Folch, "Biomolecular gradients in cell culture systems." *Lab on a Chip* 8.1 (2008): 34-57.

9. S. K. W. Dertinger, D. T. Chiu, N. L. Jeon and G. M. Whitesides, "Generation of gradients having complex shapes using microfluidic networks." *Analytical Chemistry* 73.6 (2001): 1240-1246.

10. M. A. Holden, S. Kumar, E. T. Castellana, A. Beskok and P. S. Cremer, S "Generating fixed concentration arrays in a microfluidic device." *Sensors and Actuators B: Chemical* 92.1 (2003): 199-207.

11. R. F. Ismagilov, A. D. Stroock, P. J. A. Kenis, G. Whitesides and H. A. Stone, "Experimental and theoretical scaling laws for transverse diffusive broadening in two-phase laminar flows in microchannels." *Applied Physics Letters* 76.17 (2000): 2376-2378.

12. B. R. Gorman and J. P. Wikswo, "Microscale technologies for tissue engineering and biology." *Proceedings of the National Academy of Sciences of the United States of America* 103.8 (2006): 2480-2487.

13. N. L. Jeon, H. Baskaran, S. K. W. Dertinger, G. M. Whitesides, L. Van de Water and M. Toner, "Applications of microfluidics in chemical biology." *Current opinion in chemical biology* 10.6 (2006): 584-591.

14. A. Khademhosseini, R. Langer, J. Borenstein and J. P. Vacanti, "Microscale technologies for tissue engineering and biology." *Proceedings of the National Academy of Sciences of the United States of America* 103.8 (2006): 2480-2487.

15. A. Shamloo, N. Ma, M.-m. Poo, L. L. Sohn and S. C. Heilshorn, "Endothelial cell polarization and chemotaxis in a microfluidic device." *Lab on a chip* 8.8 (2008): 1292-1299.

16. B. G. Chung, L. A. Flanagan, S. W. Rhee, P. H. Schwartz, A. P. Lee, E. S. Monuki and N. L. Jeon, "Human neural stem cell growth and differentiation in a gradient-generating microfluidic device." *Lab on a Chip* 5.4 (2005): 401-406.

17. J. Pihl, J. Sinclair, E. Sahlin, M. Karlsson, F. Petterson, J. Olofsson and O. Orwar, "Microfluidic gradient-generating device for pharmacological profiling." *Analytical Chemistry* 77.13 (2005): 3897-3903.

18. B. G. Chung, F. Lin and N. L. Jeon, "A microfluidic multi-injector for gradient generation." *Lab on a Chip* 6.6 (2006): 764-768.

19. M. S. Yang, J. Yang, C. W. Li and J. L. Zhao, "Generation of concentration gradient by controlled flow distribution and diffusive mixing in a microfluidic chip." *Lab on a Chip* 2.3 (2002): 158-163.

20. B. Mosadegh, C. Huang, J. W. Park, H. S. Shin, B. G. Chung, S.-K. Hwang, K.-H. Lee, H. J. Kim, J. Brody and N. L. Jeon, "Generation of stable complex gradients across two-dimensional surfaces and three-dimensional gels." *Langmuir* 23.22 (2007): 10910-10912.

21. V. V. Abhyankar, M. A. Lokuta, A. Huttenlocher and D. J. Beebe, "Characterization of a membrane-based gradient generator for use in cell-signaling studies." *Lab on a Chip* 6.3 (2006): 389-393.

22. T. Kang, J. Han and K. S. Lee, "Concentration gradient generator using a convective–diffusive balance." *Lab on a Chip* 8.7 (2008): 1220-1222.

23. Y. Du, J. Shim, M. Vidula, M. J. Hancock, E. Lo, B. G. Chung, J. T. Borenstein, M. Khabiry, D. M. Cropek and A. Khademhosseini, "Rapid generation of spatially and temporally controllable long-range concentration gradients in a microfluidic device." *Lab on a Chip* 9.6 (2009): 761-767.

24. A. S. Nezhad, M. Packirisamy and A. Geitmann, "Dynamic, high precision targeting of growth modulating agents is able to trigger pollen tube growth reorientation." *The Plant Journal* 80.1 (2014): 185-195.

25. J. A. Wrather and S. R. Koenning, "Estimates of disease effects on soybean yields in the United States 2003 to 2005." *Journal of nematology* 38.2 (2006): 173.

26. D. Sandhu, H. Y. Gao, S. Cianzio and M. K. Bhattacharyya, "Deletion of a disease resistance nucleotide-binding-site leucine-rich-repeat-like sequence is associated with the loss of the Phytophthora resistance gene Rps4 in soybean." *Genetics* 168.4 (2004): 2157-2167.

27. D. Sandhu, K. G. Schallock, N. Rivera-Velez, P. Lundeen, S. Cianzio and M. K. Bhattacharyya, "Soybean Phytophthora resistance gene Rps8 maps closely to the Rps3 region." *Journal of Heredity* 96.5 (2005): 536-541.

28. H. Y. Gao, N. N. Narayanan, L. Ellison and M. K. Hattacharyya, "Two classes of highly similar coiled coil-nucleotide binding-leucine rich repeat genes isolated from the Rps1-k locus encode Phytophthora resistance in soybean." *Molecular plant-microbe interactions* 18.10 (2005): 1035-1045.

29. H. Gao and M. K. Bhattacharyya, "The soybean-Phytophthora resistance locus Rps1-k encompasses coiled coil-nucleotide binding-leucine rich repeat-like genes and repetitive sequences." *BMC Plant Biology* 8.1 (2008): 29.

30. A. F. Schmitthenner, M. Hobe and R. G. Bhat, "Phytophthora sojae races in Ohio over a 10-year interval." *Plant Disease* 78.3 (1994): 269-276.

31. A. Laugier, and J. Garai, "Derivation of the ideal gas law." *J. Chem. Educ* 84.11 (2007): 1832.

32. J. S. Rowlinson, *Chemistry in Britain*. **20** (11), 1027-1027 (1984).

33. S. Kaul, et al. "Analysis of the genome sequence of the flowering plant Arabidopsis thaliana." *Nature* 408.6814 (2000): 796-815.

34. H. Jiang, Z. Xu, M. R. Aluru and L. Dong, "Plant chip for high-throughput phenotyping of Arabidopsis." *Lab on a Chip* 14.7 (2014): 1281-1293.

35. H. Jiang, Y. Jiao, M. R. Aluru and L. Dong, "Electrospun nanofibrous membranes for temperature regulation of microfluidic seed growth chips." *Journal of nanoscience and nanotechnology* 12.8 (2012): 6333-6339.

CHAPTER 3. MICROFLUIDIC CHIP FOR AUTOMATED SCREENING OF CARBON DIOXIDE CONDITIONS FOR MICROALGAL CELL GROWTH

A paper published in Biomicrofluidics

Zhen Xu, Yingjun Wang, Yuncong Chen, Martin H Spalding and Liang Dong

Abstract

This paper reports on a microfluidic device capable of screening carbon dioxide (CO_2) conditions for microalgal cell growth. The device mainly consists of a microfluidic cell culture (MCC) unit, a gas concentration gradient generator (CGG), and an in-line cell growth optical measurement unit. The MCC unit is structured with multiple aqueous-filled cell culture channels at the top layer, multiple CO_2 flow channels at the bottom, and a commercial hydrophobic gas semipermeable membrane sandwiched between the two channel layers. The CGG unit provides different CO_2 concentrations to support photosynthesis of microalgae in the culture channels. The integration of the commercial gas semipermeable membrane into the cell culture device allows rapid mass transport and uniform distribution of CO_2 inside the culture medium without using agitation-assisted convection methods, because the diffusion of CO_2 from the gas flow channels to the liquid culture channels is fast over a small length scale. In addition, automated in-line monitoring of microalgal cell growth is realized via the optical measurement unit that is able to detect changes in the light intensity transmitted through the cells grown in the culture channels. The microfluidic device also allows a simple grayscale analysis method to quantify the cell growth. The utility of the whole system is validated by growing Chlamydomonas reinhardtii cells under different low- or very-low CO_2 levels.

3.1 Introduction

Microalgae are microorganisms that can rapidly grow by using inexpensive renewable resources, such as light, CO_2, water, and certain inorganic salts, to produce biomass and oil production [1]. Compared to higher plants, microalgae have higher rates of biomass and oil production than traditional crops, due to their simple cellular structure [2]. Presently, microalgae cultivation is performed in flasks, dishes and plates [3] for laboratory research, and open raceway ponds [4] and tubular, flat and vertical photobioreactors in various pilot plants [5-9]. These systems allow small to large-scale algae cultivation to study influences of combinatorial conditions (e.g., light [10,11], temperature [12], CO_2 [13], pH [14], and nutrients [15-17]) on photosynthesis of microalgal cells. To maximize microalgal biomass and lipid production, it is critical to select and develop more efficient microalgal strains and find optimal cultivation conditions through advanced genetic and biochemical approaches and assay technologies [18]. However, traditional cultivation systems are often not suitable for rapid screening of numerous microalgal strains and their optimal growth conditions to isolate superior strains. In addition to their relatively large footprint areas, high material consumptions, and slow response times, it is considerably challenging to simultaneously create multiple sets of different environmental conditions with high accuracy and flexibility.

Microfluidics-based biotechnologies have been extensively developed to enable system miniaturization, automation, and parallelization of biochemical processes [19], as well as high-throughput culture, manipulation, and detection of cells and microorganisms [20-26]. Several microfluidic devices have been reported for on-chip cultivation, analysis, and transformation of microalgal cells under various growth conditions [27-42]. For example, toxicity screening using marine microalgal cultures in a microfluidic device was

reported.39 Microfluidic photobioreactors were also realized to study the impact of light conditions on microalgal cell growth and oil production [40,41]. In addition, microfluidic droplets were utilized to study growth kinetics of microalgae [42].

The current atmospheric CO_2 level (approximately 400 ppm, or so-called low CO_2) is one of the major limiting factors for optimal photosynthesis and biomass accumulation in many plant and algal species [43]. Microalgal cells grown under atmospheric CO_2 level (with or without active aeration) can draw more than 80% CO_2 from the medium through photosynthesis, reducing actual CO_2 level into the range of near deplete (so-called very-low CO_2 concentration) far below the nominal ambient CO_2 concentration [13,44]. Multiple acclimation states have been demonstrated in the model green alga Chlamydomonas in response to these different low- or very low-CO_2 conditions, which are driven by different inorganic carbon uptake modes and regulatory mechanism [45]. One advantage of microfluidics-based bioreactors is their small volume in which different environmental conditions can be rapidly and precisely controlled. This is especially useful to control CO_2 status for microalgal cell cultures because fast equilibrium between the gas and liquid phases can be achieved. To our knowledge, there are no any reports on development of microfluidic devices to study microalgal cell growth under various CO_2 conditions. In-line monitoring of microalgae growth has also rarely been achieved in existing microfluidic algae bioreactors.

In this paper, we report on a new microfluidic device for parallel execution of microalgal cell culture experiments and in-line monitoring of cell growth under different low- or very-low CO_2 conditions. Spatial CO_2 concentrations inside cell culture channels can be precisely obtained and uniformly distributed within only a few minutes, due to the unique integration of a hydrophobic gas semipermeable membrane into the device.

3.2 Device Design

Specifically, the device consists of a microalgal cell culture (MCC) unit, a gas concentration gradient generation (CGG) unit (Fig, 3.1a). The MCC unit is structured with multiple aqueous-filled cell culture channels at the top layer, multiple CO_2 flow channels at the bottom, and a hydrophobic gas semipermeable membrane sandwiched between these two layers (Fig. 3.1b, c). The CGG unit can generate a series of different gas concentrations to provide CO2 supplies for growing cells in the channels. The gas inlets of the MCC unit are located at the back of the unit (Fig. 3.1a). The MCC and CGG units are connected using microfluidic tubing.

The sandwiched hydrophobic gas semipermeable membrane holds the aqueous culture medium in the upper cell culture channels, while allowing CO_2 gas to diffuse from the gas flow channels into the growth medium through the embedded nanopores of this membrane. Mass transport of CO_2 into the medium is fast, as it relies on direct diffusion over a small length scale, rather than on using agitation-assisted convection methods (e.g., shaking, rotating, and bubbling) of traditional cultivation systems. Because the whole upper culture channel is exposed to the CO_2 flowing in the gas channel, the diffusion of CO_2 will lead to uniform distribution of CO2 within the aqueous-filled culture channel. In addition, the use of the nanoporous semipermeable membrane avoids large-area contact of the medium with the CO_2 flow that otherwise will cause a notorious evaporation problem often occurring with air-open microfluidic devices. Nevertheless, minor evaporation still happens at the nanopores in the membrane. To compensate for possible medium losses, two miniature reservoirs are emplaced at the inlet and outlet of each culture channel and loaded with minimal medium (Fig. 3.1). Here, the minimal medium does not have any organic carbon acetate so microalgae can only use CO_2 as carbon source. The level of medium surface in the

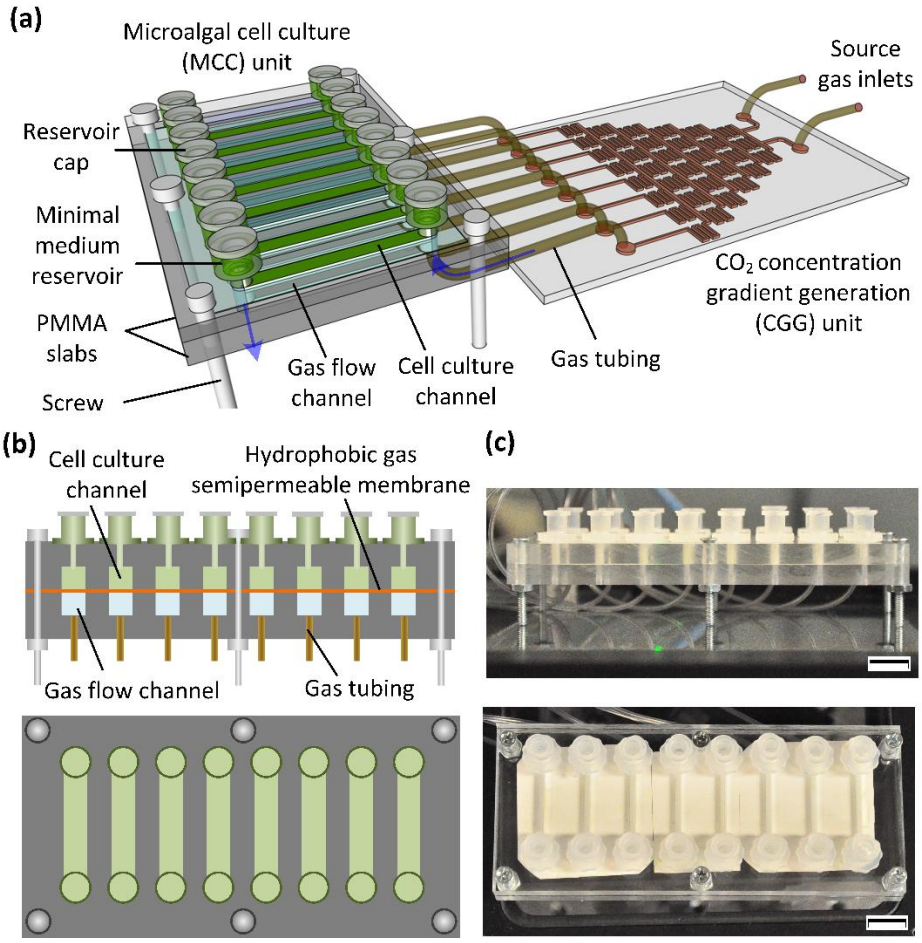

Figure 3.1 *(a) Schematic of a microfluidic device with a MCC unit and a CGG unit for growing microalgal cells under different CO2 conditions. (b, c) Side view (upper panel) and top view (lower panel) of the MCC unit (b: schematic representations; c: photos of a fabricated device). The scale bars represent 10 mm.*

reservoirs is set above the culture channel. This allows automatic refilling of the culture channel when the medium loss occurs.

Dynamic process of CO_2 diffusion from the gas flow channel to the cell culture channel was studied using a finite element analysis (FEA) based software COMSOL. The CO_2 gas diffuses through the membrane and further into the culture channel (Fig. 3.2a). The whole process was modelled using a modified transport equation as

$$\frac{\partial c}{\partial t} + \nabla \cdot (-D\nabla c) + d = 0 \qquad (3\text{-}1)$$

where c, D, and d represent the concentration, diffusivity, and constant consumption rate of CO_2, respectively [46]. The growth medium in the culture channel was in a static state. The diffusivity was set as $D = 1.44 \times 10^{-5}$ m^2/s for CO_2 to diffuse through the nanoporous membrane, and $1.92 \times 10\text{-}^{9}$ m^2/s for CO_2 to diffuse into the aqueous-filled culture channel [47]. The diffusion coefficient of PMMA of CO_2 is $D = 3.16 \times 10^{-13}$ m^2/s, which is much smaller than the diffusion coefficient in nanoporous membrane and the aqueous-filled culture channel [48]. The PMMA channels wall were treated as no-slip wall. For a normalization purpose, the constant CO_2 concentration $c = 1.0$ mol/m^3 was used. It is noteworthy that the CO_2 consumption rate of microalgal cells is significantly affected by cell photosynthesis, inducible CO_2 concentrating mechanism, and other factors [49-52]. For example, microalgal cells can actively and dynamically accumulate CO_2 at the site of ribulose-1,5-bisphosphate carboxylase-oxygenase (RuBisCO). Because of the complexity of dynamic CO_2 concentrating process inside the cell [13], it is not easy to obtain and apply a time-varying CO_2 consumption rate in Eq. (3-1). Here, to illustrate the diffusion process only, the CO_2 consumption rate was set constant at $d = 5.70 \times 10^{-10}$ $mol/(m^3 \cdot s)$ based on the information given in ref. 53. Fig. 3.2b shows the simulated time-lapse CO_2 distributions in a 500 μm-deep aqueous-filled channel above a gas semipermeable hydrophobic membrane (thickness: 200 μm; mean pore size: 220 nm). Fig. 3.2c shows that the CO_2 in the medium closer to the membrane reaches a stable level slightly earlier than that farther from the membrane. After only about 400 s, the whole culture channel has a uniformly distributed CO_2 environment.

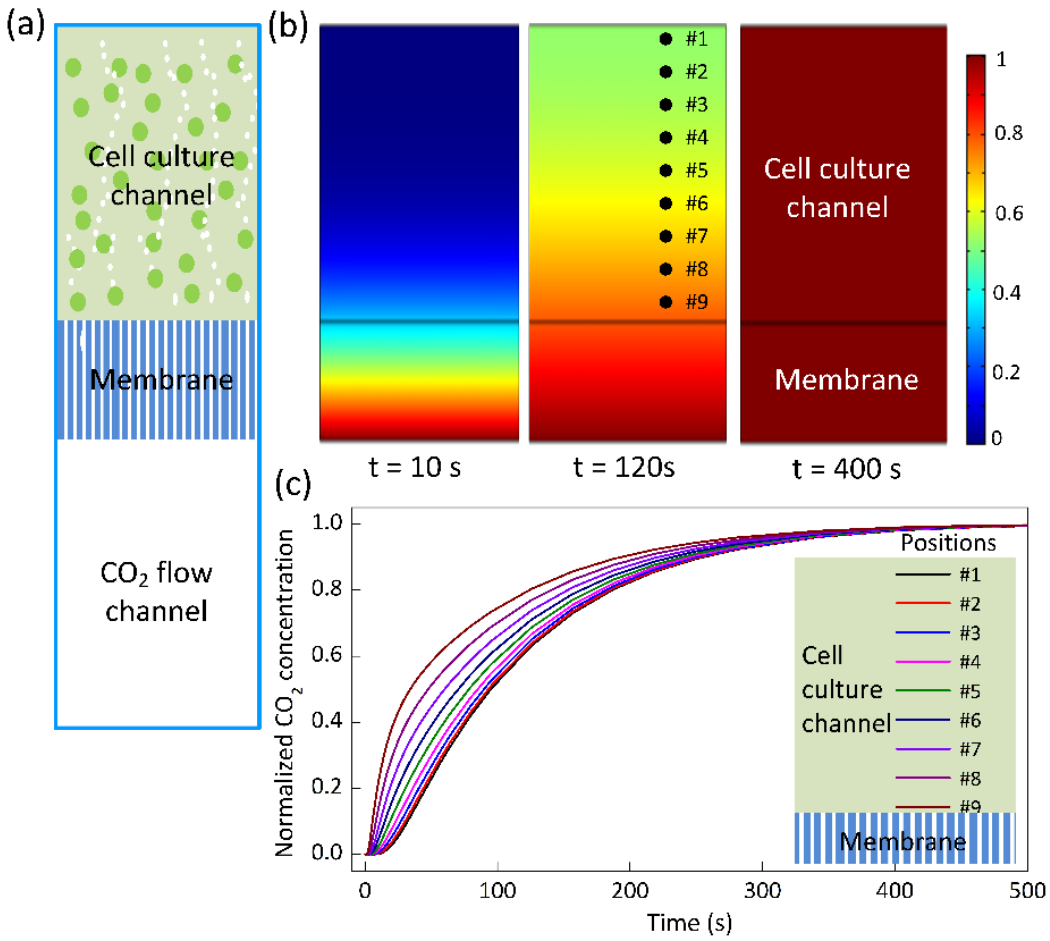

Figure 3.2 *(a) Schematic side view of a set of cell culture, gas flow channel, and hydrophobic gas semipermeable membrane. (b) Simulated time-lapse images showing the diffusion of CO2 through the membrane into an aqueous-filled culture channel with observation points #1-9. The CO2 channel is not shown here. The color bar on the right indicates the normalized CO2 concentration. (c) Simulated normalized CO2 concentration as a function of time at different sites along the height of cell culture channel. The inset shows nine different sites in the channel.*

Fig. 3.3a shows the gas CGG unit able to produce eight different CO_2 concentrations. This unit was formed with two gas inlets, eight outlets and a series of serpentine channels between the inlets and outlets [54]. All the channels in this unit were set 200 µm wide and 50 µm deep. As two source CO_2 streams (50 ppm and 280 ppm) were introduced into the device, they travelled down, repeatedly split, combined with neighboring streams, and mixed by diffusion in the serpentine channels (Fig. 3.3b). This resulted in a stable discrete gradient

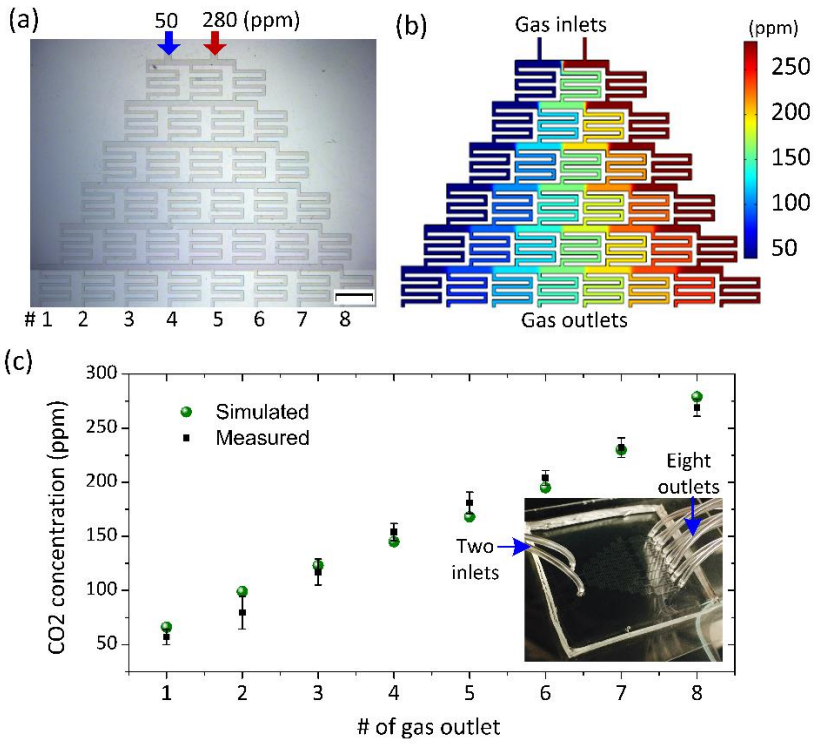

Figure 3.3 *(a) Microscopic image for the channel network of the gas CGG unit. (b) Simulated steady-state CO2 distribution. The scale bars represent 2 mm. (c) Measured and simulated CO2 levels at the outputs of the unit. The measurements were performed using a CO2 meter (Qubit Systems; Kingston, ON, Canada). The inset shows the fabricated CGG device. The result was obtained over four independent experiments with four devices.*

of CO_2 levels generated at the outlets of the device. The measured CO_2 concentrations agreed with the simulated result (Fig. 3.3c).

The cell culture and gas flow channels of the MCC unit were formed with two poly (methyl methacrylate) or PMMA plates (thickness: 0.25 inch; Plexiglas; Alsip, IL) using a milling machine (CNC Masters, Irwindale, CA). All the channels had dimensions of 0.5 mm (depth) × 1 mm (width) × 10 mm (length) and were manually aligned. The hydrophobic semipermeable membrane (thickness: 200 µm; mean pore size: 220 nm; Sterlitech; Kent, WA) was sandwiched by the PMMA plates with six cap screws (M4 × 0.7; Thorlabs; Newton, NJ). After that, 16 polypropylene reservoirs EW-45508-16; Cole-Parmer; Vernon Hills, IL) with 100 µL loading volume were glued at the ends of the culture channels. The

CGG unit was made of poly (dimethyl siloxane) or PDMS using conventional soft lithography. Finally, microfluidic tubing (Microbore PTFE tubing; 0.012" ID x 0.030" OD; Cole-Parmer, Vernon Hills, IL) was used to direct the gas flows from the outlets of the CGG to the MCC unit.

3.3 Experimental

To realize in-line monitoring of microalgal cell growth, an optical detection system (Fig. 3.4b) was built to measure transmitted light intensity (TLI) varying with growing cells in the culture channels. The detection system mainly consists of a 532-nm wavelength laser (DJ532-10; Thorlabs; Newton, NJ), a photodetector (model 1918; Newport, Irvine, CA), and a programmable motorized stage (ASI-FW1000; Applied Scientific Instrumentation, Eugene, OR). The 532-nm wavelength was chosen to minimize direct light absorption by microalgal cells [55]. The motorized stage allowed precise positioning of each culture channel under the beam spot (diameter: 0.8 mm) for the TLI measurement.

A common laboratory microalgal strain of Chlamydomonas reinhardtii (C. reinhardtii, CC620) was used as a model cell to validate the developed device. The strain was obtained from the Chlamydomonas Resource Centre and maintained on agar plates with Tris-acetate-phosphate (TAP) nutrient in a Plexiglass chamber at room temperature under light [56]. Liquid cultures were grown in flasks on an incubated orbital shaker at 125 rpm. In both the plate and liquid cultures, a 5% CO_2 flow (in air vol/vol) was maintained in the incubator.

To perform on-chip cell culture, all the device components were sterilized by filling with pure ethanol and letting them sit for 1 hr., followed by flushing the components with deionized water for 5 min and then minimal medium without carbon (consisting of 143 mg/L K_2HPO_4, 73 mg/L KH_2PO_4, 400 mg/L NH_4NO_3, 100 mg/L $MgSO_4$.7 H2O, 50 mg/L $CaCl_2 \cdot 2H_20$, 1 mL/L trace elements stock [57], and 10 mL/L 2.0 M Mops titrated with Tris

base to pH 7.1) for another 5 min. 1 mL of the strain CC620 (pre-incubated in flasks as described above) was used to mix with TAP medium in a 10-mL centrifuge tube (Corning; Corning, NY). The cells were then separated from TAP medium by centrifuging (Champion F-33V; Ample Scientific, Norcross, GA) at 2000 rpm for 5 min and mixed with 10 mL minimal medium [58].

After the cells were loaded into the culture channels using a pipette, the miniature polypropylene reservoirs were filled with the minimal medium and sealed with homemade PDMS plugs. The cells were grown under a 9-watt fluorescent lamp placed 30 cm above the culture channels. Eight CO_2 concentrations were realized at the outputs of the CGG unit (Fig. 3.3c) by infusing 50 ppm and 280 ppm source CO_2 flows into the unit through two gas flow controllers (EW-32660; Cole-Parmer, Vernon Hills, IL).

3.4 Results and Discussion

Under the generated CO_2 environments, the strain CC620 was grown in the culture channels for 48 hrs. Fig. 3.4a shows that the cell density increased differently at 48 hr, depending on the exposed CO_2 levels. To quantify the CO_2 impact, the cell growth under different CO_2 conditions was monitored using the TLI measurement setup once every 8 hrs. Ten different points were tested for each channel. Fig. 3.4c shows the relative change of TLI compared to the initial TLI value (obtained prior to cell loading with only the minimal medium in the channel). The calculation method is displayed in Fig. 3.4c where the variables of TLI_{no_cell} and TLI(t) represent the initial TLI value and the value at time t, respectively. In each channel, the cell density increased with time t owing to cell growth and division, causing to reduce the absolute value of TLI. Therefore, there appears to be an increase in the relative change of TLI over a 48-hr period under all the different CO_2 conditions (Fig. 3.4c). In addition, the relative change of TLI increased with CO_2 concentration, indicating that the

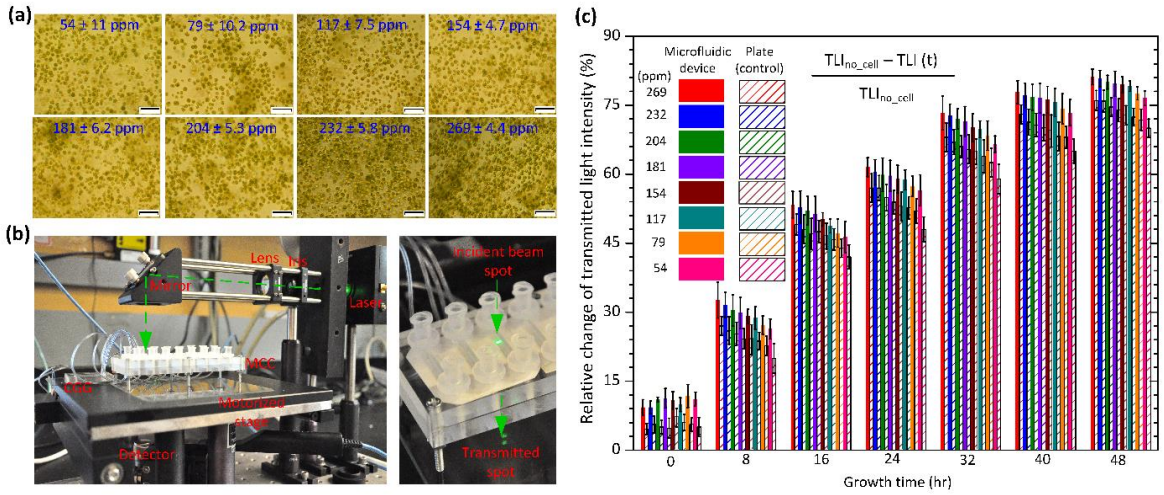

Figure 3.4 *(a) Microscopic images of C. reinhardtii strain CC620 grown in the eight channels of the MCC unit with different CO2 concentration levels labelled. The scale bars represent 40 μm. (b) TLI measurement setup (left). (c) Relative change of TLI as a function of CO2 concentration over a 48-hr period for cultivation of cells (C. reinhardtii strain CC620) in both the microfluidic device and the plates. The result was obtained over four independent experiments with four devices.*

higher CO_2 concentrations (in the tested range from 54 ppm to 269 ppm) promoted the cell growth. Specifically, at 48 hr, the relative TLI change was shown to increase from 70% at 54 ppm CO_2 concentration to 77% at 269 ppm (Fig. 3.4c).

In the control experiment, 5 ml cell suspensions (pre-incubated using the method described above) with the minimal medium were loaded in a sterile Petri dish (3.5 cm diameter; 1 cm depth; SIAL0165; Sigma-Aldrich, St. Louis, MO) emplaced inside an incubator. Eight CO_2 concentrations were provided by mixing 5% CO_2 (in air vol/vol) with dry CO_2-free air with the help of two flow controllers. The obtained CO_2 levels were the same as those used in the microfluidic culture experiment. The TLI measurement was performed outside the incubator at an 8-hr interval. It should be noted that the relative change of TLI for the control experiment exhibited an almost parallel rise over all the CO_2 levels compared to those for the on-chip growth experiment. This may be due to the larger quantity of cells initially loaded in the Petri dishes than that loaded in the microfluidic culture channels. Nevertheless, the tendencies to increase the relative change of TLI with increasing

CO_2 level agreed well between the two methods. This indicates that our device is suitable for cultivation of microalgal cells.

In addition to the TLI measurement, the present microfluidic device also allowed a simple grayscale analysis method to quantify cell growth in the channels. Such redundancy is believed to be helpful for those users who may not be able to build the in-line cell growth optical measurement unit. As the cells grew, the color of culture channel became darker. A digital camera (DFC310 FX; Leica; Wetzlar, Germany) was used to regularly take photos of the culture channels. The grayscale value (GSV; 0 = totally dark; 255 = totally bright) of the channel image was extracted by Image J (an open source image processing and analysis freeware). The change of GSV at time t was compared to its initial value at t = 0 (right after cell loading) and then further normalized by the initial GSV (see the calculation method displayed in Fig. 3.5). As shown in Fig. 3.5, under a generated CO_2 concentration, the GSV of the channel image gradually decreased in a 48-hr span, implying the increase of cell density. The higher the CO_2 concentration, the more the relative change in GSV obtained. At 48 hr, the maximum relative reduction in GSV (53%) occurred at 269 ppm and the minimum (41%) at 54 ppm. The results were also validated by the control experiment previously described, except for performing the GSV measurement in this case. Due to the different nature of the TLI and GSV methods, the obtained relative changes of TLI (Fig. 3.4c) and GSV (Fig. 3.5) are not necessary to be the same.

This work was focused on proof-of-concept for using the microfluidic device to cultivate microalgal cells under different low- or very low-CO_2 conditions. It would be the numbers of CO_2 flow and cell culture channels. It is also our interest to integrate this device with other detection methods (e.g., fluorescence) to study the lipid content of the numbers of

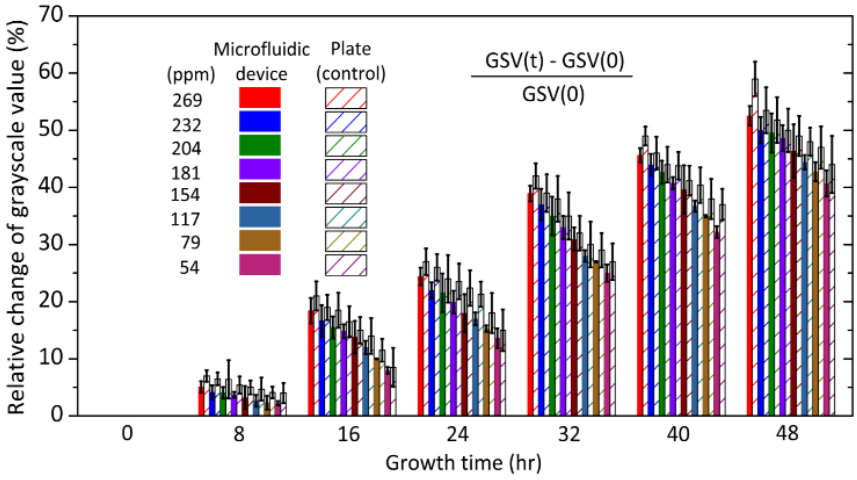

Figure 3.5 *Relative change in GSV of the images of cell culture channels containing C. reinhardtii strain CC620 growing under different CO2 levels over a 48-hr period. At time t = 0, the relative changes of GSV for all the culture channels are zero. The result was obtained over four independent experiments with four devices.*

CO_2 flow and cell culture channels. It is also our interest to integrate this device with other detection methods (e.g., fluorescence) to study the lipid content of microalgal species and strains as a function of CO_2 concentration. This will help us to better understand cellular phenomena and mechanisms (e.g., lipid metabolism, CO_2 accumulating, and environmental adaptability) controlling growth and oil content, and to find high oil producing strains. In addition, we note that although the CO_2 concentrations in the gas flow channels were measured using the commercial CO_2 sensor mentioned above, it is almost impossible to directly measure the dissolved CO_2 concentrations in the liquid growth media because the presently commercial CO_2 sensors are all too big to fit in the small culture channels. Interestingly, based on Henry's Law [59], the dissolved CO_2 concentration in the liquid culture channel is actually linear with the CO2 concentration in the gas flow channel, as the environmental temperature and air pressure are constant over time. One of our future work includes developing dissolved CO2 sensors (or pH sensors [60]) that are small enough to be embedded into the liquid culture channels of the presented microfluidic system. In addition, it would also be useful to integrate controlled chemical delivery [61,62] and temperature

control elements [63] to facilitate studying the influence of various biotic and abiotic stress on different microalgal cell species and strains.

3.5 Conclusions

We demonstrated a microfluidic device to cultivate microalgal cells under different CO_2 concentrations and perform in-line measurement of cell growth rate, which is difficult to be done in traditional large-batch growth. The integration of gas semipermeable hydrophobic membrane into the cell culture device allowed mass transportation and uniform distribution of CO_2 in culture medium within only several minutes. In addition, useful methodological redundancy for monitoring of cell growth have been developed, which will increase the adoptability of this microfluidic device by a wide range of users.

References

1. S. A. Scott, M. P. Davey, J. S. Dennis, I. Horst, C. J. Howe, D. J. Lea-Smith and A. G. Smith, "Biodiesel from algae: challenges and prospects." *Current opinion in biotechnology* 21.3 (2010): 277-286.

2. M. Packer, "Algal capture of carbon dioxide; biomass generation as a tool for greenhouse gas mitigation with reference to New Zealand energy strategy and policy." *Energy Policy* 37.9 (2009): 3428-3437.

3. A. Saeed and M. Iqbal, "Immobilization of blue green microalgae on loofa sponge to biosorb cadmium in repeated shake flask batch and continuous flow fixed bed column reactor system." *World Journal of Microbiology and Biotechnology* 22.8 (2006): 775-782.

4. O. Jorquera, A. Kiperstok, E. A. Sales, M. Embiruçu and M. L. Ghirardi, "Comparative energy life-cycle analyses of microalgal biomass production in open ponds and photobioreactors." *Bioresource technology* 101.4 (2010): 1406-1413.

5. C.Y. Chen, K.L. Yeh, R. Aisyah, D.J. Lee and J.-S. Chang, "Cultivation, photobioreactor design and harvesting of microalgae for biodiesel production: a critical review." *Bioresource technology* 102.1 (2011): 71-81.

6. D. O. Hall, F. Acién Fernández, E. C. Guerrero, K. K. Rao and E. M. Grima, "Outdoor helical tubular photobioreactors for microalgal production: Modeling of fluid‐dynamics and mass transfer and assessment of biomass productivity." *Biotechnology and bioengineering* 82.1 (2003): 62-73.

7. J. C. Ogbonna, T. Soejima and H. Tanaka, "An integrated solar and artificial light system for internal illumination of photobioreactors." *Journal of Biotechnology* 70.1 (1999): 289-297.

8. J. Pruvost, L. Pottier and J. Legrand, "Numerical investigation of hydrodynamic and mixing conditions in a torus photobioreactor." *Chemical Engineering Science* 61.14 (2006): 4476-4489.

9. C. Ugwu, H. Aoyagi and H. Uchiyama, "Photobioreactors for mass cultivation of algae." *Bioresource technology* 99.10 (2008): 4021-4028.

10. E. Collini, C. Y. Wong, K. E. Wilk, P. M. Curmi, P. Brumer and G. D. Scholes, "Coherently wired light-harvesting in photosynthetic marine algae at ambient temperature." *Nature* 463.7281 (2010): 644.

11. W. Dunstan, "A comparison of the photosynthesis—light intensity relationship in phylogenetically different marine microalgae." *Journal of Experimental Marine Biology and Ecology* 13.3 (1973): 181-187.

12. I. R. Davison, "Environmental effects on algal photosynthesis: temperature." *Journal of phycology* 27.1 (1991): 2-8.

13. P. Vance and M. H. Spalding, "Growth, photosynthesis, and gene expression in Chlamydomonas over a range of CO2 concentrations and CO2/O2 ratios: CO2 regulates multiple acclimation states." *Canadian Journal of Botany* 83.7 (2005): 796-809.

14. Y. Azov, Effect of pH on inorganic carbon uptake in algal cultures." *Applied and environmental microbiology* 43.6 (1982): 1300-1306.

15. W. A. Kratz and J. Myers, "Nutrition and growth of several blue-green algae." *American journal of botany* (1955): 282-287.

16. M. F. Pedersen and J. Borum, "Nutrient control of algal growth in estuarine waters. Nutrient limitation and the importance of nitrogen requirements and nitrogen storage among phytoplankton and species of macroalgae." *Marine Ecology progress series* (1996): 261-272.

17. J. Yang, M. Xu, X. Zhang, Q. Hu, M. Sommerfeld and Y. Chen, "Life-cycle analysis on biodiesel production from microalgae: water footprint and nutrients balance." *Bioresource technology* 102.1 (2011): 159-165.

18. R. Radakovits, R. E. Jinkerson, A. Darzins and M. C. Posewitz, "Genetic engineering of algae for enhanced biofuel production." *Eukaryotic cell* 9.4 (2010): 486-501.

19. D. Mark, S. Haeberle, G. Roth, F. von Stetten and R. Zengerle, "Microfluidic lab-on-a-chip platforms: requirements, characteristics and applications." *Microfluidics Based Microsystems*. Springer, Dordrecht, 2010. 305-376.

20. G. B. Salieb-Beugelaar, G. Simone, A. Arora, A. Philippi and A. Manz, "Latest developments in microfluidic cell biology and analysis systems." *Analytical chemistry* 82.12 (2010): 4848-4864.

21. H. Yang, X. Qiao, M.K. Bhattacharyya, and L. Dong, "Microfluidic droplet encapsulation of highly motile single zoospores for phenotypic screening of an antioomycete chemical." *Biomicrofluidics* 5.4 (2011): 044103.

22. R. A. Erickson and R. Jimenez, "Microfluidic cytometer for high-throughput measurement of photosynthetic characteristics and lipid accumulation in individual algal cells." *Lab on a Chip* 13.15 (2013): 2893-2901.

23. H. Jiang, Z. Xu, M. R. Aluru and L. Dong, "Plant chip for high-throughput phenotyping of Arabidopsis." *Lab on a Chip* 14.7 (2014): 1281-1293.

24. P. Liu, R.J. Martin and L. Dong. "Micro-electro-fluidic grids for nematodes: a lens-less, image-sensor-less approach for on-chip tracking of nematode locomotion." *Lab on a chip* 13.4 (2013): 650-661.

25. Z. Xu, H. Jiang, B. B. Sahu, S. Kambakam, P. Singh, X. Wang, Q. Wang, M. K. Bhattacharyya, and L. Dong, "Erratum:"Humidity assay for studying plant-pathogen interactions in miniature controlled discrete

humidity environments with good throughput"[Biomicrofluidics 10, 034108 (2016)]." *Biomicrofluidics* 10.5 (2016).

26. P. Liu, D. Mao, R. J. Martin, and L. Dong, "An integrated fiber-optic microfluidic device for detection of muscular force generation of microscopic nematodes." *Lab on a Chip* 12.18 (2012): 3458-3466.

27. A. Han, H. Hou, L. Li, H. S. Kim and P. de Figueiredo, "Microfabricated devices in microbial bioenergy sciences." *Trends in biotechnology* 31.4 (2013): 225-232.

28. R. E. Holcomb, L. J. Mason, K. F. Reardon, D. M. Cropek and C. S. Henry, "Culturing and investigation of stress-induced lipid accumulation in microalgae using a microfluidic device." *Analytical and bioanalytical chemistry* 400.1 (2011): 245-253.

29. D.H. Lee, C. Y. Bae, J.-I. Han and J.K. Park, "In situ analysis of heterogeneity in the lipid content of single green microalgae in alginate hydrogel microcapsules." *Analytical chemistry* 85.18 (2013): 8749-8756.

30. J. Pan, A. L. Stephenson, E. Kazamia, W. T. Huck, J. S. Dennis, A. G. Smith and C. Abell, "Quantitative tracking of the growth of individual algal cells in microdroplet compartments." *Integrative Biology* 3.10 (2011): 1043-1051.

31. A. Schaap, Y. Bellouard and T. Rohrlack, "Optofluidic lab-on-a-chip for rapid algae population screening." *Biomedical optics express* 2.3 (2011): 658-664.

32. A. Schaap, T. Rohrlack and Y. Bellouard, "Optical classification of algae species with a glass lab-on-a-chip." *Lab on a Chip* 12.8 (2012): 1527-1532.

33. D. R. Link, E. Grasland-Mongrain, A. Duri, F. Sarrazin, Z. Cheng, G. Cristobal, M. Marquez and D. A. Weitz, "Electric control of droplets in microfluidic devices." *Angewandte Chemie International Edition* 45.16 (2006): 2556-2560.

34. S. Bae, C.W. Kim, J. S. Choi, J. W. Yang and T. S. Seo, "An integrated microfluidic device for the high-throughput screening of microalgal cell culture conditions that induce high growth rate and lipid content." *Analytical and bioanalytical chemistry* 405.29 (2013): 9365-9374.

35. R. Best, S. Abalde-Cela, C. Abell, and A. G Smith, "Applications of microdroplet technology for algal biotechnology." *Current Biotechnology* 5.2 (2016): 109-117.

36. I. B. Tahirbegi, J. Ehgartner, P. Sulzer, S. Zieger, A. Kasjanow, M. Paradiso and T. Mayr, "Fast pesticide detection inside microfluidic device with integrated optical pH, oxygen sensors and algal fluorescence." *Biosensors and Bioelectron*ics 88 (2017): 188-195.

37. H. S. Kwak, J. Y. H. Kim, S. C. Na, N.L. Jeon and S. J. Sim, "Multiplex microfluidic system integrating sequential operations of microalgal lipid production." *Analyst* 141.4 (2016): 1218-1225.

38. H. S. Kim, A. R. Guzman, H. R. Thapa, T. P. Devarenne and A. Han, "A droplet microfluidics platform for rapid microalgal growth and oil production analysis." *Biotechnology and bioengineering* 113.8 (2016): 1691-1701.

39. G. Zheng, Y. Wang, Z. Wang, W. Zhong, H. Wang and Y. Li, "An integrated microfluidic device in marine microalgae culture for toxicity screening application." *Marine pollution bulletin* 72.1 (2013): 231-243.

40. M. Chen, T. Mertiri, T. Holland and A. S. Basu, Optical microplates for high-throughput screening of photosynthesis in lipid-producing algae." *Lab on a Chip* 12.20 (2012): 3870-3874.

41. H. S. Kim, T. L. Weiss, H. R. Thapa, T. P. Devarenne and A. Han, "A microfluidic photobioreactor array demonstrating high-throughput screening for microalgal oil production." *Lab on a Chip* 14.8 (2014): 1415-1425.

42. A. Dewan, J. Kim, R. H. McLean, S. A. Vanapalli and M. N. Karim, "Growth kinetics of microalgae in microfluidic static droplet arrays." *Biotechnology and bioengineering* 109.12 (2012): 2987-2996.

43. Y. Wang, D.J. Stessman, and M.H. Spalding, "The CO2 concentrating mechanism and photosynthetic carbon assimilation in limiting CO2: how Chlamydomonas works against the gradient." *The Plant Journal* 82.3 (2015): 429-448.

44. T, Yamano, K. Miura, and H. Fukuzawa, "Expression analysis of genes associated with the induction of the carbon-concentrating mechanism in Chlamydomonas reinhardtii." *Plant physiology 147*.1 (2008): 340-354.

45. Y. Wang, and M.H. Spalding, "An inorganic carbon transport system responsible for acclimation specific to air levels of CO2 in Chlamydomonas reinhardtii." *Proceedings of the National Academy of Sciences* 103.26 (2006): 10110-10115.

46. J. S. Rowlinson, *Chemistry in Britain*. **20**, 1027–1027 (1984).

47. T. R. Marrero and E. A. Mason, "Gaseous diffusion coefficients." *Journal of Physical and Chemical Reference Data* 1.1 (1972): 3-118.

48. H. Eslami, et al., Sorption and diffusion of carbon dioxide and nitrogen in poly (methyl methacrylate)." *The Journal of chemical physics* 139.12 (2013): 124902.

49. Y. Wang and M. H. Spalding, "Acclimation to very-low CO2: contribution of LCIB and LCIA to inorganic carbon uptake in Chlamydomonas reinhardtii." *Plant physiology* (2014): pp-114.

50. M. R. Badger and M. H. Spalding, "CO2 acquisition, concentration and fixation in cyanobacteria and algae." *Photosynthesis*. Springer Netherlands, 2000. 369-397.

51. G. Bozzo and B. Colman, "The induction of inorganic carbon transport and external carbonic anhydrase in Chlamydomonas reinhardtii is regulated by external CO2 concentration." *Plant, Cell & Environm*ent 23.10 (2000): 1137-1144.

52. M. R. Badger, A. Kaplan and J. A. Berry, "Internal inorganic carbon pool of Chlamydomonas reinhardtii Evidence for a carbon dioxide-concentrating mechanism." *Plant Physiology* 66.3 (1980): 407-413.

53. J. L. Gosse, M. S. Chinn, A. M. Grunden, O. I. Bernal, J. S. Jenkins, C. Yeager, S. Kosourov, M. Seibert and M. C. Flickinger, "A versatile method for preparation of hydrated microbial–latex biocatalytic coatings for gas absorption and gas evolution." *Journal of industrial microbiology & biotechnology* 39.9 (2012): 1269-1278.

54. S. K. Dertinger, D. T. Chiu, N. L. Jeon and G. M. Whitesides, "Generation of gradients having complex shapes using microfluidic networks." *Analytical Chemistry* 73.6 (2001): 1240-1246.

55. Y. Y. Huang, C. M. Beal, W. W. Cai, R. S. Ruoff and E. M. Terentjev, "Micro-Raman spectroscopy of algae: composition analysis and fluorescence background behavior." *Biotechnology and bioengineering* 105.5 (2010): 889-898.

56. D. S. Gorman and R. Levine, "Cytochrome f and plastocyanin: their sequence in the photosynthetic electron transport chain of Chlamydomonas reinhardi." *Proceedings of the National Academy of Sciences* 54.6 (1965): 1665-1669.

57. S. Surzycki, "[4] Synchronously grown cultures of Chlamydomonas reinhardi." *Methods in enzymology* 23 (1971): 67-73.

58. A. M. Geraghty, J. C. Anderson, and M. H. Spalding, "A 36 kilodalton limiting-CO 2 induced polypeptide of Chlamydomonas is distinct from the 37 kilodalton periplasmic carbonic anhydrase." *Plant physiology* 93.1 (1990): 116-121.

59. W. Gerrard, "Henry's Law and Raoult's Law." *Solubility of Gases and Liquids*. Springer US, 1976. 29-54.

60. D. Mao, P. Liu, and L. Dong, "Multichannel detection using transmissive diffraction grating sensor." *Journal of Polymer Science Part B: Polymer Physics* 49.23 (2011): 1645-1650.

61. H. Yang, W. Hong, and L. Dong, "A controlled biochemical release device with embedded nanofluidic channels." *Applied Physics Letters* 100.15 (2012): 153510.

62. H. Yang and L. Dong, "Selective nanofiber deposition using a microfluidic confinement approach." *Langmuir* 26.3 (2009): 1539-1543.

63. H.W. Jiang, Y. Jiao, M.R. Aluru, and L. Dong, "Electrospun nanofibrous membranes for temperature regulation of microfluidic seed growth chips." *Journal of nanoscience and nanotechnology* 12.8 (2012): 6333-6339.

CHAPTER 4. MULTIWELL-PLATE-BASED MICROALGAL BIOREACTOR ARRAY FOR HIGH-THROUGHPUT SCREENING OF CO2 CONCENTRATION CONDITIONS ON MICROALGAE GROWTH

A paper to be submitted to Micromachines

Zhen Xu, Yingjun Wang, Martin H Spalding, and Liang Dong

Abstract

Here, we present a high-throughput multi-well-plate-based microalgal bioreactor array to culture and screen microalgae strains grown under different carbon dioxide (CO_2) concentration conditions. The bioreactor system consists of a cell-multi-well-plate based microalgal bioreactor array, a CO_2 concentration gradient generator, and an optical screening moving stage. The customized Poly (methyl methacrylate) (PMMA) plate, including an optical routing pillar, a CO_2 inlet, a CO_2 outlet, a magnetic stir, and a growth media refilling port was fabricated. The PMMA plate was placed on the top of a traditional cell multi-well plate to construct the microalgal bioreactor array. To validate the workability of this system, Chlamydomonas reinhardtii (C. reinhardtii strains) CC620 were cultured in the developed bioreactor array, and the growth rates of cells were screened under different CO_2 concentrations. The system allows for both colorimetric analysis and transmission measurement. This work showed a potential bioreactor array for in-line screening based on microalgal culture under different CO_2 concentrations in a high-throughput way. It is believed to help accelerate the development of biorenewable energy.

4.1 Introduction

Microalgae are one of oldest microbes, living in both water columns and sediment [1]. Algal cells have a high efficiency to convert solar energy to biomass through

photosynthesis [2]. They can produce more oil for biodiesel production more efficiently than traditional crops [3-5]. Therefore, microalgae are a potential energy source of renewable energy fuel. To increase production of microalgal oil, it is important to develop better microalgae strains through genetic and bioprocess engineering to maximize efficiency of photosynthesis [6, 7]. Despite considerable efforts in recent years, significant challenges still remains including understanding how to control growth and oil content of microalgae, screening optimum environment conditions for algae growth and lipid production, and high-throughput testing methods to find high oil production strains.

Current microalgae studies are conducted by culturing microalgal cells in lab flasks [8], open raceway ponds [9-11], and photobioreactors(PBRs) [12-15]. These culture systems have enabled large scale algae growth for biofuel production. Those studies have made contributed greatly to understanding the effects of various environment factors during culturing, such as light [16], temperature [17], CO_2 [18], pH [19], and nutrients [20] on growth, photosynthesis, and hydrocarbon production. However, considering the large amount of microalgal strains and combinatorial nature of many culture factors, current conventional culture systems are less suitable for large-scale, high-throughput algae growth screening and analyzing under different environment conditions. Also, due to the large volumes of the conventional culture system, the cost is huge. Furthermore, in-line monitoring and quantification of algal growth in these culture systems is rarely achieved.

A cell multi-well culture plate, a flat plate with multiple wells, has become a standard tool in biological experiments. Because of the composition of multiple wells in a single plate, it works in a highly efficient way to conduct analytical studies. Cell culture and analysis using various multi-well plates is becoming more widely used within experimental cell

biology [21]. Many multi-well-based platforms have been developed to realize cell culture, manipulation, and detection for high-throughput bioassays. Ressler et al. developed a 24-well-plate with an interdigital electrode structure to monitor the growth of living cells. [22] Hutchinson et al. performed an automatic solid-phase microextraction (SPME) analysis system with an array of 96 SPME devices and a 96-well plate. [23] Domansky et al. investigated a high-throughput 3D liver culturing multi-well for liver toxicology and metabolism. [24] These studies have shown great promise of employing multi-well format structures to improve biological research.

In this paper, we present a high-throughput multi-well-plate-based microalgal bioreactor array system for studying microalgal growth under different CO_2 conditions. The multi-well-based design of the system realized parallelizing multiple experiments of culturing microalgal cells under different CO_2 concentrations and automatically monitoring cell growth with minimum labor. We believe this microalgal bioreactor array system can make a contribution to microalgal study.

4.2 Material and Method

4.2.1 Concept of multi-well-plate-based microalgal bioreactor

The multi-well-plate-based microalgal bioreactor is an array of microalgal bioreactor cells (Fig. 4.1a). The body of the bioreactor is a 24-well plate, covered with a customized PMMA plate. Thus, the whole bioreactor includes 24 independent microalgal bioreactor cells. Each cell consists of a culturing well, a PMMA plate, a transparent pillar, a gas inlet, a gas outlet, a media refilling tube, and a magnetic stir (Fig. 4.1b). All parts play a role in the bioreactor cell. The PMMA plate is designed to fit together perfectly with the 24-well plate. The transparent pillar works as an optical channel, transmitting white light during cell culturing and a laser during measuring. The gas inlet is set to relate to the outlet of the CO_2

concentration gradient generator, and it works as the carbon source of the culturing system. The gas outlet is sealed with a Polydimethylsiloxane (PDMS) pillar when the bioreactor is left unused. The PDMS pillar is removed once the system is in work status. The media refilling tube, which is used to refill culture media, is set to overcome evaporation issue in long-term experiments. Besides, the magnetic stir (Bel-Art Products, Wayne, NJ) is made to avoid cells settling at the bottom of the well. A single bioreactor cell simulates a natural microalgal growth environment with a specified CO_2 concentration. Therefore, the bioreactor array can be used to study microalgal growth under different CO_2 conditions identically.

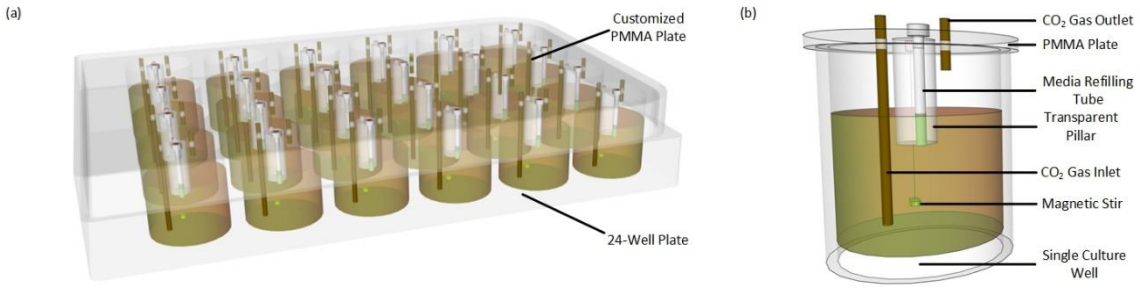

Figure 4.1 *(a) Schematic of multi-well-plate-based microalgal bioreactor. (b) Schematic of a single bioreactor well.*

4.2.2 Fabrication and assembly

The main part of the bioreactor array is the 24-well plate (Thermo Fisher Scientific, Inc; Waltham, MA). AutoCAD (Autodesk; San Rafael, CA) was introduced to design the pattern of the PMMA plate, according 24-well plate's parameters. And the plate was fabricated using a high-precision milling machine (CNC Masters; Irwindale, USA) later. Both the gas inlets and gas outlets consist of a size-to-fit steel tubing and a tygon tubing (Microbore PTFE Tubing; Cole-parmer, Vernon Hills, IL), but of different length. Then, all the parts were assembled together. Following sterilization, the bioreactor array was fitted with an O-ring. After that, a concentration gradient generator was fabricated through

traditional soft-lithograph technology using PDMS and bonded with a glass slide. Lastly, tygon tubing was used to realize the connection between the outlets of the concentration gradient generator and the gas inlets of the microalgal bioreactor array.

4.2.3 Transmitted light intensity and colorimetric detection

To achieve real-time monitoring of cell growth, a transmitted light intensity (TLI) measurement setup was built and interfaced with the cell culture device. The setup consisted of an automated moving stage (ASI-FW1000; Applied Scientific Instrumentation, Eugene, OR), a diode-pumped solid-state laser (DJ532; Thorlabs, Newton, NJ), a silicon photodetector (818-ST; Newport Corp, Irvine, CA) and a multi-function optical meter (2835-C; Newport Corp, Irvine, CA). A 532 nm wavelength laser was used to avoid direct absorption by chlorophyll. Besides, since the laser was turned on only during the measurement, its influence on algal growth was considered negligible. Time course measurement for all the culture channels was realized by placing the device on the automated moving stage. A homemade program was used to coordinate the operation of the automated stage, laser, detector, and readout devices. A laser TLI decreases with increasing cell density. Furthermore, a simple colorimetric method was also taken to estimate cell growth by taking pictures for all the growth channels using a digital camera (Leica DFC310 FX, Leica, Germany) and conducting image analysis.

4.2.4 Cell incubation and on-chip culture

To demonstrate the workability of the microalgal bioreactors array, C. reinhardtii strain CC620, a wild type of green microalgae strain, was introduced as our model microalgae. The system was used to characterize its growth under different CO_2 concentrations. C. reinhardtii strain CC620 [Chlamydomonas Resource Center] was initially maintained on an agar plate with the TAP nutrient in a Plexiglass chamber at room

temperature under ample light. Cells were moved and grown in Erlenmeyer flasks in liquid phase. All device components were treated using pure ethanol for sterilization, followed by flushing with DI water for 10 minutes and a none-carbon TAP culture medium for another 10 minutes. 1 mL C.reinhardtii strain CC620, which is mixed with TAP medium, was put in a 10 mL centrifuge tube (Corning Inc, Corning, NY), and was centrifuged (Champion F-33V; Ample Scientific, Norcross, GA) at 2000 rpm for 5 minutes. Then, the cells were separated for TAP medium, mixed with 10 mL none-carbon TAP medium in an Erlenmeyer flask.

After extracting from Erlenmeyer flask using a pipette (Finnpipette; Thermo Scientific, Pittsburgh, PA), C.reinhartii strains were loaded into a multi-well plate. The 24-well plate was covered with the PMMA plate. The gas inlets were connected to correspond CO_2 concentration gradient generator's outlets and the media refilling ports were sealed with PDMS plugs. The plate was placed on the automated stage for in-line monitoring and an external magnetic field was applied under the plate.

Different CO_2 concentration conditions, ranging from 50 ppm to 300 ppm, were created using the concentration gradient generator. To realize this, the two inlets of the concentration gradient generator were respectively connected with two gas cylinders with different CO_2 concentration, one is 50 ppm and the other is 300 ppm. The flow rates of the input gas flows were controlled by two mass flow controllers (Cole-Parmer, Vernon Hills, IL).

4.3 Results

C. reinhardtii strains CC620 in microalgal bioreactor array were cultured and screened for 10 days under eight different CO_2 concentrations to study effect of CO_2 concentration on algal growth. The growth of strains was characterized by tracking each well's cell density over time. Two methods, measuring total cell area percentage using an

image software (Image J) and measuring light intensity transmission rate of each culture well, were used to analyse the cell density.

One study was taken to analyse the algal growth in a CO_2 concentration 50 ppm. The cell density increased greatly after 10 days' culture. Strain cells covered the whole area gradually (Figure 4.2a). ImageJ was used for quantitative analysis. The result showed cell density keeping increasing in the first 4 days and curve going flat after that (Figure4. 2b). After 10 days culturing, the total cell area percentage reach 57.5% while it was only 0.17% at the first day. The growth rate was high during the first 4 days because of the low cell density and plenteous growth media. Then the growth rate reduced to a very low level in the next 6 days, when maximum cell density was achieved due to limited space and limited growth media in the bioreactor system. Light intensity measurement indicated consistent results, the light intensity transmission rate reduced rapidly at the first 4 days and kept in a low reduction rate after that. Comparing the 59% light intensity transmission rate at day 0, it was only 0.65% at day 10 as the cell density increased. Thus, two methods mutually verified their results, and both indicated similar growth tendency about algal cell density in 50 ppm CO_2 environment.

Another study was about the growth statusof algal cells under different CO_2 concentrations. Figure 4.2a shows the cell images under 8 different CO_2 concentrations in day 10. Here, the total cell area percentages under different CO_2 concentration were calculated. The cell density increased with the increase of CO_2 concentration. A higher CO_2 concentration leaded to a higher cell density. The cell density under 272 ppm CO_2 concentration is 55.6% higher than the value under 50 ppm CO_2 concentration(Figure 4.3b).

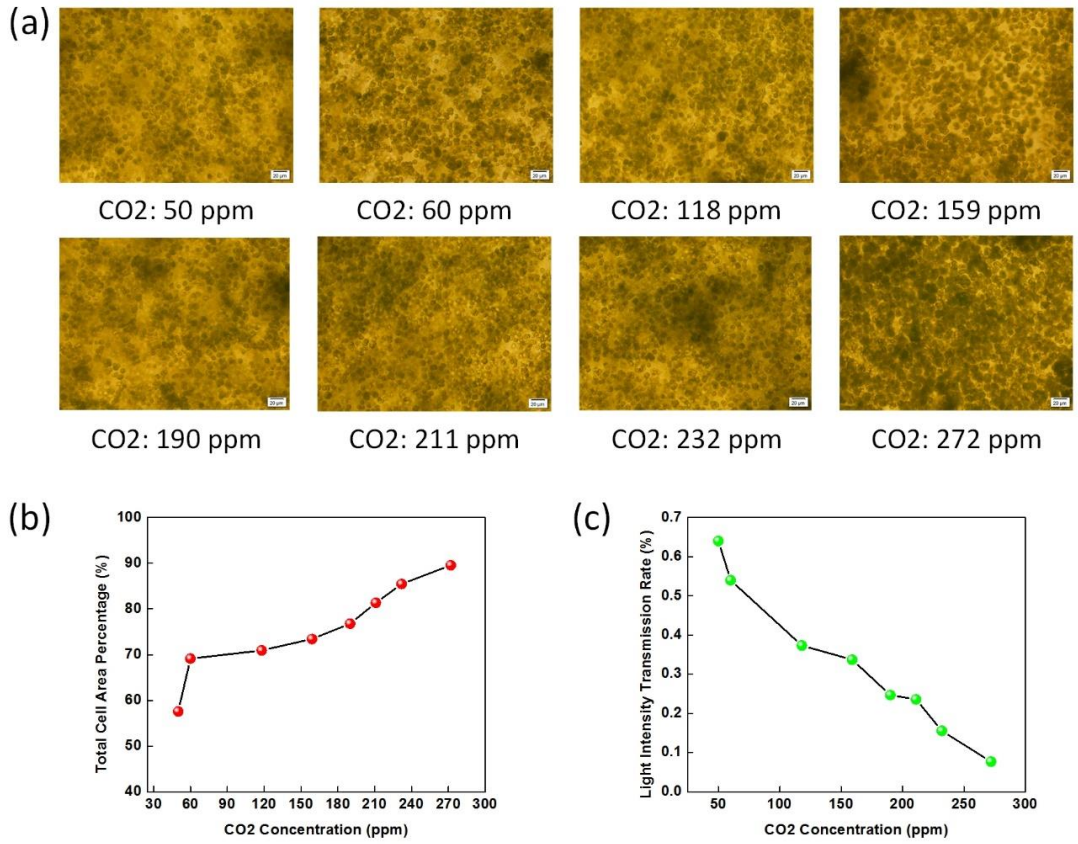

Figure 4.2 *(a) Images of C. reinhardtii strains culturing at day 10 under CO2 concentration 50 ppm, 60 ppm, 118 ppm, 159 ppm, 190 ppm, 211 ppm, 232 ppm, 272 ppm. (b) Total algal cell area for the growth images in all wells after 10-day culturing. (c) Light intensity transmission rate for all algal bioreactor wells after 10-day culturing. Scale bar: 20 µm.*

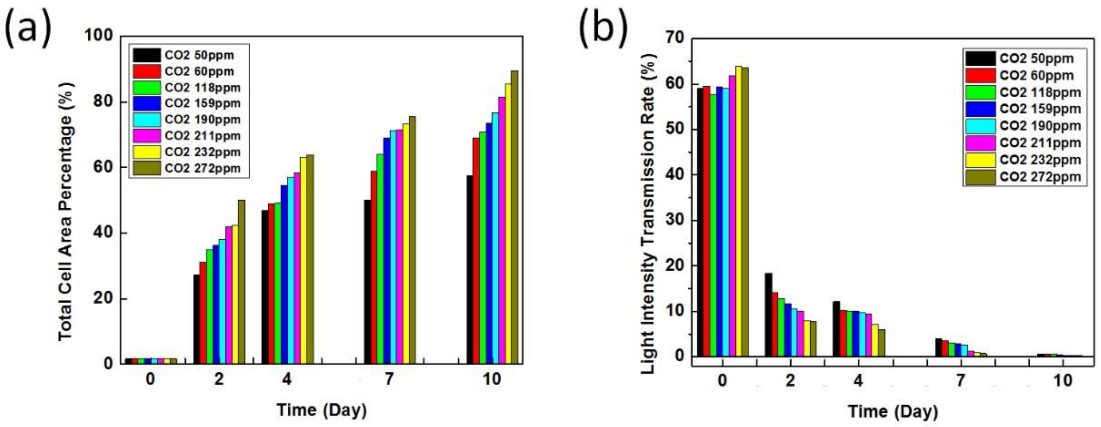

Figure 4.3 *(a) Total algal cells area percentage analysis for all bioreactors for 10 days. (b) Light intensity transmission rate for all bioreactor for 10 days.*

Another measurement based on light intensity transmission presented a close result. The light intensity transmission rate reduced from 0.64% to 0.076% while CO_2 concentration increased from 50 ppm to 272 ppm. The algal cells grew best when the CO_2 concentration is 272 ppm. As a result, CO_2 concentration effected algal growth rate under low CO_2 concentration environment (50 ppm to 300 ppm) and a higher CO_2 concentration lead to a higher growth rate of algal cell.

4.4 Discussion

Here, we have presented a high-throughput multi-well-based microalgal bioreactor array and validated the array to study C. reinhardtii strains CC620 growth under eight different CO_2 conditions. By introducing of a customized PMMA plate with functional components, including a transparent pillar, a magnetic stir, and a media refilling tube, long-term observation and real-time analysis were achieved. Comparing with traditional conventional PBRs, the bioreactor array applied identical control factors to all culture wells to investigate variable factor in a high-throughput and low-cost way.

Different from conventional PBRs, the volume of single bioreactor well is only on the scale of three milliliters. Thus, one CO_2 condition requires 5 mL of media, considering evaporation during testing, almost 160 times less than nutrient consumption compared to current conventional PBRs (800 mL/5 mL = 160). What is more, the total volume of a 24-well microalgal bioreactor array is only 265.625 mL (12.5 cm (Length) * 8.5 cm (Width) * 2.5 cm (Height)), which is equal or smaller less the volume of one traditional conventional PBR. More importantly, the miniaturized device with allows for many advantages, including faster CO_2 mass transportation, easily generated CO_2 concentration gradient environment, and in-line monitor convenience. Therefore, the small-scale device will allow many growth conditions to be built at a single time in a single device, which often is difficult to be done in

large batch growth, as it is now utilized.

Current study is focused on the effect of different CO_2 concentration for one single microalgae strain. With simple modification, the microalgal bioreactor array can be used to investigate multiple strains growth under same or multiple environment factors in the future. For instance, the gas inlets can be connected a specified CO_2 concentration to study multiple strains growth under same CO_2 concentration. Furthermore, the bioreactor array can be extended to build an integrated bioreactor to simulate natural microalgal growth environment with multiple controllable factors, including CO_2 concentration, light condition, pH value, temperature and nutrient.

4.5 Conclusions

A high-throughput multi-well-plate-based microalgal bioreactors was developed to study growth of microalgae under eight different CO_2 concentrations in parallel. The bioreactors have an observation optical pillar, a built-in magnetic stir, a gas inlet, a gas outlet, and a media refilling port in each identical well. A wild type microalgae strain, C. reinhardtii strain CC620, was cultured and analysed using the developed platform under differentCO_2 conditions. The results indicated different growth rates of C. reinhardtii strain cells under different CO_2 conditions. Comparing with traditional conventional PBRs, the system simulated a natural growth environment for microalgae and achieved real-time screening, with higher throughput and lower cost. Although we only demonstrated the design and function based on a 24-well plate, the concept is scalable to a larger system using plates with more wells, such as a 96-well plate. We hope that this developed platform can be used as a powerful tool helping algal growth investigation, especially analysing under different CO_2

concentrations and other culture factors within significantly lower material consumption and shorter time, which would accelerate developing processing of biorenewable fuel.

References

1. H.V. Thurman, and A.B. Elizabeth, *Introductory oceanography*. New Jersey: Prentice Hall, 1997.

2. P.M. Schenk, et al. "Second generation biofuels: high-efficiency microalgae for biodiesel production." *Bioenergy research* 1.1 (2008): 20-43.

3. T.M. Mata, A.M. Antonio and S.C. Nidia, "Microalgae for biodiesel production and other applications: a review." *Renewable and sustainable energy reviews* 14.1 (2010): 217-232.

4. Y. Chisti, "Biodiesel from microalgae." *Biotechnology advances* 25.3 (2007): 294-306.

5. Y. Chisti, "Biodiesel from microalgae beats bioethanol." *Trends in biotechnology* 26.3 (2008): 126-131.

6. R. Harun, et al. "Bioprocess engineering of microalgae to produce a variety of consumer products." *Renewable and Sustainable Energy Reviews* 14.3 (2010): 1037-1047.

7. K. Srirangan, M.E. Pyne, and C.P. Chou. "Biochemical and genetic engineering strategies to enhance hydrogen production in photosynthetic algae and cyanobacteria." *Bioresource technology* 102.18 (2011): 8589-8604.

8. A. Saeed, and M. Iqbal. "Immobilization of blue green microalgae on loofa sponge to biosorb cadmium in repeated shake flask batch and continuous flow fixed bed column reactor system." *World Journal of Microbiology and Biotechnology* 22.8 (2006): 775-782.

9. S. Boussiba, et al. "Outdoor cultivation of the marine microalga Isochrysis galbana in open reactors." *Aquaculture* 72.3-4 (1988): 247-253.

10. E.M. Radmann, C.O. Reinehr, and J.A.V. Costa. "Optimization of the repeated batch cultivation of microalga Spirulina platensis in open raceway ponds." *Aquaculture* 265.1 (2007): 118-126.

11. M.A. Borowitzka, "Commercial production of microalgae: ponds, tanks, tubes and fermenters." *Journal of biotechnology* 70.1 (1999): 313-321.

12. C.Y. Chen, et al. "Cultivation, photobioreactor design and harvesting of microalgae for biodiesel production: a critical review." *Bioresource technology* 102.1 (2011): 71-81.

13. J. Degen, et al. "A novel airlift photobioreactor with baffles for improved light utilization through the flashing light effect." *Journal of biotechnology* 92.2 (2001): 89-94.

14. D.O. Hall, et al. "Outdoor helical tubular photobioreactors for microalgal production: Modeling of fluid‐dynamics and mass transfer and assessment of biomass productivity." *Biotechnology and bioengineering* 82.1 (2003): 62-73.

15. M. Harker, A.J. Tsavalos, and A.J. Young. "Autotrophic growth and carotenoid production of Haematococcus pluvialis in a 30 liter air-lift photobioreactor." *Journal of Fermentation and Bioengineering* 82.2 (1996): 113-118.

16. E. Collini, et al. "Coherently wired light-harvesting in photosynthetic marine algae at ambient temperature." *Nature* 463.7281 (2010): 644.

17. I.R. Davison, "Environmental effects on algal photosynthesis: temperature." *Journal of phycology* 27.1 (1991): 2-8.

18. P. Vance, and M.H. Spalding. "Growth, photosynthesis, and gene expression in Chlamydomonas over a range of CO2 concentrations and CO2/O2 ratios: CO2 regulates multiple acclimation states." *Canadian Journal of Botany* 83.7 (2005): 796-809.

19. Y. Azov, "Effect of pH on inorganic carbon uptake in algal cultures." *Applied and environmental microbiology* 43.6 (1982): 1300-1306.

20. W.A. Kratz, and J. Myers. "Nutrition and growth of several blue-green algae." *American journal of botany* (1955): 282-287.

21. D. Vuckovic, "High-throughput solid-phase microextraction in multi-well-plate format." *TrAC Trends in Analytical Chemistry* 45 (2013): 136-153.

22. J. Ressler, et al. "New concepts for chip-supported multi-well-plates: realization of a 24-well-plate with integrated impedance-sensors for functional cellular screening applications and automated microscope aided cell-based assays." *Engineering in Medicine and Biology Society*, 2004. IEMBS'04. 26th Annual International Conference of the IEEE. Vol. 1. IEEE, 2004.

23. J.P. Hutchinson, L. Setkova, and J. Pawliszyn. "Automation of solid-phase microextraction on a 96-well plate format." *Journal of Chromatography A* 1149.2 (2007): 127-137.

24. K. Domansky, et al. "Perfused multiwell plate for 3D liver tissue engineering." *Lab on a chip* 10.1 (2010): 51-58.

CHAPTER 5. NUTRIENT SENSING USING CHIP SCALE ELECTROPHORESIS AND IN SITU SOIL SOLUTION EXTRACTION

A paper published in *IEEE Sensors Journal*

Zhen Xu, Xinran Wang, Robert J. Weber, Fellow, IEEE, Ratnesh Kumar, and Liang Dong

Abstract

This paper reports an electrophoresis based microfluidic ion nutrient sensor for the detection of anions in soil solution samples. The sensor is able to analyze concentration of various anions in extracted soil solutions with high sensitivity as well as high specificity, while it is an approach requiring no labels. The electrophoretic microchip integrates a pair of in-plane conductivity detection microelectrodes. A programmable high voltage power supply unit was designed to achieve precise control over voltage potentials needed for sample and buffer injection and ion separation. An electrical conductivity detector was designed to extract and process the changes in conductivity due to the arrivals of separated anions at the electrodes at various times. An arrival time serves to identify an anionic species, while the peak height indicates the concentration. A soil water extraction device was also designed to extract the soil solution analyte from the bulk soil, by applying vacuum suction. Only a minute amount of solution (on the order of μL) is needed for the electrophoretic measurement. Extracted soil solutions were analyzed for ionic concentrations to demonstrate the feasibility of using this microfluidic sensor, showing a limit of detection of about 7.25 μM.

5.1 Introduction

Sensors-enabled nutrient management for sustainable agriculture is of great societal interest [1-4]. In fact, “managing the nitrogen-cycle” is one of the 14 grand challenges put forth by the U.S. National Academy of Engineering. By measuring the available plant

nutrients in soil, a more precise nutrient application can be achieved in farming [5, 6]. Sensing the changes in the nutrient ion concentrations is vital for providing the nutrient-sufficient conditions for a maximal plant growth and yield [7]. Therefore, a soil nutrient sensor is important for optimizing nutrient management.

Over the past two decades, many types of soil sensors have been developed to monitor soil properties, including soil moisture [8, 9], pH [10], temperature [11], heavy metal [12], and nutrients [14]. These span various measurement techniques include electrical [8, 14], electromagnetic [15], optical [16], radiometric [17], mechanical [18], acoustic [19], or electrochemical [20]. For the detection of nutrient ions in the soil, common measurement practices include the use of ion chromatography [21], spectrophotometry [22], ion-selective electrodes (ISEs), and electrochemical sensors [23]. Among these, chromatography and spectrophotometry are limited to laboratory settings, while the goal here is design of affordable sensors for site-specific and real-time measurements. ISE-based sensors are field deployable and can convert the activity of a specific ion in a solution into an electrical signal [24]. They, however, rely on specific ion-selective membranes that may degrade over time or may not even be available for certain ions (e.g., for phosphorous ions PO43-). Enzymatic electrochemical sensors, using an ion-specific enzyme for molecular recognition, have also been developed to realize detection of a specific ion [25]. Similar to ISEs, this type of sensors are affected by their life time and the availability of the ion-specific enzymes.

To address the issues of sensor life and stability, limited by the recognition agent employed, here we present a label-free design based on the electrophoretic separation of ions and electrical measurements of the conductivity at the end of the electrophoretic channel.

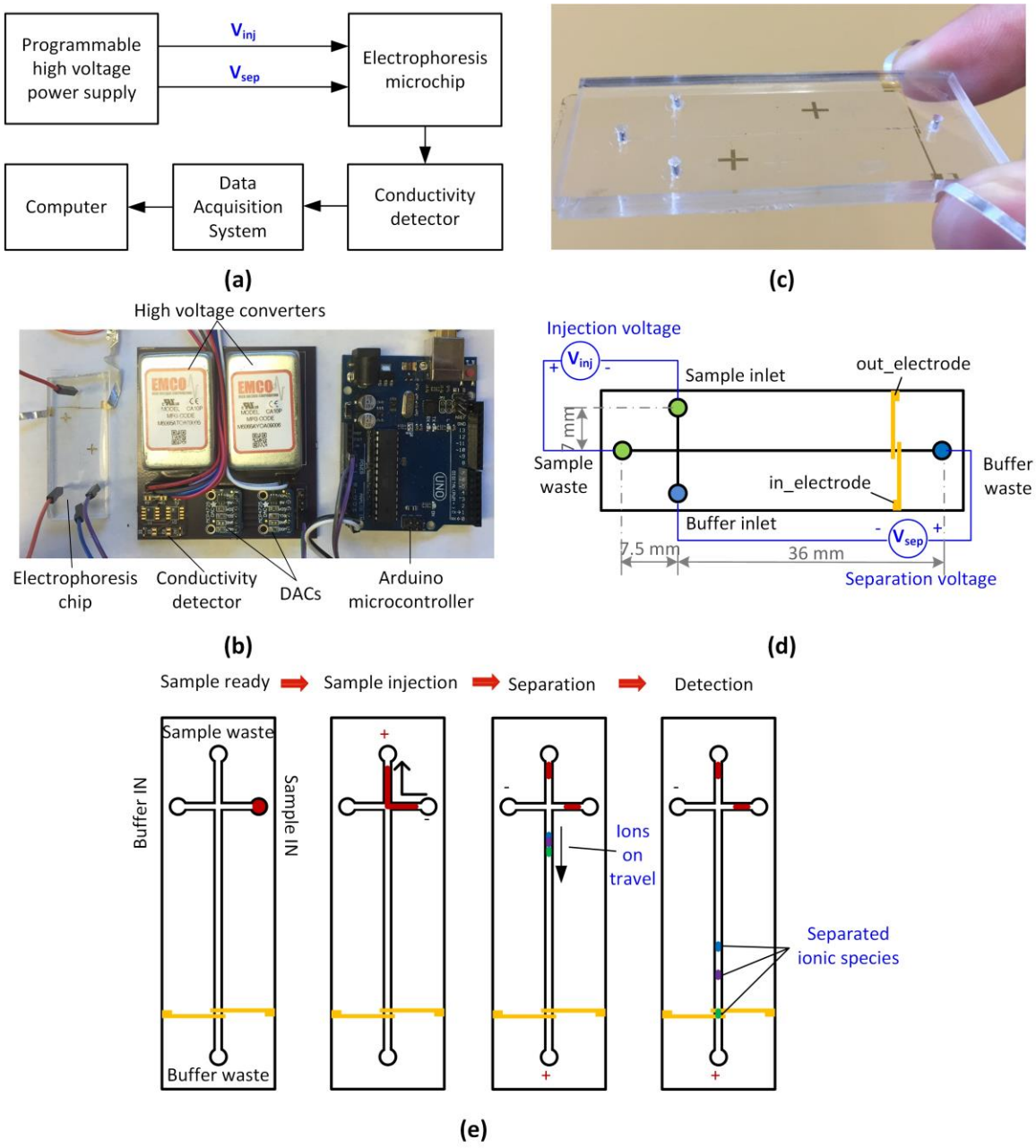

Figure 5.1 *(a) Schematic of the microfluidic electrophoretic ion sensor system. (b) Photograph of the developed microfluidic electrophoretic ion sensor system consisting of an electrophoresis microchip, a customized printed circuit board (PCB) integrating the two programmable precision high voltage power supply units, a conductivity detection unit, and an Arduino microcontroller. (c) Photograph of the fabricated electrophoresis microchip. (d) Schematic of an electrophoresis microchip, in_electrode is connected to the sinusoidal input and out_electrode is connected to the conductivity detection circuit. (e) Schematic of the operation steps of sampling injection, ion separation, and conductivity detection.*

There exist other prior applications of electrophoretic separation-based sensing. For example, capillary electrophoresis has been used for DNA separation [26], monitoring chemical reactions [27], biomolecules analysis [28], and clinical diagnostics [29]. These applications rely on the fact that bio-particles exhibit different mobility characteristics under an electric potential [30]. The commercial electrophoresis instruments with classic capillaries are often equipped with optical absorption or fluorescence detectors [31-34] and allow for a single-molecule level sensitivity but are bulky and not meant for field applications [35]. Keeping miniaturization and portability in mind, microfluidic devices for chemical analysis and biological assays have recently received considerable attention [36]. In particular, microchip-scale electrophoresis for separation and detection has been studied for many applications and is considerably compact [37-40]. In contrast to the commercial electrophoresis instruments, the microchip-based electrophoresis devices integrate simple and effective electrical detection methods [41]. This allows downscaling the detector size without scarifying sensitivity. While many microfluidic electrophoretic devices have been reported as cited above, the application to soil nutrient detection remains limited.

This paper reports a microfluidic electrophoretic nutrient sensor system capable of separating and quantifying inorganic anions in minute (micro-liter) amounts of soil solution samples. A vacuum suction-based soil solution extraction unit was also designed to enable in situ application. Different ions were separated as they travel along an electrophoretic channel under the influence of an applied electrical field, owing to their differential electrical mobilities. The sensor system includes a microfluidic electrophoresis chip with microelectrodes, a voltage application control unit, and an electrical conductivity measurement unit, all of which were designed and implemented (Fig. 5.1(a), (b)). A mixture

of anions in the extracted soil water, including chloride (Cl^-), nitrate (NO_3^-), sulfate (SO_4^{2-}), dihydrogen phosphate ($H_2PO_4^-$), was successfully separated and detected using the developed system, showing ion separation based on travel time along the electrophoretic microchannel, with the detection peak levels corresponding to the ion concentrations. As this device required only a minute amount of the extracted soil solution on the order of microliters, the sensor would make a negligible response to the measured environment. The detected ions contain the most important elements for plant growth, such as Nitrogen (N), Phosphorus (P), and Sulfur (S). Therefore, the developed sensing system has the potential to monitor soil's nutritional health. As mentioned above, no labeling process of analyte-recognition is necessary for the presented sensing approach. In addition, the design of the soil water solution extraction unit makes the overall system suitable for an in-situ application.

5.2 Principle and Design

5.2.1 Principle

The electrophoretic separation of the ions in a solution takes place due to the differences in the ion mobilities under the influence of an applied electric field. The two together determine the velocity of an ion in an electrophoretic channel:

$$v = \mu_e E \tag{5-1}$$

where v is the ion velocity, μ_e is the electrophoretic mobility, and E is the applied electric field [42]. The buffer solution used in the electrophoresis microchannel also admits an electro-osmotic flow (EOF) under the influence of the same electric field [43]. The EOF is superimposed with the ionic mobility to determine an analyte's overall electrophoretic migration rate and may reinforce or oppose it [44]. Hence, the net ion-velocity v_{net} is:

$$v_{net} = (\mu_e \pm \mu_{EOF})E \quad (5\text{-}2)$$

where μ_{EOF} denotes the EOF mobility. Accordingly, different ionic species arrive at and pass through a detector at different time points while traveling through the electrophoretic microchannel. An electrical conductivity measurement at the microelectrodes, placed at the far end of the microchannel, is a simple means to detect the arrival time and the concentrations of the separated ions. As the ions pass through the detection area, the concentrations of ionic species in the detection area change, thus changing the measured electrical conductivity. These ionic separations and the corresponding changes in the conductivity measurements show up as multiple peaks in a plot of conductivity versus time. At the low concentrations of our setting, the conductivity at any given time is given by [45]:

$$\kappa = \sum_i c_i |z_i| \lambda_i \quad (5\text{-}3)$$

where κ is the electrolytic conductivity measured at the electrodes, c_i is the molar concentration of the ionic species i in the solution, z_i is the ionic charge, and λ_i is the equivalent conductance of the i^{th} ion species.

5.2.2 Electrophoretic Microchip

The designed electrophoresis microchip is shown in Fig. 5.1(c), with its schematic shown in Fig. 5.1(d). The microchip has the dimensions of 50 mm (length) × 25 mm (width) × 4 mm (height) and is made of polydimethylsiloxane (PDMS) laid over a thin 130 µm-thick glass slide that is deposited with two gold microelectrodes on the face opposite to the PDMS layer. Two perpendicular intersecting microfluidic channels are located within the PDMS layer. The shorter channel (length: 14 mm) is used for sample loading while the longer one (length: 43.5 mm) for the ion separation. Both the channels are 200 µm wide and 50 µm

deep. The two gold microelectrodes, that are formed on the flip side of the glass substrate, are each 400 µm wide, and orthogonally crossed with the separation channel. The gap between the two microelectrodes is 200 µm [46]. Two sample and buffer inlets, and their corresponding outlets are located at the ends of the loading and the separation channels, respectively. Fig. 5.1(e) shows the fluid manipulation processes for the buffer and the analyte solutions, and to separate the ions in the analyte solution using electrophoresis.

5.2.3 Fabrication Process

The fabrication process for the microchip is schematically shown in Fig. 5.2. First, the detection electrode materials, consisting of 5 nm titanium and 80 nm gold, were sputtered on the surface of the thin glass substrate (60 mm × 25 mm × 0.13 mm, Superslip® cover glasses, Ted Pella, Redding, CA). Subsequently, a 1.5 µm-thick photoresist (AZ 5214, MicroChem Corp, Westborough, MA) was spin-coated on the device surface and then photo-patterned by conventional photolithography. After removal of titanium and gold from the unwanted area using an etchant solution (GE-8148, Transene, Danvers, MA), the device was flushed with acetone to thoroughly remove the remaining photoresist. Thereby, the microelectrodes were formed.

Next, separately, the PDMS microchannels were fabricated using soft lithography. For this step, a silicon wafer with photoresist SU-8 (3050; MicroChem, Westborough, MA) was spin-coated at 3000 rpm for 30 s to generate 50 µm-thick SU-8 on the surface. Then, the wafer was baked at 65 °C for 5 min and 90 °C for 1 hr. Subsequently, the wafer was exposed to an ultraviolet light with another photomask, baked at 90 °C for 30 min, and developed to form a master mold for the microfluidic channels. Following that, PDMS solution and its curing agent (Sylgard 184, Dow Corning, Auburn, MI) with a weight ratio of 10:1 was mixed, degassed, poured on the master mold and thermally cured at 70 °C for 2 hr on a

hotplate. The PDMS channel layer was peeled off and necessary holes were formed using a manual punch. Finally, the thin glass substrate was bonded with the PDMS channel layer by 10 sec oxygen plasma treatment using a FEMTO Plasma Cleaner (8 psi; 100 watts; Diener Electronic, Ebhausen, Germany).

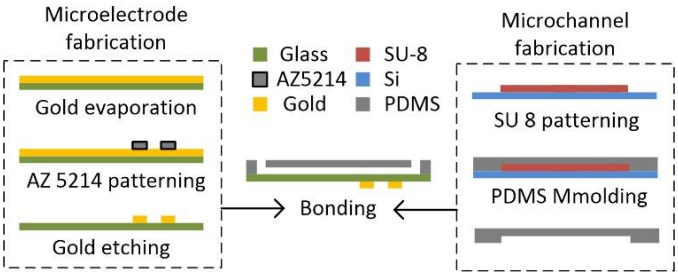

Figure 5.2 *Fabrication process for a microfluidic electrophoresis chip. A side view of the slice along the channel is shown.*

5.2.4 Programmable High-Voltage Power Supply Unit

A programmable power supply unit was designed to provide precise electrical potentials to load a sample solution and separate ions. The unit, shown in Fig. 5.1b and Fig. 5.3, includes three main parts: Two high voltage DC to DC converters (CA10P, XP EMCO, Sutter Creek, CA), two digital to analog converters (DACs, MCP4725, Adafruit Industries, New York City, NY), and an Arduino microcontroller. The microcontroller controls the two sets of DACs and DC to DC converters, with one set providing a DC voltage V_{inj} between the sample inlet and the sample waste outlet, and the other providing another DC voltage V_{sep} between the buffer inlet and the buffer waste outlet, as shown in Fig. 5.1(d). Specifically, the microcontroller provides a digital control output, which is converted to an analog DC voltage between 0 and 5 V by the DAC. The DC-to-DC high voltage module elevates the low DC voltage to a high DC voltage up to 1000 V linearly. Therefore, the voltage values V_{inj} and V_{sep} can be obtained and flexibly programmed. Two pairs of copper electric wires are

inserted into the corresponding inlets and outlets for applying the two voltages for the sample injection and the ion separation.

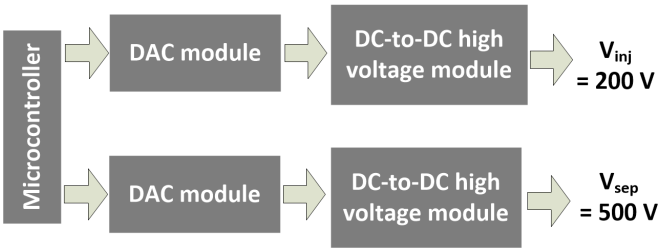

Figure 5.3 *A precision high voltage power supply designed to control the voltages for sample injection and ion separation.*

5.2.5 Conductivity detection unit

An electrical circuit model for the two microelectrodes-based detection region of the electrophoretic microchip consists of a bulk solution resistor (R_S), two parasitic capacitors (C_S) and a bypass capacitor (C_W) between the two microelectrodes, as shown in the red-dashed area of the left side of Fig. 5.4(a). This equivalent circuit was integrated with the conductivity detection unit, as shown in the blue-dashed areas in Fig. 5.4(a). The conductivity detection circuit was designed based on the principle of capacitively coupled conductivity detection (C4D) [47, 48]. The signal generator provides a sinusoidal signal of 5 mV_{p-p} on one microelectrode of the electrophoretic microchip, while its response is measured at the second microelectrode, through an I-V converter, a rectifier, and a low-pass filter. Thus, besides the sinusoidal activation, the conductivity detection circuit is used to extract, filter, amplify and transfer detected signals for analysis. The I-V convertor transforms the detected current to voltage; the voltage is rectified, and low-pass filtered to suppress the "carrier" sinusoid. A precision rectifier is set up with two diodes and an operational amplifier. The resulting signal from the circuit is acquired by a multimeter.

The equivalent circuit of the two electrodes area was analyzed to obtain an equivalent impedance Z_{eq} as in Eq. (5-4), with its resistive and reactive values given in Eq. (5-5) and (5-6) respectively:

$$Z_{eq} = R_{eq} + jX_{eq} \tag{5-4}$$

$$R_{eq} = \frac{-R_S X_S X_W + R_S X_W^2}{R_S^2 + (2X_S + X_W)^2} \tag{5-5}$$

$$X_{eq} = \frac{X_W(4X_S^2 + 2X_S X_W + R_S^2)}{R_S^2 + (2X_S + X_W)^2} \tag{5-6}$$

$$X_s = -\frac{1}{\omega C_s} \tag{5-7}$$

$$X_w = -\frac{1}{\omega C_w} \tag{5-8}$$

where R_s is the solution resistance, X_s is the parasitic reactance, X_w is the bypass reactance, and ω is the angular frequency of an applied signal.

Fig. 5.4(b) shows the measured and simulated magnitude frequency response of the output signal of the circuit shown in Fig. 5.4(a). The component values used in the simulation were identified by measurements: solution resistance, R_s = ~140 kΩ, parasitic capacitance, C_s = ~20 nF, and bypass capacitance, C_w = ~0.8 nF. The maximum response was observed at 62 kHz which was chosen as the carrier sinusoid frequency to favor a high output response for the circuit.

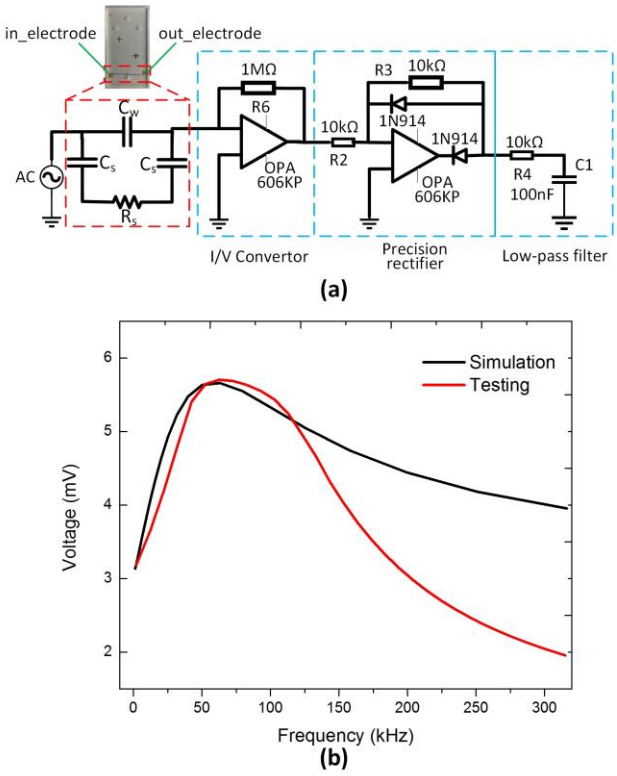

Figure 5.4 *(a) Conductivity detection circuit. (b) Measured versus simulated frequency responses of the microchip.*

5.2.6 Soil solution extraction

In additional to the electrophoretic chip and the detection unit, a vacuum-based suction unit was also designed for the in-situ extraction of soil solution. This unit consists of a suction head, a poly(methyl methacrylate) or PMMA-based collection chamber, and a mini-vacuum pump (Fig. 5.5(a)). The suction head structure is as shown in Fig. 5.5(b). A main component in the suction head is a microfiltration tubular module, consisting of a ceramic capillary tube (hydrophilic membrane composed of a blend of polyvinyl pyrrolidine and polyether sulfone; mean pore size: 0.15 μm) and high pressure polyether ether ketone or PEEK tubing. The PEEK tubing of the soil water suction unit is connected with the vacuum input of the PMMA soil water collection chamber. The vacuum output is connected the vacuum pump (VMP1625MX-12-90-CH, Virtual Industries, Inc, Colorado Springs, CO,

USA. Mini-Pump with 12-volt MAXON motor; flow rate: 1300mL/min; develops 18in/Hg. 16psi.). This collection chamber has an embedded plastic sphere (Fig. 5.5(c)). The floating sphere works as a valve and can be set to work in the ON and OFF phases (Fig. 5.5(d)). When the vacuum pump starts exhausting the air from the PMMA device, a low-pressure environment is built in the upper chamber, and the sphere valve gets stuck to the top end of the vertical channel, which is referred to as the "ON" mode. The system then begins to extract solution from soil through the suction head and accumulates it in the chamber at the

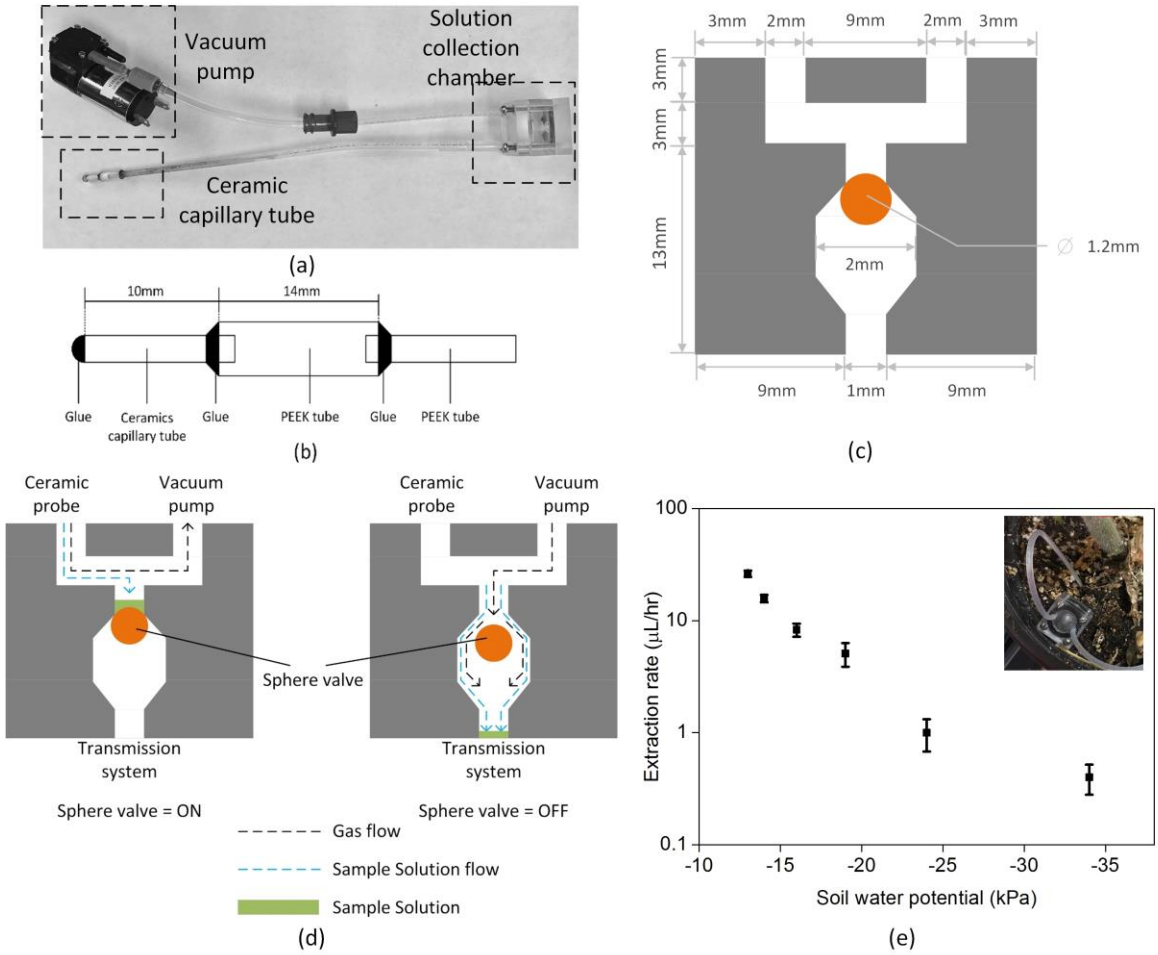

Figure 5.5 *(a) Schematic of the soil water extraction unit, consisting of a suction head, a PMMA chamber, and a vacuum pump; (b) Schematic of the suction head, ceramics capillary tube's outer diameter (OD) is 2.3 mm;(c) Schematic of solution collection chamber; (d) The ON and OFF working phases of the PMMA soil water collection chamber; (e) Measured extraction rates under different soil water potentials.*

top of the sphere valve. When the extraction is completed, the pump is switched so as to fill air into the chamber. This causes the sphere to fall down, referred to as the "OFF" mode, allowing the collected solution to be delivered below (Fig. 5.5(d)) for loading into the electrophoretic microchip.

The performance of the extraction unit was tested under different soil water potential conditions. When the soil water potential was high, which means wet soil, the extraction rate was also high (e.g., 26.3 ± 1.73 µL/hr at -13 kPa). The extraction rate dropped significantly with decreasing soil water potential (Fig. 5.5(e)).

5.3 Electrophoretic Chip Testing

The buffer solution used for on-chip electrophoresis was chosen to be 2-[N-Morpholino] ethanesulfonic acid (MES)/Histidine (HIS) 30 mM/30 mM, with 4 mmol 18-crown-6 and 0.1% methyl cellulose at 6.0 pH [49]. Both synthetic and extracted soil sample solutions were tested. The synthetic solution included a mixture of KNO_3 and Na_2SO_4 (each with 50 µM) in deionized (DI) water to evaluate the ability of the sensor to separate different ions, and different concentration solutions of KNO_3 in DI water to test the ability of the sensor to quantify nitrate ion concentrations.

Two types of real samples were prepared. The real sample of the first type (Type 1) was extracted from the soil samples collected at different locations of a Z.mays (type of maize) farm field at the Agricultural Engineering and Agronomy Research Farm (Boone, Iowa). Briefly, 10 g of field moist soil was weighed in a specimen cup. 50 mL of DI water was then added to the specimen cup and shaken on a reciprocal shaker for 1 hr. After shaking, the solution was filtered using Whatman #1 filter paper and the filtrates were collected, diluted with DI water at ratio 1 to 10, and stored at 4 ^{o}C until taken out for injection into the electrophoretic microchip [50].

The real sample solution of the second type (Type 2) was collected directly from soils by the presented soil solution extraction unit. The suction head was insert into the soil, with the extraction unit running for 1 hour to extract about 20 µL of soil solution under the soil water potential of -13 kPa.

To perform the ion concentration measurement on the electrophoretic microchip, the MES/HIS buffer solution was loaded into both the microfluidic channels by using a 3 mL syringe (Becton Dickinson, NJ, USA) with a microbore tubing (Cole-Parmer, IL, USA). Subsequently, a specific sample solution was placed at the inlet of the microchip using a pipette (Thermo Scientific, MA, USA). Next, the sample solution was injected into the shorter channel by generating and applying a 200 V between the sample inlet and the sample waste outlet for 6 sec to allow filling the intersection. Subsequently, ion separation was carried out by applying 500 V between the buffer reservoir and the buffer waste reservoir for 450 sec. The conductivity detection at the electrode was performed using a 5 mV_{p-p} excitation voltage at 62 kHz. After each test-run, the microchip was rinsed with 1 mL buffer solution for 10 times.

5.4 Results and Discussion

5.4.1 Separation of ions

Fig. 5.6 shows the output voltage of the microchip system over a period of 300 sec when the device was used to separate the anions of NO_3^- and SO_4^{2-} (50 µM each) present in the synthetic sample solution. The experimental result clearly shows two voltage peaks at two different times owing to different ionic mobilities of the NO_3^- and SO_4^{2-} ions. Note while the concentrations of the two ions were the same in the synthetic sample solution, their peak intensities were different, owing to the differences in their changes and ionic conductivities.

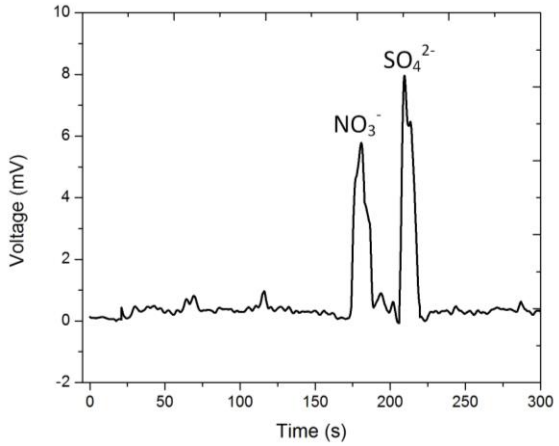

Figure 5.6 *Experimental results for separation of NO_3^- from SO_4^{2-} ions in the synthetic sample solution containing only these two ion species.*

5.4.2 Sensitivity and detection-limit from single ion detection

For the sensitivity and the detection-limit analysis, nitrate sensing was performed using the synthetic nitrate solutions of concentrations 20, 40, 60, 80, and 100 mM. Each solution was loaded into the same microchip for 3 different detection runs. Fig. 5.7(a) shows the peaks corresponding to 20, 40, 60, 80, and 100 µM of nitrate ion concentrations, all of which appeared around the same time (187 ± 3 s), indicating the high temporal accuracy of the sensor for a given ion species. Furthermore, the five nitrate concentrations can be clearly distinguished by their corresponding peak levels. Fig. 5.7(b) demonstrates that the voltage output of the sensor is almost linear to the input nitrate concentration. A linear fit of the data (Fig. 5.7(b)) indicates that the sensitivity of the sensor for the detection of the nitrate ions is approximately 0.0915 mV/µM.

The limit of detection (LOD) of the presented sensor is defined to be three times the standard deviation over the average of the voltage readout, in the absence of any analyte. The noise floor of the sensor is 0.30 ± 0.12 mV. Therefore, according to the above-mentioned definition, the LOD of the sensor is equivalent to a nitrate concentration that will result in an output voltage of 0.3 + (3 × 0.12) mV = 0.66 mV. This corresponds to LOD of around 7.25

µM. As shown in the inset of Fig. 5.7(a), it is also confirmed that the minimum detectable nitrate concentration of this sensor is 7.25 µM, which is an improvement compared to some previously reported values [51], and much lower than the amount found in agricultural soil. While this LOD is slightly higher than some ISE-based and enzymatic electrochemical sensors [26], the electrophoretic sensor has the advantage of being label-free, thereby eliminating the limit on sensor life due to the limited life of the ion selective materials.

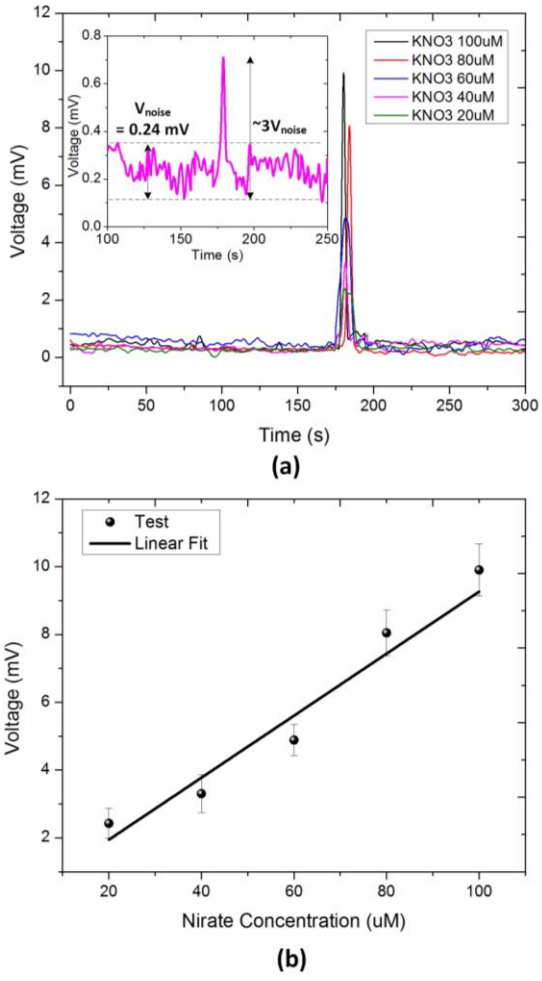

Figure 5.7 *(a) Experimental voltage response of the electrophoresis chip over a period of 300 s to different nitrate ion concentrations. (b) Output voltage of the sensor as a function of nitrate ion concentration. Coefficient of determination (R^2): 0.95013.*

5.4.3 Soil solution testing

The developed sensor was used to detect the major anions in the two types of real sample solutions collected from the soils. As mentioned in Section III, the first-type soil sample solution was obtained through the standard shaking and filtering process, and the second-type soil sample solution was collected directly by the developed extraction unit. Fig. 8 shows the result corresponding to the separated anions, under the applied electrical field, detected as time-separated voltage peaks, and served as a proof-of-principle.

In order to identify the ion types corresponding to the observed peaks, we tested four types of standard solutions independently using the microchip, each solution included only a single type of anion (each with 100 µM concentration): chloride (Cl^-), nitrate (NO_3^-), sulphate (SO_4^{2-}), and dihydrogen phosphate ($H_2PO_4^-$), respectively (Fig. 5.8(a)). These included the three important nutrients (nitrogen, phosphorus, and sulphur), plus chlorine that is considered to be the main interfering species for nitrogen. Although there are more than 4 peaks, especially in the solution extracted using a standard method, at this point only the four ions were cared to identify, for demonstrating a proof-of-principle. As discussed below, the 0.15 µm mean pore size of the extraction unit's suction head is able to filter out many extraneous particles/microbes.

The measured peaks for the 4 known ions were mapped against the results of the soil sample solution tests (Fig. 5.8(b)(c)). The difference between plots in Fig. 8(b) versus in Fig. 5.8(c) revealed a notable fact that the different extraction methods can contain different number of ion species. In fact, the ones present in the solution obtained through a standard extraction method (in Fig. 5.8(b)) are not generally the same as the ones available to the plants. Furthermore, since the pore size (0.15 µm) of the suction head used in the extraction

unit is much smaller than the pore size of Whatman #1 filter paper (11 µm) used in the standard solution extraction method, more extraneous particles/microbes were filtered out by the extraction unit, which also explains the fewer number of detected peaks in the solution extracted by the suction unit.

Using the result of mapping of the plots corresponding to the 4 known ion types against those of the two extracted solutions (Fig. 5.8(b)(c)), the peaks were labeled in Fig. 5.8 accordingly.

It is clear from the figure that the four ions in questions could be separated from each other at their given concentrations, including nitrogen from chlorine. Furthermore, using the calibration plot in Fig. 5.7(b), the detected nitrate concentration in the soil sample was found to be 210.3 ± 3.52 µM (mean ± standard deviation obtained from 5 independent experiments), which is within a 9% error-margin of the concentration value 191.2 ± 2.39 µM obtained using a sophisticated benchtop ultraviolet spectrophotometer. The slightly higher measured value for nitrate can be understood as follows: due to the closeness of the mobilities of chloride and nitrate (as noted from the proximity of their peaks), some residual chloride ions passed through the detection area while the nitrate ions started to go through that area, resulting in a slightly enhanced signal. In order to correct for such enhancement due to the overlap of the ions, one possible method would be to mathematically characterize the overlap, and algorithmically correct the reported value of the nitrate concentration. Another approach would be to increase the length of the separation channel to allow a larger gap between the two peaks and their better separation. Both these approaches are directions for future research.

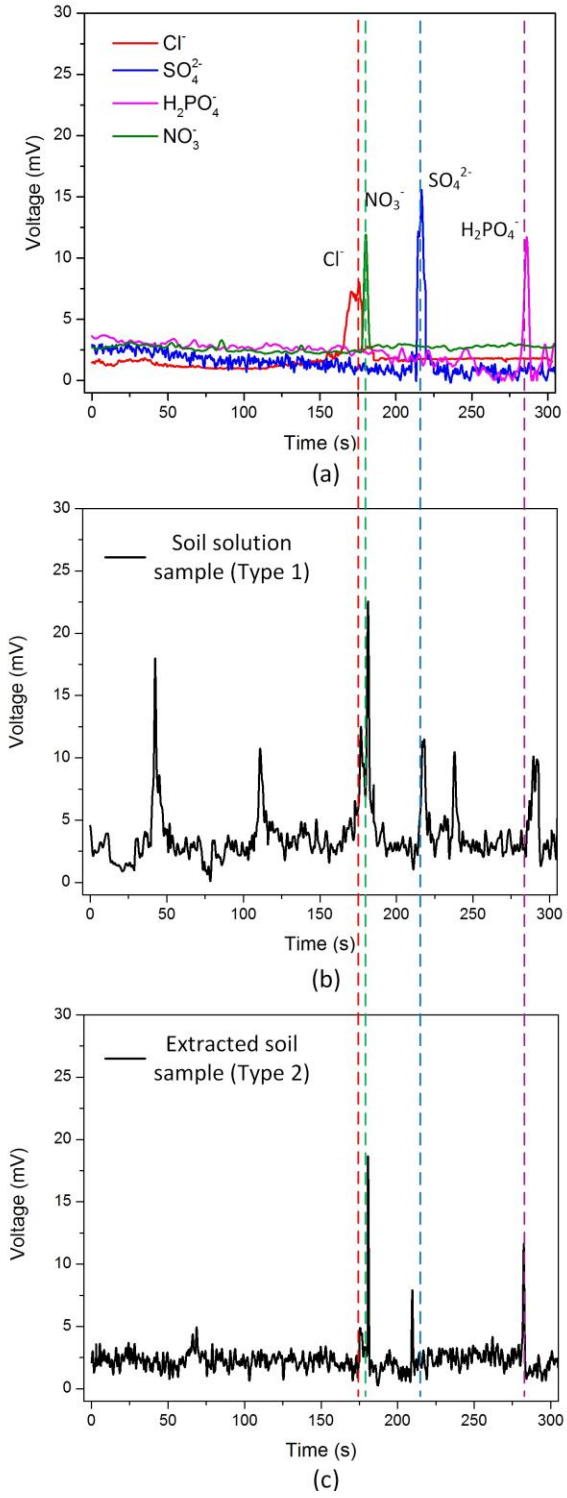

Figure 5.8 *Electropherogram of the device showing the separation and detection of anions in different samples: (a) Four synthetic samples with each containing only a single anion species (Cl-, NO3-, SO42-, or H2PO4-; each with 100 µM concentration); (b) Real soil solution sample of the first type prepared using the standard shaking and filtering method; and (c) the real sample solution of the second type directly extracted from the soil using the extraction unit. It has less peaks because the smaller pore filter removes many of the particulate matters and microbes.*

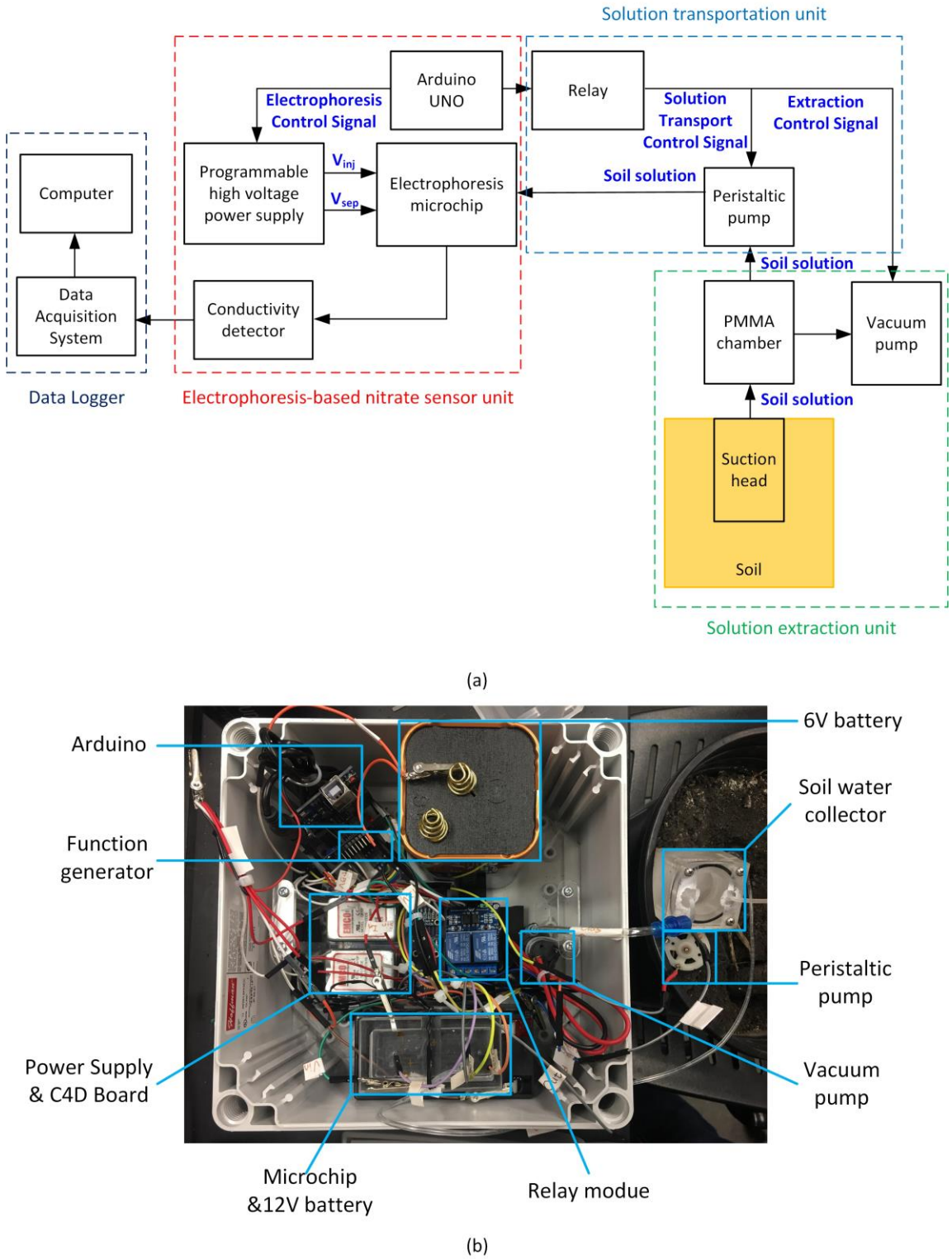

Figure 5.8 *Integrated system, (a)Schematic of integrated system, including solution extraction unit, solution transportation unit, electrophoresis-based nitrate sensor unit, and data logger. (b) image of integrated system.*

5.5 Integration System (not part of the IEEE Sensors paper)

Here an integrated system, including soil solution sampling unit, solution transportation unit, electrophoresis-based nitrate sensor unit, and data logger, was developed. The structure of data logger, electrophoresis-based nitrate sensor unit and solution extraction unit have been discussed in section 5.2. Here, the solution transportation unit was consisted of peristaltic pump and a relay module. The peristaltic pump is used for solution transportation and the relay module works as the switch for peristaltic pump and vacuum pump. Arduino UNO board, as the control centre, is programmed to control the performance of the whole system. Firstly, the Arduino UNO board sends an extraction control signal to turn on Vacuum pump and the solution extraction unit starts to sampling soil solution from soil. The sampled solution is stored in the PMMA chamber. Then the Arduino UNO board sends solution transportation control signal and turn on the peristaltic pump. The peristaltic pump delivers the collected soil solution from PMMA chamber to the sample inlet reservoir on the electrophoresis microchip. After that, the Arduino board sends out electrophoresis control signal to high voltage power supply system to start electrophoresis-based nitrate sensing process. The conductance data is collected and analysed by the data logger unit.

5.6 Conclusion

A microfluidic microchip nutrient sensing system was developed to extract, separate, detect, and quantify nutrient ions in soil sample solutions. The feature of in situ soil solution extraction is unique and innovative, enhancing the existing soil nutrient sensing technologies. The system can be used for extracting and testing analytes from other sources (e.g., water). Using this system, a mixture of anions presents in the soil solution extracted using the new suction unit as well as from an existing standard method was separated and detected via distinguishing peaks, separated over time. Further, a good linear relation between a single ion

(nitrate) concentration and detected signal peak was demonstrated. This together with a limit of detection of ~7.25 μM for nitrate ions demonstrated a good performance of the proposed detection system. The design and implementation of the soil solution extraction unit makes the entire sensing system suited for in situ applications. The extraction unit is driven by the water potential gradient. Also, the smaller-sized pores in the suction heads ensures that many of the impurities (particles/microbes) are automatically filtered out. In order to make the sensing system fully ready for an in-situ adoption, it would additionally require its integration with a wireless communication unit, such as one reported in [4]. A fully integrated sensing system has great prospects in nutrient management for precision farming.

Future research work would include (i) integrating the electrophoretic microchip sensor system with the soil solution extraction unit, a pumping unit for delivery of buffer solution and waste, external storage and waste reservoirs, and a wireless communication capability to realize a finished prototype for in situ soil nutrient monitoring, (ii) improving the microchip design, e.g., thinning down the glass substrate to further increase the output signal strength and thereby the sensitivity and LOD, (iii) optimizing the detection circuit to reduce noise floor and thus further lowering the detection limit of the system, and (iv) expanding the ability of the device to detect and quantify also the cations besides the anions.

References

1. A. Bah, S. Balasundram, and M. Husni, "Sensor technologies for precision soil nutrient management and monitoring." *American Journal of Agricultural and Biological Science* (2012).

2. K. Goulding, S. Jarvis, and A. Whitmore, "Optimizing nutrient management for farm systems." *Philosophical Transactions of the Royal Society of London B: Biological Sciences* 363.1491 (2008): 667-680.

3. H. Sahota, R. Kumar, and A. Kamal, "A wireless sensor network for precision agriculture and its performance." *Wireless Communications and Mobile Computing* 11.12 (2011): 1628-1645.

4. J. Huang, R. Kumar, A. Kamal, and R. Weber, "Development of a wireless soil sensor network." *2008 Providence, Rhode Island, June 29–July 2*, 2008. American Society of Agricultural and Biological Engineers, 2008.

5. P. Robert, "Precision agriculture: a challenge for crop nutrition management." *Plant and soil* 247.1 (2002): 143-149.

6. N. Zhang, M. Wang, and N. Wang, "Precision agriculture—a worldwide overview." *Computers and electronics in agriculture* 36.2 (2002): 113-132.

7. C.H. Ho, S.H. Lin, H.C. Hu et al., "CHL1 functions as a nitrate sensor in plants." *Cell* 138.6 (2009): 1184-1194.

8. G. Pandey, R. Kumar, and R. J. Weber, "A Low RF-Band Impedance Spectroscopy Based Sensor for In Situ, Wireless Soil Sensing." *IEEE Sensors Journal* 14.6 (2014): 1997-2005.

9. F. Kizito, C. Campbell, G. Campbell et al., "Frequency, electrical conductivity and temperature analysis of a low-cost capacitance soil moisture sensor." *Journal of Hydrology* 352.3-4 (2008): 367-378.

10. S. Staggenborg, M. Carignano, and L. Haag, "Predicting soil pH and buffer pH in situ with a real-time sensor." *Agronomy journal* 99.3 (2007): 854-861.

11. T. Jackson, K. Mansfield, M. Saafi et al., "Measuring soil temperature and moisture using wireless MEMS sensors." *Measurement* 41.4 (2008): 381-390.

12. Z. Zou, A. Jang, E. MacKnight et al., "Environmentally friendly disposable sensors with microfabricated on-chip planar bismuth electrode for in situ heavy metal ions measurement." *Sensors and Actuators B: Chemical* 134.1 (2008): 18-24.

13. J. V. Sinfield, D. Fagerman, and O. Colic, "Evaluation of sensing technologies for on-the-go detection of macro-nutrients in cultivated soils." *Computers and Electronics in Agriculture* 70.1 (2010): 1-18.

14. D. Corwin, and S. Lesch, "Apparent soil electrical conductivity measurements in agriculture." *Computers and electronics in agriculture* 46.1 (2005): 11-43.

15. K. Sudduth, S. Drummond, and N. Kitchen, "Accuracy issues in electromagnetic induction sensing of soil electrical conductivity for precision agriculture." *Computers and electronics in agriculture* 31.3 (2001): 239-264.

16. E. Ben-Dor, and A. Banin, "Near-infrared analysis as a rapid method to simultaneously evaluate several soil properties." *Soil Science Society of America Journal* 59.2 (1995): 364-372.

17. J. Reeves, G. McCarty, and T. Mimmo, "The potential of diffuse reflectance spectroscopy for the determination of carbon inventories in soils." *Environmental pollution* 116 (2002): S277-S284.

18. R. Verschoore, J. Pieters, T. Seps et al., "Development of a sensor for continuous soil resistance measurement." *Precision Agriculture. Wageningen Academic Publishers, Wageningen, The Netherlands* (2003): 689-695.

19. T. E. Grift, M. Z. Tekeste, and R. L. Raper, "Acoustic compaction layer detection." *Transactions of the ASAE* 48.5 (2005): 1723-1730.

20. S. Birrell, and J. Hummel, "Multi-sensor ISFET system for soil analysis." *Precision agriculture* 97 (1997): 459-468

21. D. L. Jones, "Organic acids in the rhizosphere–a critical review." *Plant and soil* 205.1 (1998): 25-44.

22. C.W. Chang, D. A. Laird, M. J. Mausbach et al., "Near-infrared reflectance spectroscopy–principal components regression analyses of soil properties." *Soil Science Society of America Journal* 65.2 (2001): 480-490.

23. R. R. Price, J. W. Hummel, S. J. Birrell et al., "Rapid nitrate analysis of soil cores using ISFETs." *Transactions of the ASAE* 46.3 (2003): 601.

24. E. Bakker, and M. Telting-Diaz, "Electrochemical sensors." *Analytical chemistry* 74.12 (2002): 2781-2800.

25. M. A. Ali, W. Hong, S. Oren et al., "Tunable bioelectrodes with wrinkled-ridged graphene oxide surfaces for electrochemical nitrate sensors." *RSC Advances* 6.71 (2016): 67184-67195.

26. A. T. Woolley, D. Hadley, P. Landre et al., "Functional integration of PCR amplification and capillary electrophoresis in a microfabricated DNA analysis device." *Analytical Chemistry* 68.23 (1996): 4081-4086.

27. M. W. Lada, T. W. Vickroy, and R. T. Kennedy, "High temporal resolution monitoring of glutamate and aspartate in vivo using microdialysis on-line with capillary electrophoresis with laser-induced fluorescence detection." *Analytical chemistry* 69.22 (1997): 4560-4565.

28. C. S. Effenhauser, G. J. Bruin, A. Paulus et al., "Integrated capillary electrophoresis on flexible silicone microdevices: analysis of DNA restriction fragments and detection of single DNA molecules on microchips." *Analytical Chemistry* 69.17 (1997): 3451-3457.

29. C. L. Colyer, T. Tang, N. Chiem et al., "Clinical potential of microchip capillary electrophoresis systems." *Electrophoresis* 18.10 (1997): 1733-1741.

30. Y. Huang, K. L. Ewalt, M. Tirado et al., "Electric manipulation of bioparticles and macromolecules on microfabricated electrodes." *Analytical chemistry* 73.7 (2001): 1549-1559.

31. Z. Liang, N. Chiem, G. Ocvirk et al., "Microfabrication of a planar absorbance and fluorescence cell for integrated capillary electrophoresis devices." *Analytical Chemistry* 68.6 (1996): 1040-1046.

32. M. Albin, R. Weinberger, E. Sapp et al., "Fluorescence detection in capillary electrophoresis: evaluation of derivatizing reagents and techniques." *Analytical chemistry* 63.5 (1991): 417-422.

33. J. Webster, M. Burns, D. Burke et al., "Monolithic capillary electrophoresis device with integrated fluorescence detector." *Analytical Chemistry* 73.7 (2001): 1622-1626.

34. M. L. Chabinyc, D. T. Chiu, J. C. McDonald et al., "An integrated fluorescence detection system in poly (dimethylsiloxane) for microfluidic applications." *Analytical chemistry* 73.18 (2001): 4491-4498.

35. C. Dongre, H. J. Hoekstra, and M. Pollnau, "Capillary electrophoresis and multicolor fluorescent DNA analysis in an optofluidic chip." *Capillary Electrophoresis and Microchip Capillary Electrophoresis: Principles, Applications, and Limitations* (2013): 247-266.

36. H. Craighead, "Future lab-on-a-chip technologies for interrogating individual molecules." *Nature* 442.7101 (2006): 387-393.

37. D. R. Reyes, D. Iossifidis, P.-A. Auroux et al., "Micro total analysis systems. 1. Introduction, theory, and technology." *Analytical chemistry* 74.12 (2002): 2623-2636.

38. P.A. Auroux, D. Iossifidis, D. R. Reyes et al., "Micro total analysis systems. 2. Analytical standard operations and applications." *Analytical chemistry* 74.12 (2002): 2637-2652.

39. A. T. Woolley, and R. A. Mathies, "Ultra-high-speed DNA fragment separations using microfabricated capillary array electrophoresis chips." *Proceedings of the National Academy of Sciences* 91.24 (1994): 11348-11352.

40. M. Smolka, D. Puchberger-Enengl, M. Bipoun, et al. "A mobile lab-on-a-chip device for on-site soil nutrient analysis." *Precision Agriculture* 18.2 (2017): 152-168.

41. T. Kappes, B. Galliker, M. A. Schwarz et al., "Portable capillary electrophoresis instrument with amperometric, potentiometric and conductometric detection." *TrAC Trends in Analytical Chemistry* 20.3 (2001): 133-139.

42. E. Knutson, and K. Whitby, "Aerosol classification by electric mobility: apparatus, theory, and applications." *Journal of Aerosol Science* 6.6 (1975): 443-451.

43. G. Yao, "A Computational Model for Simulation of Electroosmotic Flow in Microsystems." *Technical proceedings of the 2003 nanotechnology conference and trade show.* Vol. 1. No. 9. 2003.

44. V. M. Ugaz, and J. L. Christensen, "Electrophoresis in microfluidic systems," *in Microfluidic Technologies for Miniaturized Analysis Systems*, New York: Springer, 2007. pp. 393-438.

45. M. R. Wright, " Conductance: The Ideal Case " in An introduction to aqueous electrolyte solutions, Hoboken, NJ: John Wiley & Sons, Inc., 2007. pp.421-474.

46. F. Opekar, P. Tůma, and K. Štulík. "Contactless impedance sensors and their application to flow measurements." *Sensors* 13.3 (2013): 2786-2801.

47. J. A. Fracassi da Silva, and C. L. do Lago, "An oscillometric detector for capillary electrophoresis." *Analytical Chemistry* 70.20 (1998): 4339-4343.

48. A.J. Zemann, E. Schnell, D. Volgger, and G.K. Bonn, "Contactless conductivity detection for capillary electrophoresis." *Analytical chemistry* 70.3 (1998): 563-567.

49. P. Schmitt-Kopplin, "Determination of small ions with capillary electrophoresis and contactless conductivity detection." *Capillary Electrophoresis: Methods and Protocols* (2008): 3-19.

50. R. Hood-Nowotny, N. Hinko-Najera Umana, E. Inselbacher, P. Oswald-Lachouani, and W. Wanek, "Alternative methods for measuring inorganic, organic, and total dissolved nitrogen in soil." *Soil Science Society of America Journal* 74.3 (2010): 1018-1027.

51. P. Kubáň, and P. C. Hauser, "Application of an external contactless conductivity detector for the analysis of beverages by microchip capillary electrophoresis." *Electrophoresis* 26.16 (2005): 3169-3178.

CHAPTER 6. CONCLUSIONS

We have developed multiple microfluidic-based miniature systems, including controllable discrete humidity chamber, micro PBR system, and in-situ soil nutrient sensor, to study important problems in agriculture. The developed devices or approaches will benefit for understanding the seed-pathogen interactions, responding of microalgae to different low CO_2 conditions, and nutrient cycling of soil health in a high throughput way.

Firstly, we have presented a simple approach that generate a controlled discrete humidity gradient in two types of devices rapidly. The device was a two-layer system with a top freeway layer and a multiple-compartmented-wells bottom layer. A water source and a desiccant source were preloaded at two ends of the bottom layer. With the combination of evaporation, convection and diffusion, a stable discrete humidity gradient would be generated fast and maintained for long term. Then, the built system was used to study the soybean-P.sojae interaction under a set of humidity conditions. Furthermore, this approach is also workable in smaller scale devices with shorter generation time. And it also is suitable for multi research purposes within simple medication.

Second, we developed a new microfluidic device with a concentration gradient generator to culture and analysis growth of microalgal cells under different CO_2 concentrations. What's more, the developed culture system achieves in-line screen and analysis. In the presented system, a gas semipermeable hydrophobic membrane was used to achieve evenly distribution of CO_2 in a single culture cell within a few minutes.

Third, we developed a high-through multi-well-plate-based microalgal bioreactors to study growth of microalgae under eight different CO_2 concentrations in parallel. The bioreactors have observation optical pillar, built-in magnetic stir, gas inlets and outlets and

media refilling port. A wild type microalgae strain, C. reinhardtii strain CC620, was cultured and analyzed using the developed platform in accurate CO_2 conditions. The results showed different growth rates under different conditions. The system simulated natural growth environment for microalgae and achieved real time screening, with higher throughput and lower cost than traditional conventional PBRs.

Lastly, we developed a microchip-based nutrient sensing system to realize soil solution extraction and analysis. The developed system has four units: soil solution extraction unit, solution transportation unit, electrophoresis-based sensor unit, and data logger. Controlled by a programmable Arduino board, the presented system can soil solution sampling, delivery, and analysis automatically. To demonstrate the workability of the system, soil solution was collected, transported, injected, separated and detected via distinguishing peaks.

In summary, all the presented technologies have demonstrated their workability in several areas in biorenewable investigation and modern agriculture. Due to the properties as good flexibility and low cost, those technologies can be applied in more areas of biorenwable energy and modern agriculture. They should be powerful tools to accelerate the investigation of biorenewable energy and modern agriculture.

Future research work would focus on performance improvement and dimension miniaturization of the nutrient sensor system, including (i) reducing power consumption of the integrated system, (ii) optimizing the detection circuit to improve detection stability, reduce noise and enlarge signal-to-noise ratio to improve detection resolution, (iii) reducing solution transportation rate to achieve more precision control of solution delivery.